editor@sciencepub.net
http://www.sciencepub.net

ISSN: 1545-0740

Nature and Science

Volume 1, Number 1, 2003

Nature and Science

The **Nature and Science** is an international journal to enhance our natural and scientific knowledge spreading in the world under the free publication principle. Any valuable paper to describe natural phenomena/existence or report scientific researches/pursuits will be acceptable, including both natural and social sciences. Papers submitted could be reviews, objective descriptions, research reports, opinions/debates, news, letters, and all other information nature and science related. The journal is calling for papers and looking for more co-operators and editors.

Introductions to Authors

1. General Information

(1) Goals: As an international journal published in print and on the web, the Nature and Science is dedicating to the dissemination of fundamental knowledge in all areas of nature and science. The main purpose of the Nature and Science is to enhance our knowledge spreading in the world under the free opinion publishing principle. It publishes full-length papers (original contributions), reviews, rapid communications, and especially it publishes any debate and opinion in all the fields of nature and science.

(2) What to Do: The Nature and Science provides a place for discussion of the scientific news, research, theory, philosophy, profession and technology - that drive scientific progress. Research reports and regular manuscripts that contain new and significant information of general interest are welcome.

(3) Who: All people are welcome to submit manuscripts in any fields of nature and science.

(4) Publication Costs: US$20 per printed page of an article to defray costs of the publication will be paid by the authors when the submission or after the acceptance. Extra expense for color reproduction of figures will by paid by authors (estimate of cost will be provided by the publisher for the author's approval).

(5) Journal Copies to Authors: One hard copy of the journal will be provided free of charge for each author, and 50 offprints (reprints) of each article will be provided free of charge for the article's correspondence author (or the first author).

(6) Additional Copies Bought by Authors: Additional hard copies and offprints could be purchased with the price of US$4/issue and US$0.2/page-offprint (mailing and handling cost included). The offprints must be ordered prior to printing of the journal.

(7) Distributions: Web version of the journal is freely opened to the world without any payment or registration. The journal will be distributed to the selected libraries and institutions for free. US$5/issue is for the subscription of other readers.

(8) Advertisements: The price will be calculated as US$400/page, i.e. US$200/a half page, US$100/a quarter page, etc. Any size of the advertisement will be accepted.

2. Manuscripts Submission

(1) Submission Methods: Electronic submission through email is encouraged and hard copies plus an IBM formatted computer diskette would be also accepted.

(2) Software: The Microsoft Word file will be preferred.

(3) Font: Normal, Times New Roman, 10 pt, single space.

(4) Indent: Type 2 space in the beginning of each new paragraph.

(5) Manuscript: Don't use "Footnote" or "Header and Footer".

(6) Cover Page: Put detail information of authors and a short title in the cover page.

(7) Title: Use Title Case in the title and subtitles, e.g. "**Debt and Agency Costs".**

(8) Figure and Table: Use full word of figure and table, e.g. **"Figure 1.** Annul Income of Different Groups**", Table 1. Annual Increase of Investment".**

(9) References: Cite references by "last name, year", e.g. "(Smith, 2003)". References should include all the authors' last names and initials, title, journal, year, volume, issue, and pages etc.

Reference Examples:

Journal Article: Hacker J, Hentschel U, Dobrindt U. Prokaryotic chromosomes and disease. Science 2003;301(34):790-3.

Book: Berkowitz BA, Katzung BG. Basic and clinical evaluation of new drugs. In: Katzung BG, ed. Basic and clinical pharmacology. Appleton & Lance Publisher. Norwalk, Connecticut, USA. 1995:60-9.

(10) Submission Address: editor@sciencepub.net, Marsland Company, P.O. Box 753, East Lansing, Michigan 48826, The United States, 517-862-6881.

(11) Reviewers: Authors are encouraged to suggest 2-5 competent reviewers with their email and mailing addresses.

2. Manuscript Preparation

Each manuscript is suggested to include the following components but authors can do their ways:

(1) Title page: including the complete article title; each author's full name that family name appears with uppercase; institution(s) with which each author is affiliated, with city, state/province, and zip code; and the name, complete mailing address, telephone number, facsimile number (if available), and e-mail address for all correspondence.

(2) Abstract: including Background, Materials and Methods, Results, and Discussions.

(3) Key Words.

(4) Introduction.

(**5) Materials and Methods**.

(**6) Results**.

(**7) Discussions**.

(**8) References**.

(**9) Acknowledgments**.

Journal Address:
Marsland Company
P.O. Box 753
East Lansing, Michigan 48826
The United States
Telephone: (517) 505-7688
E-mail: editor@sciencepub.net
Homepage: http://www.sciencepub.net

Contents

NATURE AND SCIENCE

Call for Papers

Dear Friends:

Do you have scientific research results, opinions/debates or review papers to be published? The new international academic journal "Nature and Science" (ISSN 1545-0740) is inviting you to publish your papers. Please visit http://www.sciencepub.net and send your manuscripts to editor@sciencepub.net.

The Nature and Science is an international journal to enhance our natural and scientific knowledge spreading in the world under the free publication principle. Any valuable paper to describe natural phenomena/existence or report scientific researches/pursuits will be acceptable, including both natural and social sciences. Papers submitted could be reviews, objective descriptions, research reports, opinions/debates, news, letters, and all other information nature and science related.

As a formal academic journal, the Nature and Science is registered in the United States and published in the both print and Internet online versions from November of 2003. The journal is calling for papers and looking for more co-operators and editors.

To cover the publication expenses of printing and website maintenance, the journal will charge authors limited publication fee (US$20/page for print version, and US$5/page for Internet online version). For the printed version, at least 1 hard copy of printed journal for each author and 100 offprints (reprints) for each article will be provided to authors by free charge.

If you have anything including research reports, review papers or any other related article to be published, it is a good chance. At least it is better than letting your precious achievements sleep in your drawers. If you have some friends for this, let them contribute papers also. Let's work together to promulgate our research results/opinions, to do what we can do.

Papers in all the fields are accepted: including natural science and social science.

Thank you for your support!

Marsland Company
P.O. Box 753
East Lansing, Michigan 48826
The United States
Telephone: 517-862-6881
E-mail: editor@sciencepub.net
Homepage: http://www.sciencepub.net

The Nature of Time and Space

Hongbao Ma

Department of Medicine, Michigan State University, East Lansing, MI 48824, USA, hongbao@msu.edu

Abstract: Related to human activities, there are two aspects of the world: One is the observed world (epistemology) and the other is the existed world (ontology). This article discusses the nature of time and space from the epistemological and the ontological aspects. From the epistemology angle, time and space are relative (observed). From the ontology angle, time and space are absolute (existed) and the universe is a timeless world, which means that all the past, the present and the future exist eternally. [Nature and Science 2003;1(1):1-11].

Key words: time; space; nature; universe; ontology; epistemology

Contents

1. Introduction

Does the past still exist? Where is the past? Does the future exist already and wait us to meet? Does the life still exist after death? What is time? What is space? Is there an absolute time or space in the universe or not? St Augustine, who died in AD 430, said: "If nobody asks me, I know what time is, but if I am asked then I am at a loss what to say" (Barbour, 2000; Folger, 2000). This answer is true for most of the people on the earth.

Related to human's activities, there are two aspects of the world: One is the observed world and the other is the existed world. For the observed world concept, it is related to epistemology, empiricism, idealism, mentalism, immaterialism, spiritualism, subjectivity, and measurement, etc. For the existed world, it is related to ontology, naturalism, materialism, physical entity, and existence, etc.

According to Webster's Dictionary: "Time – The system of those sequential relations that any event has to any other, as past, present, or future; indefinite and continuous duration regarded as that in which events succeed one another"; "Space – The unlimited or incalculably great three-dimensional realm or expanse in which all material objects are located and all events occur" (Webster's, 2003). According to the New Webster's Dictionary: "Time - The measure of duration. A particular part or point of duration"; "Space: Extension. Internal between points or objects quantity of time" (New Webster's, 2003). As another reference, according to the Hyperdictionary: "Time is the continuum of experience in which events pass from the future through the present to the past" (Hyperdictionary, 2003). From the definitions we can see that the time and space have both the observed (measure) and existed (duration and extension) characterizations.

The modern physics is mostly talking about the measured time and space with observations and mathematics, but ignoring the existed time and space (Hawking, 1996). According to the relativity, a traveler could see that the time and the space are shrink as his/her observation, if it is true. But he/she cannot change the time and space. The time and space are still the same time and space no matter there is a traveler to observe it or not. The time and space do not shrink, but the observer feels them shrink. There are essential conflicts of the time and space concepts between the observed and existed aspects. If we only think about the measured world, including time and space that are measured by human, we should say that there is nothing if the measurers die.

In this article, I will describe and discuss the nature of time and space from both the observed aspect and the existed aspect.

2. Newton's Concepts

In 1687, Sir Isaac Newton (1/4/1643-3/31/1727) created precise notions of time, space and motion. Newton's time and space concept is absolute. According to Newton's theory, time flows with perfect uniformity forever and space is a limitless container. Nothing in the universe affects the time's flow. The space stretches from infinity to infinity. The time and space are more fundamental than matters. It can be imagined as an empty world without matter but not a matter world without time and space. All the things in the Newtonian world are at definite positions and conditions. All the things in the universe move through absolute space according to the definite laws of motion. If all the conditions of the universe are known at some instant, the laws determine all the future movements, and also all the history of the universe can be known. This is so called mechanical determinism. Even though the Newton's mechanical determinism has been criticized by relativity and quantum theories, it is still considered as the true verity of the objective world from the ontological angle.

3. Classic Relativity

Motion is observed when something moves relatively to other things. Observers moving relatively to each other report different descriptions for the motion of an object, but the objects obey the same laws of motion regardless of reference system. The laws of physics are the same in all inertial reference systems (Galilean principle of relativity). For example, measurements in one inertial reference system yield the same forces as measurements in any other inertial reference system.

Observers in different reference systems can reconcile different velocities they obtain for an object by adding the relative velocity of the reference systems to that of the object (However, this procedure breaks down for the velocities near that of the light according the Einstein's special relativity). In a reference system accelerating relatively to an inertial reference system, the law of inertia does not work without the introduction of fictitious forces that are due entirely to the accelerated motion. Centrifugal force arises in rotating reference systems and is an example of inertial forces. The earth is noninertial reference system as it rotates always.

4. Special Relativity

In 1905, Albert Einstein (3/14/1879-4/18/1955) set up the special relativity with the two basic postulates:

1. The laws of physics are the same in all inertial reference systems.
2. The speed of light in a vacuum is a constant value regardless of the speed of the source or the speed of the observers.

The first postulate says that there is no absolute space and any inertial reference system is just as good as any other. This is a reaffirmation of the Galilean principle of relativity. According to Galilean's classical relativity, a traveler in a ship moving with a constant velocity could not conduct experiments that would determine whether the ship is moving or at rest. However, a theory by the Scottish physicist James Clerk Maxwell describing the behavior of electromagnetic waves, such as light and radio, yielded unexpected results. In Newton's laws, reference systems moving at constant velocities are equivalent to each other. However, if one system accelerates relatively to another, the two reference systems are not equivalent. The Newton's laws depend on acceleration and not on the velocity. The acceleration of a reference system can be detected, but its velocity cannot be detected absolutely. In Maxwell's theory the velocity of the electromagnetic waves appears in the equations rather than their acceleration. Maxwell's equation and Galilean principle of relativity were apparently in conflict. To reconcile the contradiction between the principle of relativity and Maxwell's equation, Einstein supposed an absolute reference system in the universe, which depended on his second postulate of special relativity: There is a speed limit. According to Newtonian mechanics a charged particle (charge q, mass m) in a constant electric field E can be accelerated to an arbitrary velocity: $v(t)=qEt/m$. The velocity could be arbitrarily big according to the equation. But, the Einstein's special relativity supposes that particles cannot be accelerated beyond the light speed $c=3\times10^8$ m/s (Kogut, 2001). As the Figure 1 shows, according to Newton's law, the relative velocity of the light to the observer should be $v'=c+v$, but the relativity denies the rule called addition of velocities in Newton's world and gives the result as $v'<c+v$ or $v'=c$, with the speed limit postulate. It rests on Newton's ideas of absolute time and space. As my opinion, the speed limit is the postulated idea by the theory of special relativity and it is an idealistic concept.

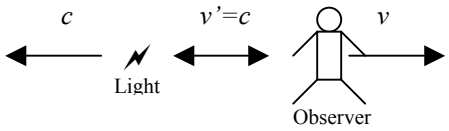

Figure 1. A light moves to the left direction with the speed c and an observer moves to the right direction with the speed v. According to the Einstein's special relativity, the speed of the light observed by the observer is also c, rather than $c+v$.

5. General Relativity

In the second half of 1915, Einstein expanded on his general theory of relativity and most definitely included "time" as a very important factor. According to the general relativity, the laws of physics are the same in all reference systems, and constant acceleration is

completely equivalent to a uniform gravitation (gravitational mass=inertial mass). One of Einstein's postulates of this theory states that the fabric of space-time, in the vicinity of a large mass, is curved. This "curvature" can be observed affecting the motion of other bodies in the vicinity in a way that is manifested as a force. This is called the force of gravity. Another tenet of Einstein's relativity notes the slowing of "time" at high speeds. According to the theory of relativity, some space-time future and past are relative to every space-time point P (Figure 2) (Zeh, 1992).

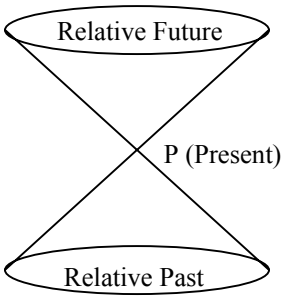

Figure 2. Local space-time structure according to the theory of relativity. Space-time future and past are defined relatively to every event P and independently of any frame of reference.

Although the general relativity has been universally accepted by modern science, many questions still need asked. Is acceleration relative? If there is no absolute space in the universe, what is the reference of the acceleration motion? We can say that there is no way to determine which of two inertial reference systems is really at rest and which is absolute motion, but we really feel the absolute acceleration if the system is accelerated. Accelerated to what? It does not need reference to determine acceleration and the acceleration is absolute. Be absolute to what? As my conclusion the answer should be "space". The space is the absolute reference in the existed world. The space is absolute.

6. Quantum Mechanics

The submicroscopic atomic world of the quantum mechanics and the vast cosmic world of the general relativity provide a radically different conception of time each, and physicists simply don't know how to reconcile the two views. Specifically, DeWitt hijacked the Schrödinger equation, named for the great Austrian physicist who created it. In its original form, the equation reveals how the arrangement of electrons determines the geometrical shapes of atoms and molecules. As modified by DeWitt, the equation describes different possible shapes for the entire universe and the position of everything in it. The key difference between Schrödinger's quantum and DeWitt's cosmic version of the equation - besides the scale of the things involved - is that atoms, over time, can interact with other atoms and change their energies. But the universe has nothing to interact with except itself and has only a fixed total energy. Because the energy of the universe does not change with time, the easiest way to solve what has become known as the Wheeler-DeWitt equation is to eliminate time. In theories of quantum mechanics, time is essentially taken for granted, and it simply regularly ticks away in the background, just as it does in our own lives. Time in the quantum theory has no remarkable properties at all. That is not agreed in the general relativity. The pictures of time in the general relativity and the quantum mechanics are fundamentally incompatible (Peskin, 1995).

7. Simultaneous Events

According to Einstein's special theory of relativity, the time clock varies and the simultaneity is relative from the different observers. There is no universal way to say if two specific physical events are simultaneous or not. (Kirkpatrick, 1995). With Figure 3, the following gives the description. For the two events X and Y, observer A can say that they are the simultaneous events, observer B can say that X is after Y, and observer C can say that X is before Y (Figure 3). What is true? My answer is that there is no answer. The real thing is that the events X and Y are existed events. The differences of time order gotten from different observers are their description on an observed world, not an existed itself. All the history is there forever, and all the future is there already. There is neither before nor after in the nature.

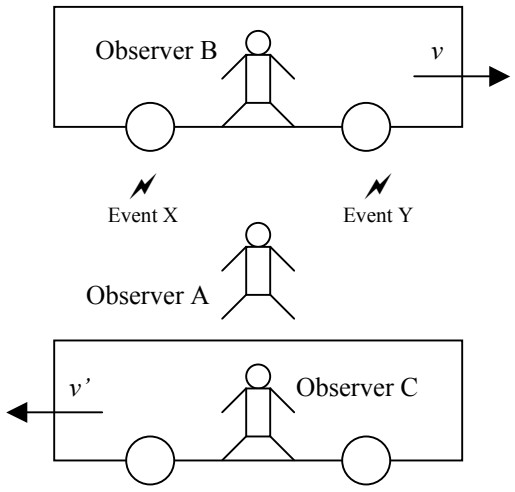

Figure 3. There is no universal way to say if two specific physical events are simultaneous or not according to the special theory of relativity. As for the events X and Y, if it is simultaneous for observer A, the event Y will happen before the event X for observer B and after the event X for observer C.

8. Time Dilation

According to the special theory of relativity, time interval increases with the object's moving speed (Figure 4).

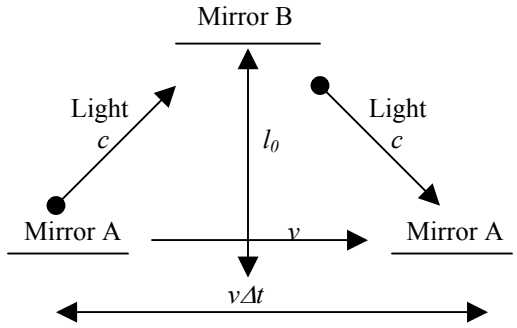

Figure 4. The demonstration of the time dilation. In a moving box at the velocity *v* of right direction, a light ray emits from mirror A and travels to mirror B (length AB) then reflects back to mirror A (length BA).

As Figure 4 shows, the light ray travels along the line segment AB and then along BA back to mirror A. The distance mirror A in Figure 4 travels between sending and receiving the light ray is $v\Delta t$. The distance the light ray travels is: AB+BA=$2\sqrt{l_0^2+(v\Delta t/2)^2}$. (1)

The light ray also travels at the speed limit *c* in the box according to special relativity postulate 2, so

AB+BA= $c\Delta t$ (2)

Here the equation (2) is subjectively assumed that the light speed is limited to *c* as the special relativity supposes.

Combining equations (1) and (2) it gets:

$$c\Delta t=2\sqrt{l_0^2+(v\Delta t/2)^2}\ .$$

$$\Delta t=\frac{2l_0}{\sqrt{c^2-v^2}}=\frac{2l_0/c}{\sqrt{1-v^2/c^2}}$$

$$\Delta t=\frac{\Delta\tau}{\sqrt{1-v^2/c^2}},$$

where $\Delta\tau=2l_0/c=\Delta t\sqrt{1-v^2/c^2}$.

This result is called "time dilation". The time interval in a moving system, Δt is dilated by a factor of

$$\gamma\equiv\frac{1}{\sqrt{1-v^2/c^2}}.$$

Two experiments, one in 1971 and the other one in 1977, confirmed the predictions of the time dilation (Kirkpatrick, 1995). Time dilation is an observed phenomenon.

Table 1 gives the calculated values of the adjustment factor for the different speeds of the moving systems.

Table 1. The Values of the Adjustment Factor for Various Speeds

Speeds	Adjustment Factor (γ)
Fastest subsonic jet plane	1.0000000000006
3 times speed of sound	1.000000000005
50% of speed of light	1.15
80% of speed of light	1.67
99% of speed of light	7.09
99.99% of speed of light	70.7
99.9999% of speed of light	707
The speed of light	∞

9. Lorentz Contraction

If the constancy of the speed limit implies time dilation, it must also affect the measurements of the length of moving objects. This is the Lorentz contraction (Kogut, 2001). It can be described with Figure 5.

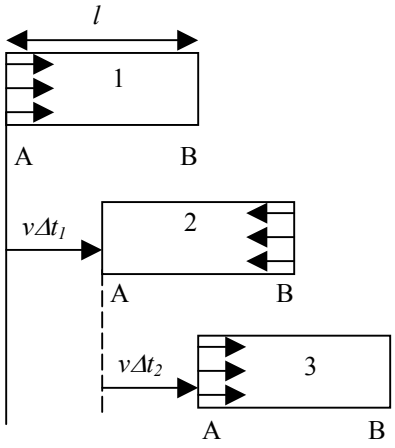

Figure 5. The demonstration of the Lorentz contraction. In a moving box at the velocity *v* of right direction, a light ray emits from mirror A and travels to mirror B (length AB) then reflects back to mirror A (length BA).

In the first image of Figure 5, light ray leaves mirror A and heads toward mirror B (from left to right). In the second image, the light ray reaches mirror B after a time Δt_1. Mirror A has moved a distance $v\Delta t_1$ to the right, so

$c\Delta t_1=l+\Delta t_1$. (3)

In the third image of Figure 5, the light ray leaves mirror B and is reflected to mirror A. Between images 2 and 3, a time Δt_2 has passed, so mirror A moves an additional distance $v\Delta t_2$:

$c\Delta t_2=l-v\Delta t_2$. (4)

Where the minus occurs because the light ray is moving from mirror B to A while mirror A is moving to the right direction for the $v\Delta t_2$.

$\Delta t=\Delta t_1+\Delta t_2$

$$\Delta t=\frac{l}{c-v}+\frac{l}{c+v} \qquad (5)$$

$$\Delta t = \frac{2l/c}{1 - v^2/c^2}.$$

From $\Delta t = \gamma(2l_0/c)$, it gets

$$l = l_0/\gamma = \sqrt{1 - v^2/c^2}\, l_0. \quad (6)$$

This is called Lorentz contraction because l is less than l_0. This result is conducted from the time dilation. It is the observed result.

10. Gravity and Light

According to the special relativity, gravitation alters space. One of the arguments of this is that space is distorted when a gravitational field bends light. Relativity denies the Newtonian space view of the flat-space (Euclidean) and takes the warped space-time view. According to Einstein's general theory of relativity a gravitational field alters time, and the gravitational time dilation is caused (Pickover, 1998). But, according to my opinion, the fact is that the clocks run slower in a gravitational field, rather than the time elapse slower. Light is bent by gravity (Figure 6). The light is wave-particle, so that it is possible for light to move as a curve, rather than straight line only, just like any other object to travel in the three-dimension space with any contrail. This is not space bent, but the light bent. There is no gravitational time dilation existed.

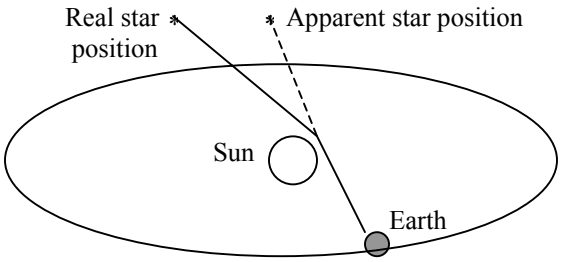

Figure 6. The path of starlight is bent as it passes the sun. This effect has been greatly exaggerated in this drawing.

11. Gravitational Waves

When Einstein proposed his general theory of relativity, he also postulated the existence of gravitational waves. In many ways gravitational waves should be analogous to electromagnetic waves. The acceleration of electric charges produces electromagnetic waves such as light, radio, radar, TV, and x-rays, etc. Gravitational waves should result from the acceleration of mass. Both carry energy through space, and decrease in intensity as the inverse square of the distance from the source. But, the gravitational waves have not been detected yet. Why? First, the gravitational force is 10^{43} times weaker than the electromagnetic force. Second, the detectors are less sensitive in intercepting gravitational waves by at least another factor of 10^{43}. The detection of gravitational waves is one of the most fundamental challenges of the modern science. Although there is no direct evidence of gravitational waves detected, there is strong indirect evidence for the existence of the gravitational waves. In 1974 Joseph Taylor and Russell Hulse discovered a pair of neutron stars orbiting each other at very close range. Neutron stars normally have masses slightly larger than the mass of our sun but they are only 10 km in diameter. The electrons and protons in neutron stars combine and form neutrons under the condition of high density, and the neutron stars consist almost entirely of neutrons. The two neutron stars Taylor and Hulse observed orbit each other every eight hours and the orbital speed is 0.13% of the light speed. One of the neutron stars is a pulsar that gives a pulse of radiation every 59 milliseconds. These pulses of radiation like a clock that is as good as any atomic clock. This clock allows very precise timings of the orbits and almost 20 years of measurements indicate that the orbital period is decreasing. In fact, it is decreasing at precisely the rate expected from the loss of energy due to gravitational radiation, possibly the gravitational wave. The 1993 Nobel Prize of physics was awarded to Taylor and Hulse for this contribution (Kirkpatrick, 1995).

As a personal opinion, I think that the gravitational waves will be detected directly, and it is only a matter of the development of technology and the improvement of the detecting sensitivity. As it has no evidence to say that the speed of gravitational waves travel with the light speed limitation, the detection of gravitational waves will affect the concepts of the relativity and the nature of time and space.

12. Big Bang

According to the modern cosmological principle, the universe was formed about 15 billion years ago. For the beginning, a tremendous explosion started the expansion of the universe. This explosion is known as the big bang model. At the point of this event all of the matter, energy, time and space were contained at one point. Supposing that there was neither time nor space before the big bang. This occurrence was not a conventional explosion but an event filling all of the space with all of the particles of the embryonic universe rushing away from each other. This phenomenon of galaxies moving farther away from each other is known as the redshift. Redshift says that the light ray will shift to a longer wavelength (red direction) if the light source moves from the observer. The faster the moving, the more the redshift. Light from the farther galaxies has a bigger redshift, which shows that the farther the stars, the fast they are moving. The origin of the big bang theory can be credited to Edwin Hubble. With the redshift observation, Hubble made the conclusion that the universe is continuously expanding. He discovered that a galaxy's velocity is proportional to its distance

from the observer. Galaxies that are twice as far from us move twice as fast. Another consequence is that the universe is expanding in every direction. This observation means that it has taken every galaxy the same amount of time to move from a common starting position to its current position. Just as the big bang theory provided for the foundation of the universe, Hubble's observations provided for the foundation of the big bang theory.

Since the big bang, the universe has been continuously expanding and there has been more and more distance between clusters of galaxies. The big bang theory received its strongest confirmation when Arno Penzias and Robert Wilson, who later won the Nobel Prize in 1978 for the discovery of the cosmic background radiation in 1964 (Lidsey, 2000).

The temperature of the universe at any given time is directly related to the size and age of the universe. It often proves convenient to measure the age of the universe directly in terms of its temperature. A higher temperature corresponds to an earlier time. When the universe was one second old its temperature was about ten billion degree. Matter in the form of atoms would not have been present that time (Lidsey, 2000; Delsemme, 1998). Even most modern cosmologists agree that the big bang model represents an accurate description of the very early universe, at least for the time after about one second, what existed prior to the big bang is completely unknown. Especially, it is unreasonable to believe that there was neither time nor space before the big bang (origin of the universe).

13. Black Hole

According to the general relativity, a black hole is a region of space that has so much mass concentrated in it that there is no way for a nearby object to escape its gravitational pull. Light inside the black hole is bent back on itself and never escapes. Stars begin to collapse and the matter density would gradually increase within the black hole. In the general relativity, gravity is a manifestation of the curvature of space-time. Massive objects distort time and space, so that the usual rules of geometry do not apply anymore. This distortion of space is extremely severe near a black hole. In particular, a black hole has something called an event horizon. This is a spherical surface that marks the boundary of the black hole. Objects can pass in through the horizon, but they cannot get back out. In fact, once anything crosses the horizon, it will be doomed to move inexorably closer and closer to the center of the black hole (Al-Khalili, 2003).

The black hole theory does not show what will happen for the gravitational waves from a black hole. Even the postulate of relativity that makes light speed as the speed limitation keeps matter escaping from the black hole, whether the speed of gravitational waves obeys this limitation is not clear.

14. Twin Paradox

As I have described in this article, time could be relative and dilative according to relativity from the epistemological point. But, from the ontological angle, time could be neither relative nor dilative. People in different inertial systems can stop their experiments, come together, and compare clocks. They should be able to resolve the question of which clock is really running slower. This makes the apparent paradox, called the twin paradox. Suppose that twins decide to do a time-dilation experiment. One twin gets in a spaceship and flies away from the earth. The spaceship travels out to a distant star and returns to the earth. The twin staying on the earth observes that clocks in the spaceship run slower than on the earth. Therefore, the twin in the spaceship ages more slowly. The twin should return from the journey at a younger age than the one who stays at home. Meanwhile, the twin in the spaceship observes that the clocks on the earth are running slower, as he will see that earth moves from him (relatively). So, the earth-bound twin will age slower and should be the younger age the reunion. Thus, we have a paradox. How can each twin be younger than the other? The answer by the physics now is that the twin in the spaceship is taking the trip and his clock is slower. This is supposed that the situation is not symmetric and the spaceship accelerates to leave or turns around to return. But, if there is no absolute space, it will be no way to define which system is accelerated. The two objects should be relative to be accelerated if no absolute space existed. The fact is that we really feel the accelerate force if we take the trip. So that, the only possible answer is that the absolute reference should be the absolute space. The theory of relativity is wrong in this point.

15. Length Paradox

Suppose that an experimenter takes a pole of 9 m long at 80% of the speed of light relatively to a box of 6 m long. Knowing about the length contraction according to the Lorentz contraction by special relativity, the experimenter proposes that the pole can certainly fit the box when it pass through the box for a while, as the following calculation:

For the pole, original length l_0=9 *m,* v=0.8 *c.* For the pole's length l when it moves at v, according to Lorentz contraction [equation (6)]:

$$l = l_0 \Big/ \gamma = \sqrt{1 - v^2 / c^2}\, l_0 =$$

$$9 \times \sqrt{1 - (0.8c)^2 / c^2} = 9 \times \sqrt{1 - 0.64} = 5.4 \text{ (m)}.$$

As 5.4<6, the pole certainly can fit the box when the pole passes through the box for a while.

For the box, it also moves at the speed of 0.8 *c* toward the pole (relative moving). According to the Lorentz contraction either, it is impossible for the box to fit the pole at any instant as the box is too small to the pole, as the following calculation:

For the box, original length l_0'=6 *m,* v'=0.8 *c*. For the box's length *l'* when it moves at *v'*:

$$l' = l_0' / \gamma = \sqrt{1 - v'^2/c^2}\, l_0' =$$

$$6 \times \sqrt{1 - (0.8c)^2/c^2} = 6 \times \sqrt{1 - 0.64} = 3.6 \text{ (m)}.$$

As 3.6<6, the box certainly cannot fit the pole when the box passes through the pole.

For the same event, it is impossible for the pole to fit the box but for the box cannot fit the pole. So that we can get the conclusion that the length cannot contract from the ontological angle and the Lorentz contraction by special relativity is wrong at this point. From ontological point, the length (space) as an objective existence has the absolute meaning and the Lorentz contraction is at the epistemological level.

16. Probability Paradox (Oppugn the Second Law of Thermodynamics)

The first law of thermodynamics is stated as "the energy of the universe is fixed", or "the energy is a function of state", i.e., there is no net energy change in any cyclic process: $\oint dE=0$. The second law of thermodynamics could be formulated in four different ways: (1) Heat cannot flow from a colder body to a hotter one automatically; (2) Entropy must increase; (3) No cyclic process can convert heat entirely to work; (4) In any cyclic process the heat *Q* transferred to the system from its surroundings at the temperature T must obey an inequality: $\oint dQ/T<0$ (Hoover, 1999).

The second law of thermodynamics is a statistical result (Savitt, 1990; Uffink, 2001). As an example: take ten billion red liquid particles and ten billion white liquid particles, and arbitrarily mix all the particles in a container. Suppose that there is no interaction between any two of the particles. After a certain time, there is almost no possibility that all the red particles are in a half of the box and all the white particles are in the other half part of the box. It cannot separate the red and white particles without outside energy input. This suppose is depended on all the red particles are same and all the white particles are same, but the red ones and white ones are different. This distinguishability comes from the human eye as we see some particles are red and others are white. The true story is that all the particles are really different. There are twenty billion particles that can be numbered from one to twenty billion. The concept of entropy is an epistemological concept rather than ontological concept. The basic ground for the thermodynamics is to consume that the matter particles are divided into groups with human's idea, but not the nature itself. According to thermodynamics, the particles belonging to the same group are the same, and those belonging to different category are different. But, the true fact for the nature is that all the particles are different. Any two particles in the universe are different. Even one particle is not the same ones when it is at any two different times. There is no reason to say that the difference between any of two same color particles is smaller than the difference between any of two particles with different color. We say that red particle A is more similar to red particle B than white particle A, and this is depended on the human's intuition. It is certainly possible that red particle A is less similar to red particle B than white particle A. The key point is that we must know that any true existent distribution of the twenty billion particles has the same possibility to appear as the distribution of all red ones are in one half of the container and the all white ones are in the other half of the container.

As a metaphor, let's think about this dilemma: A 20-year-old guy is charged with killing another guy with a knife by cutting the victim's neck publicly. Many people really saw this event and went to court as witnesses. But, the attorney of the killer says in the court: "The cut location was on the 16.5555555555 cm from the top of the victim's head with the 1.3333333333 cm deep and 3.3333333333 cm wide. According to the statistical calculation, it needs about 10^{20} times to make one time cut of this. If my client made the cut one time per second, it needs at least 20 million years to get this cut done ($60\times60\times24\times1000000=8.64\times10^{10}$). My client is only 20 years old. How could my client do this within his 20 years even if he cut with all his time? This against the second law of thermodynamics and the principle of statistics." Even plenty evidence and witnesses are there to prove this killing, how is the judger going to make the judgment if he respects the statistical theory and the second law of thermodynamics and the science?

The fact is that the basic statistical principles and the second law of thermodynamics are useful tools in human practice, but they are not the true natural existence.

17. Uncertainty Principle

The famous Heisenberg's uncertainty principle states: The more precisely the position (of a subatomic particle) is determined, the less precisely the momentum is known in this instant, and vice versa. According to this argument by the German physicist Werner Heisenberg, we cannot make any measurements on a system of atomic entities without affecting the system. The more precise our measurements, the more we disturb the system. Furthermore, the measured and disturbed quantities come in pairs, the more precisely we determine one half of the pair, and the more we

disturb the other. In other words, the more certain we are about the value of one, the more uncertain we are about the value of the other. This is the essence of the uncertainty principle. Mathematically, it says that the product of the uncertainties of these pairs has a lower limit equal to Planck's constant. For example, the pair of variables that is connected by the uncertainty principle is energy and time: $\Delta E \Delta t > h$ (E is energy, t is time and h is Planck's constant) (Kirkpatrick, 1995). From the description we can see that the uncertainty principle is a mathematical results even with observed supports.

The uncertainty principle is a measurable principle, not an existent principle. It is the epistemological principle rather than the ontological principle. Not to say if it is right or wrong, this uncertainty principle is depended on the ability of human brain and muscle to determine the position and momentum of an object. But, it does not say anything if the position and momentum certainty existing in the same time or not. Even the measurement is principle important for technology and maybe also for science, the real essence of the world is its existence, rather than its measurability. The existence is 0 and 1. This means that all in the natural world only have two conditions: existence and non-existence. It is not the natural fact that a physical object can exist in the probability x: $0<x<1$. It must be: $x=0$ or $x=1$. The uncertainty principle does not show the real world.

18. Three-dimensional Time

Suppose that a signal travels in the three-dimensional space with velocity v at any direction that represented by the variable distance s. The distance s to reach any particular point in the three-dimensional space will be the summation of x, y, and z:

$$S^2=x^2+y^2+z^2 \qquad (7)$$

$$vt=s \qquad (8)$$

Substituting the above:

$$v^2t^2= x^2+y^2+z^2$$

$$t^2=(x^2+y^2+z^2)/v^2$$

$$t^2=(x^2/v^2)+(y^2/v^2)+(z^2/v^2)$$

$$t^2_x= x^2/v^2$$

$$t^2_y= y^2/v^2$$

$$t^2_z=z^2/v^2$$

$$t^2= t^2_x+t^2_y+t^2_z \qquad (9)$$

From equation (9) we can see that the time of a signal to travel in the three-dimensional space is three dimensions either. The nature of time could be three dimensions according to the above mathematical calculation. This three-dimensional time concept is obtained from the mathematical calculation rather than the ontological existence. Mathematical results are at the epistemological level. If any mathematical result is in conflict with the possible existence, I persist that the possible existence is true.

19. The Measurement of Time

The modern idea of time is the fourth dimension of the space. We measure the length, width and depth of an object in order to define its place in space, and we now recognize the importance of its fixed position at the time of the measurement.

Three systems of time measurements are in use: (1) universal time (Greenwich Mean Time) – derived from the rotation of the earth on its axis; (2) ephemeris time – derived from the revolution of the earth around the sun; (3) atomic time – derived from the operation of the atomic clocks. Universal time is the mean solar time of the prime meridian on which the city of Greenwich of England is located. The universal time is the basis for the standard time used for the reckoning of civil time. Ephemeris time is the time scale of dynamical astronomy that is used for the precise study of the motion of celestial bodies. Atomic time is the time measurements of the time interval related to the physical phenomena. The time measurement tools are normally called clocks.

There are many kinds of clocks in the human history, such as water clock, sand clock, glass clock, pendulum clock, quartz-crystal clock, atomic clock, etc. The typical method to measure time is the pendulum. A given pendulum completes a certain fixed number of oscillations while the earth rotates once on its axis relative to the stars. A simple pendulum whose length is one meter, for example, always completes 43,047 oscillations while the earth rotates once on its axis (Markowitz, 1988).

The most discussions on time measurement by the relativity are clock. The clock is a man-made tool to measure the time. This is an epistemological concept.

20. Absolute Time and Space

Both the relativity and quantum mechanics are thinking about how to measure the time with a clock and how to measure the space with a ruler. They are at the epistemological (or empiricism) level. To reveal the essence of nature, we need to discuss the time and space from the ontology, or naturalism point. From the ontology angle, the key point is not about how to make the accurate measurements, but how to understand the real nature existence.

If there is no absolute space existing, all the movements including the accelerative movement are relative. But, we really feel the accelerative movements if we take an accelerative carriage and we do not need any moving or static reference to feel this acceleration. How can we feel the acceleration as our experience if there is no absolute reference system to be referenced? Considering the earth or a big star as the reference system is really objective. The light pathway can be curved, but it is the light's pathway is curved, rather than the space is curved. There is no reason to say that

the light ray must travel on a specific surface of a space. We can assume that the phenomenon of light ray curved is the light passes through the continuous surfaces of absolute space when the gravitational force influences the light, rather than the space is curved by the gravitation (Figure 6). Even we agree with the concepts of time dilation and Lorentz contraction, we still should consider them as a linguistic question, rather than the scientific tenet. For the body in an inertial system, the moving is relative. If we do not give a reference, we cannot verify its motion. But, for the accelerated motion, it does not need to define a reference. How do we know the absolute acceleration without an absolute reference? The only possibility is that there is an absolute reference – the absolute space. The size of space can be measured small under a specific physical condition such as an moving object, but the space itself cannot be changed by human observation. The real space is absolute!

Time is a strange being. It is everywhere and is always running. In all literatures, sciences and mythologies time always goes in one direction-forward. According to the relativity time can be zero or stand still at the speed of light. But time never vanishes. It is the current belief that time can be removed and introduced into the universe thereby showing that total universal time is constant. This is a weird concept. People can see the time arrow goes in one direction in the macro-world, but never see it goes vice versa. In the micro-world, according to the quantum calculation, scientists get the two-way time arrow objectively. Why? The reason is that the intelligence of human brain cannot feel the true existence of the micro-world running. This is the science tricking brain. The clocks can run slower under a specific physical condition such as an object moving, but the time cannot elapse slower by human's measurements. Time is the natural existence phenomenon. Nobody can make the time dilate or shrink by his/her measuring activity. The real time is absolute!

21. Timeless World

I have discussed the nature of time and space partly from the epistemological angle depended on the common scientific notions. Now, let's think about the timeless world concept from the ontological angle.

For the past, where is it now? For the future, where does it stay? These questions have been asked in the whole history of human society (Hawking, 1988, 2002). I am convinced of the timeless world naturally. In my view, everything in the universe will never change. Time and motion are nothing more than illusions. In the universe, every moment of every individual's life - birth, death, and anything in between - exists forever. Everyone is eternal. That means each and every one of us is immortal. The universe has neither past nor future. All the things in the past, present, and future exist forever. The concepts of past, present and future are depended on the human brain. The total universal time is constant. It is a matter of experimentally proven fact that this seemingly universal flow of time does not exist. Lapses of time, as they are measured by the recurrence of periodic events, are not impervious to everything but rather depend upon the relative motion of the two systems whose periodicities are being compared and the positions of the systems are in a gravitational field.

A ship with over-light speed can catch the image of the past events. This happens only because the light goes out but not because there is the real past time. This is just like what we see a movie tape with the reversed direction. The fact is that everything exists already and forever. We see that there are past and future because we are living in our time arrow. This is the absolute time. The key question for us is how to testify that the past still exists and the future has existed already.

22. Determinism

Classic Newtonian mechanics and the newer quantum mechanics have been sources of many debates about the role of cause and effect in the natural world. With Newton's law of motion came the idea that specifying the position and momentum of a particle and the forces acting on it allowed the calculation of its future motion (Roberts, 2003). Everything is determined. It was like that the universe is an enormous machine. Since the universe has been made of existence condition, its future is predetermined. This idea is known as the Newton's mechanical determinism. This notion must also be extended to living organisms. Newton's mechanical determinism has been criticized by the relativity and the quantum theories.

Even though humans could not determine the positions and momenta of all the objects at a specific time, according to the Heisenberg's uncertainty principle, and there are limitations of the abilities for the human intelligence to know the future of the world, the nature knows the future. The future is predetermined by nature. All things in the future are real existence in the future according to the timeless world tenet, no matter we can pre-know or not. For natural existence fact, we must say that the "determinism (predetermine)" is true, not the "prophetism (precognition)" is true. Everything of the world in future is there – somewhere in future, no matter whether we do know the detail or not.

Time, space, memory and mind are related. To talk about this I want to mention the old Zen parable of the three Buddhist monks who were arguing about a waving flag. The first monk said that the flag was moving, not the wind. The second monk said that the wind was moving, not the flag. Then the third monk smiled and said: "It is neither the wind nor the flag that is moving - it is your minds". This provided a hint for the nature of

our knowledge. The principles and theories we created, such as the relativity, the uncertainty principle, the second law of thermodynamics and the probability theory, etc., all are the moving of our mind. Maybe we will never know the complete functions and future of the universe with our limited ability. But the nature does know. The natural determinism is the natural existence that is not depended on our knowledge or our abilities.

23. Discussions and Conclusions

A lot of discussions on the topics of nature of time and space have been made and the relativity and the quantum theories were challenged (Butterfield, 2003; Hawking, 2001; Hoover, 2003; Morriston, 1999; Myrvold, 2003).

Motion is everywhere in the universe. In one second, a human heartbeat takes place and the earth moves about 30 km around the sun, and a beam of light travels 300,000 km (7 times around our earth). In addition, the earth rotates on its axis at almost 1,600 km and revolves around the sun at approx 100,000 km per hour. This entire solar system is moving toward the star Vega at about 19 km per second and our Milky Way galaxy is traveling toward the Great Andromeda galaxy at about 80 km per second.

Space is defined by saying where a thing may come to be or has been. It is the separator of objects. Time is a similar separator of chronological events (when things have been or may come to be). The whole universe is an entity connected by the space-time field. The whole universe is one thing.

There are two aspects for the concept of time and space: One is the measured time and space (subjective, epistemology), and the other is the physical time and space (objective, ontology, physical entity). As the space expands, it is no reason to say that the space expands or the ruler shrinks, neither to say that time dilates or contracts. The only accepted natural fact is that we get the message of something sometimes getting bigger (so called expanding or dilating) and sometimes becoming smaller (so called shrinking or contacting).

To describe the universe on the largest scale, Einstein weaved time and space together into the very fabric of the universe. As a result in the general relativity, there is no invisible framework, no clock ticking outside the universe against which to measure events. How could there be? Time and space joined together cause weird consequences: Space and time curve around stars and other massive bodies and make light bend away from straight-line paths. Does time seem to slow down or even come to a full stop near the black holes? The concepts on these topics by modern science are at the idealist point.

The mistakes of the relativity are to consider that all the existence is relative but the light/light speed is absolute. Light is only a form of electromagnetic radiation existing in the universe with the wave and particle properties. From this point, as any other forms of the existence, light cannot be the standard to judge the nature of time and space. All the existences in the universe are existing, including all the energy, matter, moving, space, time, etc. The existence is absolute, no matter someone observing/measuring it or not. After Albert Einstein died on April 18, 1955, the universe still exists absolutely. The existence is not depended on whether Heisenberg could measure it precisely or not.

We have no way to ontologically recognize all the past, present, or future existence. The contemporary intelligent people could monitor the instantaneous state of the processing of inputs by the brain. However, what perceived has been delayed in the perceiving process because in the course of this perceiving procedure, a finite amount of time is taken to encode and process the inputs. The processed information is transferred to a tape called memory, which is often modified in the process of accessing. From epistemology, we consider that the future is modifiable by intervention in real time, while the past is not. The human brain, by a process of participation, transforms visual inputs in the form of light waves into the objective reality. We see the world through our eyes and we think about the world with our brain cells (Brown, 1998). Light rays are the bridge from the body to the spirit through the tunnel of the mind. Furthermore, we can also feel the real world and measure the world with our skin, nose, tongue, hand, etc. All the physical parts of our body can be used to feel and measure the world. So, making the light as the absolute reference is totally wrong. We trust our observations but we know that the world we observe is the observed world, and sometimes it is not the real existed world. Even we must depend on our observations, but we should think about what it really is (Rose, 1998).

According to the big bang theory, time began with the big bang, an explosion of a singularity (Earman, 1999). The theory is very vague on the how, when, where, and why of that singularity. Was it located in space? If so, space has no beginning and space must be absolute. Some scientists consider the big bang to be a rapid expansion of space. If space can expand, then it is in motion, and thus it cannot be a dimension that defines motion. If we say the beginning of the universe, we need to ask "beginning of what?" According to the modern cosmology, the concept of time has no meaning before the beginning of the universe. It did not exist then. So that we can see that the modern cosmological concept on the time and space is wrong. Linear time is based on a historical perspective of events that rush ahead, one following the other, in a straight line. The passage of light is an event. Events occur in time and space. Time and space measure the when and where of

events. Light passes through space during a time span. It is not the passage of light through space creates time.

Ontologically, the time and space can neither contract nor expand. If we really want to say that time and space can contract or expand, we must create other words to define the concepts of those kinds of "time" and "space", rather than the time and space we have defined already. The modern physics and cosmology, such as the relativity and the quantum theory, are defining the contraction/expansion of time/space with the linguistic tricks, rather than the scientific philosophy.

Contemporary astrophysics says that it has significant evidence revealing that the universe is open (expanding only, not oscillating). When this conclusion is combined with other types of cosmological observations, it would seem that the universe originated at a singularity (an absolute temporal boundary) approximately 15 billion years ago. This intends to give conclusions about a causative power outside of space-time asymmetry (i.e., a Creator), and the nature of space-time and causality (Spitzer, 2001).

If we say that the universe is finite, we must ask and answer what is the outside of the universe. Although this is an ancient question, it is still the question that nobody can answer reasonably. "Nothing" is not the satisfied answer to the outside of the universe of the finite model.

Although the quantum information theory that combines physics, computer science and information theory has succeeded in harnessing the special features of the sub-atomic world to devise fast algorithms, to decipher unbreakable codes, and to teleport quantum states (Hagar, 2003), and this gives quantum theory new features, the quantum theory still conflicts with the real physical existence.

Correspondence to:
Hongbao Ma
B326 Clinical Center
Department of Medicine
Michigan State University
East Lansing, MI 48824, USA
Telephone: 517-432-0623 (O); 517-355-7880 (H)
Email: hongbao@msu.edu

References

Al-Khalili J. Black holes wormholes & time machines. Institute of Physics Publishing, Bristol, United Kingdom. 2003:78-107.

Barbour J. The End of Time – The next revolution of physics. Oxford University Press. New York City, New York. 2000:11-3.

Brown JW. Foundations of cognitive metaphysics. Process Studies 1998;27(1-2):79-92.

Butterfield J, Isham C. Spacetime and the philosophical challenge of quantum gravity, in Physics Meets Philosophy at the Planck Scale: Contemporary Theories, in Quantum Gravity, Callender C (ed), Cambridge University Press, Cambridge, Britain. 2001:33-89.

Callender C. Philosophy of space-time physics, in The Blackwell Guide to the Philosophy of Science, Machamer P (ed), Blackwell Press, Cambridge, Britain. 2002:173-98.

Delsemme A. Our cosmic origin: From the big bang to the emergence of life and intelligence. Cambridge University Press. Cambridge, United Kingdom. 1998:28-37.

Dowe P. The coincidences of time travel. Philosophy of Science. 2003;70(3):574-89.

Earman J, Eisenstaedt J. Einstein and singularities. Studies in History and Philosophy of Modern Physics. 1999;30B(2):185-235.

Folger T. From here to eternity- Imagine a universe with no past or future, where time is an illusion and everyone is immortal. Discover 2000;21(12):54-61.

Hagar A. A Philosopher looks at quantum information theory. Philosophy of Science 2003;70(4):752-75.

Hawking SW. A brief history of time: from the big bang to black holes. Bantam Books, New York, NY, USA. 1988:16-25.

Hawking SW, Penrose R. The nature of space and time. Princeton University Press. Princeton, NJ, USA. 1996:3-36.

Hawking SW, Penrose R. The nature of space and time. International-Studies-in-Philosophy 2001;33(4):126-7.

Hawking SW, Thorne KS, Novikov I, Ferris T, Lightman A. The future of spacetime. W. W. Norton & Company, Inc., New York, NY, USA. 2002:57-62.

Hoover KD. Nonstationary time series, cointegration, and the principle of the common cause. The British Journal for the Philosophy of Science 2003;54(4):527-51.

Hoover WG. Time reversibility, computer simulation, and chaos. World Scientific Publishing Co. Pte. Ltd. River Edge, NJ, USA. 1999:41-2.

Hyperdictionary. http://www.hyperdictionary.com/dictionary/time. 2003.

Kirkpatrick LD, Wheeler GF. Physics. Saunders College Publishing. New York, NY, USA. 1995:274-83.

Kogut JB. Introduction to relativity. Harcourt/Academic Press. Burlington, MA, USA. 2001:12-20.

Lidsey JE. The big bang. Cambridge University Press. Cambridge, United Kingdom. 2000:55-65.

Markowitz W. Time. In Collier's Encyclopedia. Macmillan Educational Company. New York, NY, USA. 1988;22:318-25.

Monk NAM. Conceptions of space-time: Problems and possible solutions. Studies in History and Philosophy of Modern Physics. 1997;28B(1):1-34.

Morriston W. Must the past have a beginning? Philo1999;2(1):5-19.

Myrvold WC. Relativistic quantum becoming. The British Journal for the Philosophy of Science 2003;54(3):475-500.

New Webster's Dictionary, Weston, FL, USA. 2003:161,173.

Peskin ME, Schroeder DV. An introduction to quantum field theory. Addison-Wesley Publishing Company. New York, NY, USA. 1995:781-800.

Pickover CA. Time: A traveler's guide. Oxford University Press. New York, NY, USA. 1998:25-33.

Roberts JT. Leibniz on force and absolute motion. Philosophy of Science 2003;70(3):553-73.

Rose S. Lifelines. Oxford University Press. New York City, New York. 1998:136-41.

Savitt SF. Epistemological time asymmetry. Proceedings of the Biennial Meetings of the Philosophy of Science Association 1990;317-24.

Spitzer RJ. Indications of creation in contemporary astrophysics. Ultimate Reality and Meaning. 2001;24(3):209-54.

Uffink J. Bluff your way in the second law of thermodynamics. Studies in History and Philosophy of Modern Physics. 2001;32B(3): 305-94.

Webster's New Universal Unabridged Dictionary. Barnes & Noble Publishing, Inc. New York, NY, USA. 2003:1827,1984.

Zeh HD. The physical basis of the direction of time. Springer-Verlag. New York, NY, USA. 1992:8-11.

Empirical Study of Capital Structure on Agency Costs in Chinese Listed Firms

Hongxia Li*, Liming Cui**

* School of Management, Harbin University of Science and Technology, Harbin, Heilongjiang 150080, China; ** Aston Business School, Aston University, Birmingham, B4 7ET, UK.
lhx_2002@hotmail.com, Liming_cui@hotmail.com.

Abstract: This study examines the impact of capital structure on agency costs in 211 non-financial Chinese listed firms for the period 1999-2001. There are two main findings. (1) Firms with high debt to asset ratio have high ratio of annual sales to total assets and high ratio of return-on-equity. If a firm has a high debt to asset ratio, creditors are much more concerned about the payment of interest and repayment of principal and will have incentives to monitor the firm. Thus, a capital structure with high debt decreases agency costs. (2) Positive and significant correlation is identified between ownership concentration and the return-on-equity ratio. This is because the largest shareholders have a strong interest in firm performance and therefore a high ability to reduce agency costs. Our empirical results further illustrate that firms have inclination of refinancing through stock market and harm small shareholders' interest. [Nature and Science 2003;1(1):12-20].

Keywords: capital structure; agency costs; corporate governance

1. Introduction

The Chinese stock market was established in the early 1990s. By listing on the stock exchange, state-owned enterprises (SOEs) have improved their debt to asset ratio, and promoted their development by directly financing from the stock market. After 10 years' development, there are more than 1200 listed firms on the two stock exchanges now. The total market capitalisation at the end of March 2001 was RMB (Chinese dollar) 5 trillion, 54% of the last year's GDP. This shows that listed firms play a significant role in the national economy. On the other hand, China still has much to do on reform in corporate governance[1]. For historical reasons, the majority of China's listed firms were restructured and transformed from previous state-owned enterprises or other government controlled entities[2] and there are many problems left with the governance structure. The central problem with the governance structure is the ambiguous definition of the controlling power of the state shares. This led to the false placement of state property. "Inside control" problem is serious[3]. Secondly, state shares are uniquely big and there is serious impingement upon the interests of small shareholders. Thirdly, the board of directors is formed mainly by executive directors and controlling shareholders, directors lack integrity obligations, failing to perform their duties industriously[4]. Additionally, there is not much pressure of dividend from shareholders, so re-financing of listed firms usually place the order of debt after additional or right shares. By pecking order pattern of financing observed in advanced country corporations, firms obtain capital by making greater use of internal finance followed by debt and turning to stock market finance only as a last resort. Jensen's (1986) free cash flow theory considers debt can mitigate the agency problems between shareholders and managers of firms and motivate management to act in the interests of the shareholders. How would their financing patterns differ from those of advanced country firms? How to decide the best strategy of refinancing?

There has been much research conducted concerning the agency problem in developed markets. There are three general ways in which to reduce the conflicts of interest between managers and the shareholders: 1) Increasing management ownership because high management ownership aligns the interests of management and shareholders (Jensen, 1993; Ang,

The financial support provided by the Heilongjiang Province Natural Science Fund G01-10.

[1] In its narrowest sense, corporate governance is about the relationship of the owners or shareholders of a firm with its manager (Iskander and Chamlou, 2000), which is often characterized by economists as the "agency problem".

[2] About 75% of listed firms are formerly state-owned. Another 10% are firms that mostly had significant shares held by SOEs. Only less than 10% of listed firms are formerly private-owned firms or foreign-invested firms, which in most cases had SOEs as their joint venture partners. See the website of China Securities Regulatory Commission: www.csrc.gov.cn

[3] The "inside control" viewpoint was aired in 1995 by Japanese scholar Masahiko Aoki.

[4] Wu Jinglian, June 8, 2001. The behaviour of control shareholders and corporate governance. Shanghai security news.

1999). 2) Monitoring management by large shareholders (Shleifer, 1986). 3) Using debt financing to discipline managers (Jensen, 1986; Stulz, 1990). The first option is not the focus of this study. This is because the vast majority of China's listed firms are formerly state-owned or state-controlled firms. The management holding of shares is extremely low, about 0.03% of the total shareholding[5], and it is subordinate to controlling shareholders. This situation will not change in the near future. Similarly, the second option is also excluded. The state holds shares of most listed firms in great concentration, listed firms, is not really separated from controlling shareholders in personnel, financial affairs and assets. Due to the complicated market and administrative process associated with the reform of Chinese property system, many constraints were present on reducing agency costs through the first two options. Thus our research concentrated on the third option mentioned: the impact of capital structure on agency costs.

The contribution of this study is two-dimensional. Firstly, it contributes to the literature of the impact of capital structure on agency costs in Chinese listed firms. Plenty of research about Chinese corporate governance has focused mainly on ownership structure, Xu (2000), Zheng (2002), Shi (2000), Zhang (1996), etc. The focus of this research is to study the interrelationship between the capital structure of listed firms and agency costs of equity. Secondly, among the limited research, Yang et al (2001) analyses the interrelationship between the capital structure of listed firms and agency costs. No empirical analysis has been conducted so far. This paper will fill the gap in this area. It provides evidence on firm capital structure and agency costs measured in terms of ratio of sales to total assets and ratio of return on equity. We wish to provide evidence through empirical study as to how would capital structure influence agency costs.

This paper is structured as follows. Section 2 gives previous relevant literature review. Section 3 describes the current status of Chinese corporate governance, section 4 presents the methodology including empirical model and sample. Section 5 gives the empirical results, and section 6 concludes.

2. Literature Review

Agency problems are caused by the separation of ownership from control in large firms (Berle, 1932). Jensen and Meckling (1976) apply agency theory to the modern corporation and formally model the agency costs of external equity[6]. Managers who own anything less than 100% of the residual cash flow rights of the firm have potential conflicts of interest with the outside shareholders, since they choose to reinvest the free cash rather than return it to investors (Jensen, 1976, 1986). The conflict arises when there is moral hazard inside the firm, which is called the agency costs of equity. This agency problem can be solved by increasing management ownership because high management ownership aligns the interests of management and shareholders (Jensen, 1976). Other possibilities include monitoring of management by large shareholders (Shleifer, 1986), and the use of debt financing to discipline managers (Jensen, 1986; Stulz, 1990).

2.1 Managerial Ownership and Agency Costs

Managerial ownership has considered non-linear forms (Morck, 1988; McConnell, 1995; Kole, 1995). Jensen (1993) "convergence of interest" hypothesis suggests that managerial shareholdings help align the interests of shareholders and mangers, and as the proportion of managerial equity ownership increases, so does corporate performance. In contrast, Morck et al (1988) argued that high level of managerial ownership could lead to 'entrenchment', as external shareholders find the actions of such managers difficult. Kole's (1995) argument suggests that managerial ownership may impact large and small firms differently with respect to value. Ang examined the relationship between agency costs and managerial ownership for small firms, and Singh et al tested same work on the relationship for large firms.

2.2 Concentrated Ownership and Agency Costs

An important line of agency costs literature relates to concentrated ownership. Stiglitz (1985) has argued that one of the most important ways of value maximization by firms is through concentrated ownership of the firm's shares. Shome and Singh (1995) replicate this result and provide evidence that the large shareholder's presence improves accounting performance. Large shareholders thus address the agency problem as that they both have a general interest in profit maximisation, and enough control over the assets of the firm to have their interests respected. Many scholars argued that outside large shareholders reduce managerial entrenchment (Shleifer, 1986; Kang, 1995; Yosha, 1996; Porta, 1998, 1999; Park, 1995; Denis, 1996).

However, this does not exclude the possibility of rising concentration of share ownership to depreciate the market value of the firm (Huddat, 1993; Admati, 1994). The control shareholders often have better access to information, hold more power in selecting management and involve in key decision-makings. Especially when the manager holds fewer shares[7] and is subordinate to

[5] The statistics get from: www.csrc.gov.cn.

[6] Jensen and Meckling model the agency costs of debt in this paper. However, for our purposes in this paper, it is the agency costs of equity that are relevant.

[7] Morck, Shleifer, Vishny (1988) showed in their empirical study that the proportion of equity held by

controlling shareholders, control shareholders impinge upon the interests of small shareholders by way of non-division of dividends and diversion of profits. The exploitation of small shareholders by controlling shareholders constitutes ex ante an expropriation threat that reduces managerial initiative and non-contractible investments and may come into conflict with performance-based incentive schemes (Burkart, 1997).

2.3 Debt and Agency Costs

Another strand of the agency literature has focused on the role of debt as a means of disciplining managers. Grosseman and Hart (1982) were the first to argue that managers could pre-commit to work hard by using debt rather than equity. Similarly, Jensen's (1986) free cash flow theory considers additional debt beneficial since the firm attempts to improve the productivity of its assets as a result of additional debt acquired. Debt not only reduces the free cash flow but also provides discipline to management through the debt market. Debt monitoring hypothesis is formalised by Harris and Raviv (1990) and Stulz (1990) and empirically demonstrated by Maloney et al. (1993). Shleifer and Vishny (1997) provided extensive survey about the role for debt in reducing the conflict of interests between managers and shareholders [8]. On the other hand, increased leverage also has costs. As leverage increases, the usual agency costs of debt rise, including bankruptcy cost (Jenson 1986). Myers (1977) pointed to the debt overhang problem where firms may forego good projects if they have significant debt outstanding. The reason is that for a firm facing financial distress, a large part of the returns to a good project go to bondholders. Therefore, in choosing their debt-equity level, firms should trade off between the agency costs of debt and the agency costs of equity. By appropriately allocating refinance between equity and debt, capital structure can balance the conflicts between investors and management as well as that between management and creditors.

Finally, two previous studies most closely related to this study are Ang et al (1999) and Singh (2002). In the first case, Ang et al provided evidence on corporate ownership structure and agency costs measured in terms of asset utilization and operating expenses. Ang used data on small business in America to examine how agency costs vary with a firm's ownership structure. They find agency costs 1) are higher when an outsider rather than an insider manages the firm; 2) are inversely related to the manager's ownership share; 3) increase with the number of non-manager shareholders, and 4) to a lesser extent, are lower with greater monitoring by banks. In the second study, Singh and Davidson extend the work of Ang's analysis of relationship between corporate ownership structure and agency costs to large publicly traded corporations. Using slightly different measures of agency costs[9], they analysed multi-period data for the year 1992 and 1994, and studied not only inside ownership structure as a determinant of agency costs, but also the role of outside large equity holders in disciplining the management. They found outside large shareholders' ownership may only have a limited effect on reducing agency costs and board size was negatively related to asset turnover, and unrelated to discretionary expenditures.

In this paper, following their example we use ratio of sales to assets as one of the measures of agency costs[10]. Additionally, we use ROE as an alternative measure of agency costs to analyse the possible impact of variables on agency costs in Chinese listed firms. Although ROE is a more manipulability measure in economic sense, the regulating authorities in China use this particular ratio as a standard to decide whether a firm is qualified for right shares or additional shares. It is one of the most strictly regulated ratios in China and is widely used for comparative purpose.

3. Chinese Corporate Governance

3.1 Ownership Structure and Corporate Governance

The main characteristic of the Chinese corporate governance is the over concentration of equity structure. Most of the listed firms in China are transformed from state-owned enterprises. Ownership structure displays the phenomenon of the co-existence of control shareholders, who are normally related to the state and many other small and comparatively weak shareholders. State shares are uniquely large. Statistics show that the state holds shares of most listed firms in great concentration. Of the listed companies, 54% of the equities belong to the state or state-owned corporate

managers and the valuation of the firm and proportion is in inverted U-shape.

[8] Several articles model the benefits and costs of debt, the benefit is usually the reduction in the agency cost, such as preventing the manager from investing in negative net present value projects, or forcing him to sell assets that are worth more in alternative use. The main costs of debt is firms may be prevented from undertaking good projects because debt covenants keep them from raising additional funds, or else they may be forced by creditors to liquidate when it is not efficient to do so.

[9] Use the SG & an expense ration instead of operating expenses to measure agency costs.

[10] Singh found the SG&A expense ratio not significantly influenced by ownership. This is because governance variables are not as visibly related to cash flows generated by firms that are sales revenues. We conducted a similar analysis and didn't find any significance relationship either.

persons[11]. Among the 1104 listed firms on Shenzhen and Shanghai stock markets, the proportion of shares of the number one shareholder had reached 45% and the second largest shareholder made up 8%.

The management level lacks long-term incentive and restraining mechanism. The board of directors is mainly formed by control shareholders. The lack of independent directors makes it difficult to display their regulating and balancing roles. Among all the directors of the listed firms, 73.3% have the background of state shares (27.9%) or shares of state-owned corporate persons (45.4%). Since the manager holds fewer shares, and is subordinate to controlling shareholders, the agency problem between shareholders of a firm and its manager has turned into the second dimension of the agency problem in a firm, the conflict between the controlling shareholders and small shareholders.

3.2 Leverage and Corporate Governance

The central goal of corporation, including public listing, is to establish "a modern enterprise system" in China, featuring the corporate governance structure that separates the government from enterprises. Another objective is to raise capital for SOE's and reduce their high level of debt to asset ratio by increasing direct finance through selling equity to the public. The vast majority of China's listed firms are formerly state owned or state controlled firms, mostly large and better performing firms. Before initial public offering, they do their best to dispose of the debt. So, the debt to asset ratio of listed firms is lower during the first couple of years after initial public offering.

According to capital structure theory, the way to refinance is determined by the cost of capital. In developed capital market, the top managers are restrained by shareholders and creditors, facing the pressure of paying dividend and debt. The empirical results show that listed firms obtain capital first from internal sources, then from debt, and last from equity. Capital cost influences the style of financing. In China, due to the special ownership structure of listed firms, state share is absolutely the largest among total shares and the representatives of state shares are usually absent. This reduces the restriction to management, and the managers would over pursue the control right of cash flow. The consequence is that re-financing of listed firms would have partiality for equity rather than debt. Additionally, there is not much pressure of dividend from shareholders, so refinancing of listed firms in China usually place the order of debt after additional or right shares.

The optimal debt-to-equity ratio is the point at which firm value is maximised, the point where the marginal costs of debt just offset the marginal benefits. The over low level of debt to asset ratio reflected the poor management of corporate financial gear of Chinese listed companies. Refinancing through equity is not the optimal strategy to reduce their capital cost. It's not a common phenomenon for a modern corporate to rely almost totally on it's own capital, using none or merely little debt. One of the most important reasons that Chinese listed companies don't bother to use debt is the fact that they generally can obtain "free capital" easily from the equity market. In order to limit the "equity financing thirst", China Security Regulatory Commission requires[12] that the debt to asset ratio of listed firms who want to add shares on stock market must have higher debt to asset ratio than the average level of the same industry (Table 1). Listed firms have paid more attention to their capital structure since then, and it helps to improve the capital structure of listed firms.

4. Data and Methodology

4.1 The Data

The sample was a pool of several data of firms listed on the China (Shanghai and Shenzhen) Stock Exchanges from 1999 to 2001. 211 listed firms[13] were randomly chosen excluding finance and insurance industry, ST (special treatment)[14] and PT (particular transfer)[15] firms were not included in the sample either. The accounting data was obtained from listed firms' annual reports from 1999 to 2001, which were published on the web site (http://www.csrc.gov.cn) of China's Securities Regulatory Commission (CSRC). The inside and outside ownership information and board size

[11] State shares are held by government bodies such as state asset management agencies, or institutions authorised to hold shares on behalf of the state such as a wholly state-owned investment firm. Legal person shares are shares held by any entity or institution with a legal person status, including an SOE or a firm controlled by an SOE.

[12] In Table 1, the debt to asset ratio is the industry average level of listed firms. The industry classification conforms to the first grade industry classification of Chinese Stock Exchange. This policy was announced on March 18th 2001.

[13] There were 1160 listed firms on stock market in the end of 2001. Sample =1160 - (43 ST firms +8 PT firms) * 20% - 11 firms IPO after 1999 =211 firms.

[14] Shanghai Stock Exchange and Shenzhen stock exchange declared emerging abnormal phenomenon from some listed firms' financial statements. Such listed firms' stock was specially treated. The stock is called ST stock. There are 43 ST firms in China's two stock exchanges at the end of 2001.

[15] Listed firms that have continuous 3-year loss are called PT firms. There are 8 PT firms at the end of 2001.

Table 1. Listed Firms Industry Average Debt to Asset Ratio (%)

Industry Classification	(1)	(2)	(3)	(4)	(5)	(6)	(7)	(8)	(9)	(10)	(12)	(11)	(13)
Average Debt to asset ratio	39.2	30.60	47.74	39.93	54.71	36.97	49.21	61.94	91.74	73.65	38.70	42.51	63.38

(1) Agriculture, Forestry, Animal Husbandry and Fishing. (2) Mining. (3) Manufacture. (4) Reduction and Distribution of Electricity, Gas and water.(5) Construction. (6) Transport, Storage and Post. (7) Information transmission, Computer services and software. (8) Whole sale and Retail sale.(9) Finance and Insurance. (10) Real estate. (11) Resident service and other service. (12) Disseminate and Culture. (13) Synthesis. Material source: http://www.bigsun.com.cn/data/agora/20020730/125466.hml.

Table 2. Sample Descriptive Statistics

Variable	1999		2000		2001		Pooled	
	Mean	Median	Mean	Median	Mean	Median	Mean	Median
Assets turnover	0.5335	0.4783	0.5500	0.4591	0.5634	0.4503	0.5575	0.4608
Return on equity ratio %	11.4210	10.4800	9.9839	9.6400	7.2498	7.8200	9.6150	9.5500
Debt to asset ratio %	40.4895	38.5374	39.6272	38.7600	41.4436	41.1300	40.4429	40.0496
Outside block ownership:								
The largest shareholder %	48.7506	49.0200	46.3133	45.5000	46.3500	45.9700	46.6115	47.2100
The five largest shareholders %	61.6255	61.6600	59.2176	60.1000	58.3813	58.9900	59.6540	60.5100
Total sales (RMB 10000)	90894.29	46347.96	116239.10	65616.90	136408.90	73046.00	115986.3	62795.68
Board size	9.6540	9.0000	9.7678	9.0000	9.7915	9.0000	9.7300	9.0000
Managerial ownership %	0.0441	0.0191	0.0316	0.0154	0.0273	0.0116	0.0343	0.0150

The data in this table contain 211 non-financial companies listed on the Stock Exchange of China. Outside block ownership is defined as percentage of total stock held by the largest shareholder and the five largest shareholders. Debt to asset ratio is debt divided by total assets in the end of accounting year. The size of the board of directors measures board size by determining the number of board members. Managerial ownership is the percentage of shares owned by managers.

information were obtained from the web site: http://www.cnlist.com and http://www.cninfo.com.cn.

The sample was a pool of seven ratios of firms listed on the China (Shanghai and Shenzhen) Stock Exchanges from 1999 to 2001 (Table 2). The debt to asset ratio includes data of firms' assets turnover, return on equity, debt to asset ratio, outside block ownership (the percentage of shareholding of the largest and five largest shareholders), firm total sales, board size and managerial ownership.

4.2 Methodology

The methodology we use is a system of simultaneous equations.

The system of two equations to be estimated is:

Agency costs=$\beta_0+\beta_1$capitalstructure$+\beta_2$Conc$+\beta_3$Size $+\beta_4$board$+\sum\beta_j Dum_{jt}$ (1)

Capital structure=$\beta_5+\beta_6$Conc$+\beta_7$ROE$+\beta_8$Val (2)

(Conc – concentration)

We use two alternative measures for agency costs. The first measure for agency costs is the ratio of annual sales to total assets (asset utilization), following the research of Ang et al (1999). This ratio measures management's ability to employ assets efficiently. A high ratio of annual sales to total assets shows a large amount of sales and ultimately cash flows that are generated for a given level of assets. While a high asset turnover may be identified with efficient asset management practices and hence shareholders value creation, a low asset utilisation reflects asset deployment for unproductive purposes. Therefore, higher asset turnover has less agency conflict.

We use an additional measure of agency costs, the ratio of return on equity (ROE), as a measure of profitability. This indicator measures profitability from a different angle. In China, most listed firms were transformed from state owned enterprises. In order to protect the value of state assets, fixed assets depreciation rates are centrally determined and often are artificially low, thus leading to an upward bias in fixed asset estimates. Current assets include some stockpiled goods that either cannot be sold at their book value, or cannot be sold at all. ROE is clearly a more preferable indicator of profitability, matching the common usage of the market economics. Profit is the return to equity holders; therefore higher turn on equity has less agency conflict.

Independent variables were chosen mainly based on the existing agency literature. The first variable used is capital structure, measured by debt to asset ratio (total debt divided by total book assets). The second variable used is ownership concentrations. Ownership concentration is measured by the proportion of the shares held by the largest shareholder to the total shares and the share proportion of the top five largest shareholders. The third categories of variables are control variables. They are included in the regressions to control for other potential influences on the agency costs of firms. The variables included are the size of board of directors, firm size, and industry Dummies.

The number of board members measures the size of the board of directors. The measure of a firm's size is the logarithm of total sales. The industry dummy variable is Chinese listed firms' classified 13 industries, excluding financial firms. This provides 11 industry dummy variables in the multiple regression models.

To solve potential endogenous problems, whether the ratio of return on equity or the debt to asset ratio is simultaneous is tested. On one hand, the debt to asset ratio can affect return on equity. Firstly, an increase in the debt to asset ratio, through financial charges would reduce profit. A high debt-asset ratio, finally, should imply a high degree of external control as creditors, concerned about the payment of interest and the repayment of the principal. Creditors have incentives to monitor the enterprise. A higher degree of supervision could lead to higher profitability. Secondly, by using debt, ROE would increase even though the profit doesn't increase, with a constant equity. On the contrary, obtaining capital through equity would reduce ROE. On the other hand, ROE affect the leverage, with a high level of ROE, listed firms can get funds from newly accumulated profits or from stock market by additional or right shares. The debt to asset ratio may depend not only on ROE but also on the ownership structure. If there is high ownership concentration, the control shareholders might want to reduce the dividend, implying a low debt to asset ratio. However, if the equity value growth is high, the firm can obtain plenty of cash flow, and impact on debt to asset ratio. We use Val to measure the equity value growth. This valuation is used by Leech and Leahy (1991) and is calculated as the market value of the firm at the end of its accounting year, divided by the book value of equity.

Thus, with two equations, one determining agency costs, and the other determining the debt to asset ratio, another exogenous variable is needed in the determination of the debt to asset ratio in order for equation (1) to be identified. This is outside ownership concentration. When agency costs is measured by asset turnover, using only equation (1) would suffice. When agency costs are measured by ROE, the debt to asset ratio is an endogenous variable and two equations are necessary.

5. Empirical Results

Empirical results are presented in Table 3 (Panel A & B) and Table 4. Table 3 presents the OLS regression analysis result that analysed agency costs, measured by asset utilisation and ROE respectively. Panel A gives the result of agency costs measured by asset utilisation and Panel B gives the result of agency costs measured by ROE. Table 4 presents the result of the simultaneous equation of ROE.

5.1 Agency Costs Measured by Ratio of Annual Sales to Total Assets

In panel A of Table 3, dependent variable proxy for agency costs is the ratio of annual sales to total assets. There are three groups of independent variables: capital structure variables, ownership concentration variables and control variables. Rows 1 and 2 report the

Table 3. Multivariate Regression Analysis debt to Asset Ratio and Ownership Concentration to Agency Costs

Panel A: Agency costs as measured by the ratio of annual sales to total assets.

Panel B: agency costs as measured by ratio of return on equity.

Regress -ion	Constant	Debt to asset ratio	Ownership concentration %		Control variables			Adj-R-squared
			The largest shareholder	The five largest shareholders	Board size	Firm Size (log -sales)	Industries	
Panel A:								
Row 1	0.1411	0.0072	0.0026					0.0912
	(2.2505) **	(7.8303)***	(2.9038)***					
Row 2	0.2093	0.0069		0.0012				0.0806
	(2.6118) ***	(7.4990)***		(1.0415)				
Row 3	-1.1820	0.0028	0.0002		-0.0094	0.1718	Yes	0.3986
	(-8.0504)***	(3.4429)***	(0.2773)		(-1.9838)**	(14.4776)***		
Row 4	-1.2294	0.0027		0.0010	-0.0088	0.1716	Yes	0.3995
	(-7.9337)***	(3.3710)***		(0.9863)	(-1.8553)**	(14.8980)***		
Panel B:								
Row 5	5.0937	0.1287	0.0279					0.0684
	(4.0120)***	(6.9215)***	(1.4925)					
Row 6	2.7343	0.1251		0.0626				0.0762
	(1.7017)*	(6.8009)***		(2.7472)***				
Row 7	8.9014	0.1416	0.02619		-0.5538	0.1217	Yes	0.1663
	(2.5744)***	(7.4026)***	(1.3788)		(-4.9447)***	(0.4356)		
Row 8	7.2598	0.1364		0.0377	-0.5447	0.1817		
	(1.9893)**	(7.1781)***		(1.6420)*	(-4.8468)***	(0.6694)	Yes	0.1674

Values in parentheses are t values. *10% level, ** 5% level ***1% level

Equation. (1): Agency costs $=\beta_0+\beta_1$capital structure $+\beta_2$Conc $+\beta_3$ Size $+\beta_4$ Board $+\sum\beta_j$ Dum$_j$

Table 4. Impact of Debt to Asset Ratio on the Ratio of Return on Equity (2SLS results)

Regression	Constant	Debt-to-asset %	Ownership Concentration		Control Variables			Return on Equity %	Equity Market-to-Book Value
			The largest shareholder %	The five largest shareholders%	Board	Firm size (log sale)	Industries		
Eq. (1)									
1999	-29.9728	0.9154		0.0585	-0.0186	0.1813	No		
	(-74.9606)***	(254.1369)***		(22.2788)***	(-1.6130)	(6.7096)***			
2000	-20.9198	0.6317		0.0345	-0.0140	0.3565	Yes		
	(-36.2628)***	(187.1876)***		(9.9195)***	(-0.8665)	(9.0342)***			
2001	-50.1593	0.8332		0.1354	-0.1589	1.5859	Yes		
	(-9.3704)***	(18.7996)***		(4.3807)***	(-1.0291)	(4.3131)***			
pool 1	-25.6625	0.6978	0.1198		-0.0179	0.1859	Yes		
	(114.1235)***	(428.5688)***	(102.6309)***		(-2.6085)***	(11.3209)***			
pool 2	-26.2627	0.6868		0.0895	-0.0385	0.3490			
	(-61.7831)***	(235.0715)***		(35.6543)***	(-3.0672)***	(12.0077)***	Yes		
Eq.(2)									
1999	31.3633			-0.0577				1.0353	0.0795
	(5.3222)***			(-0.6591)				(2.4545)**	(0.2693)
2000	26.1591			-0.06832				1.5447	0.3620
	(3.5698)***			(-0.6374)				(3.6285) ***	(0.8032)
2001	41.1093			-0.2024				0.7980	1.4301
	(6.7670)***			(-1.9635) **				(1.9841)**	(4.0992)***
pool 1	34.7605		-0.1694					1.3532	0.1105
	(12.1722)***		(-3.2660)***					(4.4911)***	(0.5409)
pool 2	34.7928			-0.13278				1.3031	0.2024
	(9.1036)***			(-2.1735)**				(4.4705)***	(1.0390)

Equation. (1): $ROE=\beta_0+\beta_1$ Capital structure $+\beta_2$Conc $+\beta_3$ Size $+\beta_4$ Board $+\sum\beta_j Dum_{jt}$
Equation. (2): Capital structure= $\beta_5+\beta_6$Conc $+\beta_7$ROE $+\beta_8$Val
Values in parentheses are t values. *10% level, ** 5% level *** 1% level

regression result on capital structure together with the largest shareholder concentration and the five largest shareholders' concentration respectively. Rows 3 and 4 report the regression result including the control variables: board size, firm size and industry dummies.

In all of the four rows mentioned above, a positive relationship between agency costs and capital structure was identified, all significant at a better than 1% level. This proves that firms with a higher debt to asset ratio are more efficient in their asset utilization. This result supports Jensen's (1986) theory of free cash flow, which considers additional debt beneficial as the firm attempts to improve the productivity of its assets as a result of additional debt acquired. Such positive relationship between capital structure and asset utilization is also identified by Gorman (2000), Ang (1999) and Singh (2001).

We found mixed result for the largest shareholder concentration, a positive relationship with agency costs displayed in Row 1, while an insignificant relationship was found in Row 3 when regressed with other control variables. For the five largest shareholders' concentration, no significant relationship was identified with agency costs. This proves that control shareholders don't have much interest in improving their asset utilization ratio. This result is found by Signh et al (2001) too, as they report that the proportion of equity held by outside block owners does not relate to agency costs as measured by asset utilization.

Among the control variables, the coefficients for the control variables for board size are negative and significant at 5% in relation to the asset turnover ratio as displayed in both Row 3 and Row 4. This shows that large boards reduce asset utilization and they are detrimental to shareholders' interest. This is because the function and work procedures of board of directors are not standardized. The amounts of shares held by directors are extremely low (Table 1, managerial ownership). Many directors are appointed by the government, and they are not paid by the listed companies, but paid by some government institutes instead. This way they hardly find their own interest align with the company. In the absence of integrity obligation, directors fail to perform their duties industriously to improve the firms' asset utilization. The negligence of large shareholders together with smaller shareholders' lack of supervision incentive, the smaller shareholders would choose to 'vote with feet', which would deteriorate the 'insider control' problem among the management of listed companies. The firm size factor among the control variables shows a positive relationship to asset utilization, significant at 1%. Hence the agency costs would be lower for a larger firm. Large firms have more efficient corporate governance. There are five industries' coefficients significant with asset turnover. They are electricity, transportation, wholesales, real estate and service industry. Except for wholesales, the coefficients of other industries are negatively related to asset turnover.

5.2 Agency Costs Measured by Ratio of Return on Equity

In Panel B of Table 3, dependent variable proxy for agency costs is ROE instead of asset utilization as in

Panel A, with the independent variables identical to that of Panel A. Row 5 and Row 6 report the regression result on capital structure with largest shareholder ownership concentration and five largest ownerships' concentration respectively. Row 7 and Row 8 result including also the control variables: board size, firm size and industry dummies.

As expected, we found a positive relationship between capital structure and ROE, significant at 1% level, confirmed the result in Panel A. Firms with a higher leverage level have a higher return on equity. This conforms to the theory that creditors, concerned with the repayment of the debt, would exert positive influence on the management of the firm and thus improve the firm's profit return. The ownership concentration, however, displayed different result than that of Panel A: they are positive with ROE at 1% and 10% respectively in Row 6 and Row 8. Comparing to the asset utilization result, our ROE result proves that large shareholders concern about their profitability. The highly concentrated ownership would benefit the operation of the business. For the control variables, the board size result is consistent with that of Panel B and showed negative relationship with ROE, both significant at 1%. Firm size displayed positive relationship with ROE, but not significant. The industry dummy variable for the 11 industries doesn't show any significance, except one at a 10% level. Together with the industry result from Panel A, it proves the industry factor doesn't play any significant role in deciding the agency costs.

Since the debt to asset ratio could be an endogenous variable, to solve the potential endogeneity problems we need two equations, one determining the ratio of return on equity, and the other determining the debt to asset ratio. Table 4 reports the two stage least-squares regression results.

For equation (1), both the pooled data result and the result of each individual year show that the debt to asset ratio has positive relationship with the ratio of return on equity at significant better than 1% level. This result supports Jensen's (1986) debt monitoring hypothesis. This is examined by Harris and Raviv (1990) and Stulz (1990) and empirically demonstrated by Maloney et al. (1993) and Gul and Tsui (1998). Highly leveraged firms should be subject to better supervision than those listed firms whose assets are primarily financed through "free" equity that comes with little monitoring.

The result for the largest and the five largest shareholders' concentration is identical to each other. They are both positive to ROE at significant better than 1 percent level in equation (1) in all the results. This finding supports the view that large shareholders play an active role in corporate governance (Shleifer, 1986; Yafeh, 1996; Denis, 1996). However, all the results are negative on debt to asset ratio (equation 2). Although they are only significant at the pooled level, except for year 2001, this shows the large shareholders prefer to refinance through equity than debt. The reason of an increased significance of the third year and for the pooled result is because CSRC requires the average return on equity level over the last three year (from 2001) must be more than 10% to be qualified for additional share. Thus if a firm's return on equity ratio is higher than this level, they like to finance from equity more than debt. This result conforms to Shleifer and Vishny's (1997) theory that large shareholders claim they both have a general interest in profit maximization, and enough control over the assets of the firm to have their interests respected.

Our results also provide new evidence for the second dimension of agency problem: the conflict between large shareholders and small shareholders. Since the boards of directors are mainly constituted by large shareholders in China, the boards' decisions reflect large shareholders' will. The positive relationship between large shareholder and ROE confirmed by our data (Table 4) proves that the large shareholders are very concerned about the agency problem to maximize their own benefits. Higher return on equity would mean more profits for the large shareholders. However, the non-significant positive relationship between larger shareholder and asset utilization found in Table 3 (panel A) illustrated they are not genuinely interested in improving the firm utilization. Again their significant negative relation with debt to asset ratio, their prejudice against using debt the less costly capital, proves that they are sacrificing the smaller shareholders' interest for their own good. Although large investors can be very effective in solving the agency problem, they may also inefficiently refinance the firm through equity while using debt could have maximize the firm value. Driven by their own interest they may also redistribute the wealth of the firm from other small investors. Because small shareholders unlike creditors, they are not promised any payments in return for their financial investment in the firm, and have no claim to specific assets of the firms.

Board size has a negative relation to agency costs, and its coefficient is not significant at each individual year, but significant at a better than 1% level at pooled level. The individual level result is that the large shareholders are motivated to care for the company performance. This somehow counter-effects the negative effects of the overall board members' 'shirking' behavior. However, this kind behavior would reveal itself more clearly through pooled year by members' seeking more discrete ways to enhance their own interest at the firms' cost. Large companies are more efficient in dealing with agency problems. All the results of ROE are positive to the capital structure, significant at either better than 1% or 5%. The equity market-to-book value is not significant.

6. Conclusion

There have been many research conducted concerning agency costs in developed markets, however, not enough attention has been paid to emerging market like China. The contribution of this study is two-dimensional. Firstly, it contributes to the literature of the impact of capital structure on agency cost in Chinese stock market. Secondly, among the limited research concerning capital structure, Yang et al (2002) analyses the interrelationship between the capital structure of listed firms and agency costs in a descriptive way. However, no empirical analysis has been conducted so far. This paper provides statistical evidence on firm capital structure and agency costs measured in terms of ratio of sales to total assets and ratio of return on equity.

The forces working on firms' capital structure in other countries also work in a quite similar way in China. The results indicate that firms with a higher debt to asset ratio have a higher ratio of sales to assets and a higher ratio of return on equity, and this relationship is statistically significant at better than 1 percent level. Capital structure theories suppose that managers make financing decisions so as to maximize value of equity for shareholders. This finding is supportive of the theory put forth by Williams (1987) that additional debt decreases agency costs and the theory by Jensen (1986) that debt can reduce the agency costs of free cash flow by reducing the cash flow available for spending at the discretion of managers. The ownership structure also affects capital structure. Firms with higher Ownership Concentration tend to have lower debt to asset ratio. Why do Chinese listed firms have such a low leverage? One possible reason is that Chinese firms prefer and have access to equity financing once they go public as most firms enjoy a favorable high stock price.

Our results also support Shleifer and Vishny's (1997) statement is that large shareholders claim that they both have a general interest in profit maximization, and enough control over the assets of the firm to have their interests respected. However, we also find that large shareholders are mostly concerned about their personal benefits, thus failing to improve the asset turnover. The absolute control of listed firms' large shareholders makes it difficult for small shareholders to vote against the board's decision. This results in firms' inclination of refinancing through stock market and it harms the small shareholders' interest.

Correspondence to: Hongxia Li
School of Management, Harbin University of Science and Technology
Harbin, Heilongjiang 150080, China
Telephone: 01186-451-664-2515
Cellular phone: 01186-13030027575
E-mail: **lhx_2002@hotmail.com**

References

Ang J, Cole R, Lin J. Agency costs and ownership structure. Journal of Finance 1999;55:81-106.

Berle A, Means G. The modern corporation and private property. New York: MacMillan. 1932.

Denis DK. Twenty-five years of corporate governance research and counting. Review of Financial Economics 2001;10:191-212.

Fama E, Jensen M. Agency problems and residual claims. Journal of Law and Economics 1983;26:327-49.

Filbech G, Gorman RF. Capital structure and asset utilization: the case of resource intensive industries. Resources Policy 2000;26:211-8.

Glen J, Lee K, Singh A. Competition, corporate governance and financing of corporate growth in emerging markets. Working paper/Accounting and Finance Discussion paper, RePEc: cam: camafp:00af46.http://www.econ.cam.ac.uk/dae/repec/cam/pdf/afp46.pdf.

Hart O. Firms contracts and financial structure. Oxford University Press, London. 1995.

Hirota S. Are corporate financing decisions different in Japan? An empirical study on capital structure. Journal of Japanese and International Economies 1999;13:201-29.

Holz CA. The impact of liability-asset on profitability in China's industrial state-owned enterprises. China Economic Review 2002;13:1-26.

Jensen M, Meckling W. Theory of the firm: Managerial behaviour, agency costs and ownership structure. Journal of Financial Economics 1976;3:305-60.

Jensen M. Agency costs of free cash flow, corporate finance, and takeovers. American Economic Review 1986;76:323-9.

Jorge A, Chan-Lau. The impact of corporate governance structures on the agency costs of debt. IMF Working Paper WP/01/204.

Kevin HS. Managerial ownership and performance of firms: Evidence from the UK. Journal of Corporate Finance 1999;5:79-101.

La Porta R, Lopeze-de-Silanes F, Sheifer A. Corporate ownership around the world. Journal of Finance 1999;54:471-517.

Laura M Cha. The future of China's capital market and the role of corporate governance. Luncheon speech at China business summit. www.csrc.gov.cn/csrcsite/enews/efi20010427.htm.

Lu T, Wang W. Corporate governance reform: China and World. Economic Management Publishing House, Beijing. 2002.Page 42-58

Maug E. Board of directors and capital structure: Alternative forms of corporate restructuring. Journal of Corporate Finance 1997;3:113-39.

Shleifer A, Vishny R. A survey of corporate governance. The Journal of Finance 1997;52:737-83.

Singh M, Wallace ND. Agency costs, ownership structure and corporate governance mechanisms. Journal of Banking & Finance 2003;27(5);793-816.

Sun Y, Huang Z. Ownership structure & efficiency of listed companies in Chinese listed companies, Economic Research 1999;12.

Tam OK. Ethical issues in the evolution of corporate governance in China. Journal of Business Ethics 2002;37:303-20.

Wang X, Xu LC, Zhu T. Is public listing a way out for state-owned enterprises? The case of China. Working paper series No 200111. http://www.ncer.tsinghua.edu.cn/research/paper/PaperContext.asp?yearID=2001

Yupana. W. An empirical study on the determinants of the capital structure of Thai firms. Pacific-basin Finance Journal 1999;7:371-403.

Xu X, Wang Y. Ownership structure and corporate governance in Chinese stock companies. China Economic Review 2000;10:75-98.

Yan Y. An analysis of question between capital structure and agency costs in Chinese listed firms. Accounting research 2001;9 (www.e521.com).

Yishay Y, Yosha O. Large shareholders and banks: Who monitors and how? Manuscript, Hebrew University, Jerusalem, Israel, 1996.

Zhang W. Ownership corporate governance and the agency relationship. Economic research 1996;9.
http://www.jjxj.com.cn/news_detail.asp?keyno=189

Zheng J. Agency conflict, equity value and path dependence in reducing state-hold shares. Conference paper: corporate governance reform: China and World, www.iwep.org.cn/cccg.

Pore-filled Membranes Capable of Selective Negative Rejections

Wayne Jiang*, Ronald F. Childs*, Alicja M. Mika*, James M. Dickson**

* Department of Chemistry and ** Department of Chemical Engineering, McMaster University, Hamilton, Ontario L8S 4M1 Canada, wenyi@chemistry.mcmaster.ca

Abstract: Pore-filled cation-exchange membranes containing poly(styrene-sulfonic acid) have been evaluated in pressure-driven separation of inorganic salts. The membranes are capable of separating single and mixed solutes at low pressures (low fluxes). The separation performance is affected significantly by salt concentration and concentration ratio of mixed salts. The observation of negative separation of counterions particularly at low operating pressures is unique. This type of separation may allow the selective removal of multivalent couterions and their replacement by monovalent couterions. [Nature and Science 2003;1(1):21-26].

Key words: pore-filled membranes; pore-filling; ion-exchange; polyelectrolyte; negative rejection; nanofiltration

Introduction

The phenomenon of negative rejection, a process in which a solute is found to be more concentrated in the permeate than in the feed in pressure driven membrane separation processes is possible but not normally observed, equation 1.

$$\text{Rejction}\,(\%) = \frac{C_f - C_p}{C_f} \times 100\% \qquad (1)$$

where C_f and C_p are the concentrations of the solute in the feed and permeate, respectively. There are a limited number of reports of the phenomenon in the literature (Mika, 1995; Hoffer, 1968; Hayashita, 1983). The negative rejections of acids (Mika, 1995) has been observed experimentally in membrane nanofiltration processes and calculated negative rejections of anions (Hoffer, 1967) or anion complexes (Hayashita, 1983) have been reported in multi-anion systems in reverse osmosis. The membranes used were collodion membranes, which have little practical significance in modern water treatment. The early work of Hoffer and Kedem (1968) briefly reported the experimental finding of negative cation rejection using a negatively charged membrane. Recently, Nielsen and Jonsson (1994) have reported modelling studies of negative rejections in multi-anionic solutions. We are not aware of modelling and experimental studies of negative cation rejections.

The work described here makes use of negative cation rejection, which has been found with pore-filled cation-exchange membranes. The "Pore-filling" concept was developed by Childs and coworkers (Mika, 1995). This concept is illustrated in Figure 1. The pores of substrate membranes are filled with a wide range of polymers followed by functionalization of the incorporated polymers. These stable, robust membranes with new functionality have shown exceptional performance in desalination, organic substance removal, and gas separation. Patent protection has been sought for this type of membrane and its uses by Childs and coworkers (Mika, 1999; Rilling, 1999; Komkova, 2003). These include specifically the preparation of the membranes, the use of membranes for ultra-low pressure water softening and gas separation device. The present work adds a new dimension to the already pore-filled membranes.

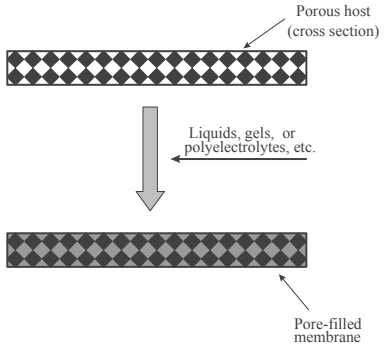

Figure 1. Pore-filling Concept. Functionality such as polyelectrolyte or hydrogel is incorporated into the pores of the substrate membrane to form a stable, robust, and high performance membrane.

Experiments

Material

The membranes used in this work were cation-exchange membranes containing poly(styrene-divinylbenzene sulfonic acid)-filled in a polyethylene membrane. The substrate membrane fabricated by the 3M Company was a polyethylene microfiltration membrane and its properties are listed in Table 1. The preparation and characterization of pore-filled ion-exchange membranes have been described in elsewhere (Jiang 1999, 2003). Inorganic reagents used, NaOH, NaCl, HCl, $MgCl_2$, and Na_2SO_4 (Aldrich), were all AR grades. Pure water used in this study was RO permeate water that was further deionized and carbon filtered. The pH of feed solutions in this work was adjusted to be neutral using NaOH and

HCl.

Table 1. Properties of Substrate Membrane

Material	Polyethylene
3M Product ID	PE-1 #533-10
Thickness (μm)	45 [a]
Porosity (%)	78 [a]
Pore size [a] (μm)	0.19
Water permeability (kg/m^{2}kPa)	1.45 [b]

[a.] Data provided by 3M.
[b.] Measured at 100 kPa (*14.3 p.s.i.*)

Pressure-driven Measurement

The pressure-driven system used in this study was a 6-cell nanofiltration/reverse osmosis (NF/RO) testing system (Mehdizadeh, 1990). The system consisted of an 8-liter feed tank and was running continuously. The effective membrane area was 15.08 cm^2. The flow rate of the feed solution was controlled at 1.00±0.05 L/min throughout the experiments. The temperature of the NF/RO system was controlled between 22 and 26°C and the results of fluxes were corrected to 25°C. The rejection of inorganic solutes or ionic species were calculated by the following equation 1. The flux was calculated from the following equation:

$$\text{Flux (kg/m}^2\text{s)} = \frac{\alpha_T \, m}{\tau \, A_m} \qquad (2)$$

where m was the mass of permeate collected over the time τ, A_m was the active membrane area, and α_T was the temperature correction factor calculated by the following empirical equation (Sourirajan, 1970):

$$\alpha_T = -0.575 \ln T + 2.85 \qquad (3)$$

where T was the temperature in Celsius (°C).

Results and Discussion

Our previous work (Jiang, 2003) reported fabrication and characterization of pore-filled cation-exchange membranes containing poly(styrene-sulfonic acid). Thus, a typical pore-filled membrane was selected for this study and its properties are list in Table 2. The experiments were carried out by using pure water, single solute (NaCl or $MgCl_2$), mixed solute (NaCl and $MgCl_2$), and tap water as the feed. Both the feed and permeate were collected and the concentrations of the solutes were measured. The experimental error in salt concentration measurement was less than 2.5% (Jiang, 1999).

Table 2. Properties of the Pore-filled Membrane Used in the NF/RO System

Degree of crosslinking	2.5%
Mass of polystyrene incorporated	83%
Thickness (μm, wet)	67 [a]
Ion-exchange capacity (eq/g)	1.92 [a]
Water content (%)	67 [a]
Water permeability (kg/m^{2}kPa)	0.66 [a]

[a.] Reference (Jiang, 2003)

Single Solute System

The rejection and flux results for single solute system are given in Figure 2. The solution flux, for single salt,

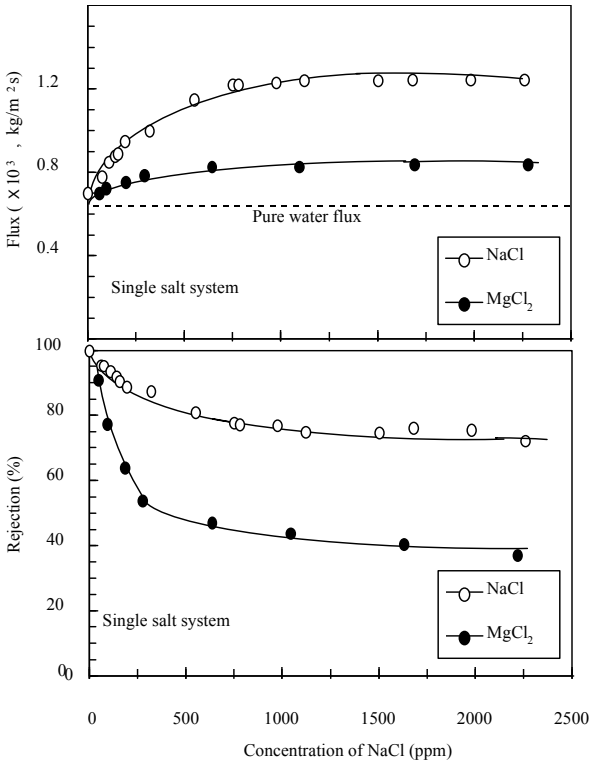

Figure 2. Rejection and flux as a function of concentration for single solutes; single salt systems were NaCl and $MgCl_2$; 2000 kPa pressure at 25°C.

is greater than the pure water flux (the dotted curve). As can be seen, a significant increase in flux was observed between 0 and approximately 500 ppm but the flux did not change dramatically in a wide concentration rage, i.e., from approximately 500 to 2500 ppm. The solution flux decreases with increasing valency of the counter-ion. This is not often seen for RO/NF thin film composite membranes. The confirmation of the crosslinked polyelectrolyte gels of the pore-filled membrane strongly depends upon ionic strength of the contacting solution and the nature of the salt. For example, besides higher effect of charge screening than the monovalent counter-ions (Na^+), the bivalent counter-ions (Mg^{2+}) in the membrane interact with two fixed charges, resulting in "ionic crosslinking". This kind of "ionic crosslinking" may lead to a decrease in pore size. Hence, the flux of single $MgCl_2$ is expected to be lower than that of single NaCl. Another effect (steric effect) may add to the ionic crosslinking effect. Another

possible explanation is that the ion size of the hydrated, bivalent Mg^{2+} is larger than that of Na^{+}. Thus, a hydrated bivalent Mg^{2+} ion is more difficult to go through pores of the membrane than a monovalent Na^{+} ion.

It is known that usually Donnan exclusion, size exclusion, and the requirement of charge neutrality all contribute to the mechanism of the salt rejection in nanofiltration/reverse osmosis processes. From Donnan exclusion considerations, the co-ions dominate the rejection of salts. However, size exclusion is of minor importance for these pore-filled membranes as evidenced by the reported low rejections of sucrose. Strathmann and co-workers (Peeters, 1998) pointed out that the permeation of ions through charged membranes in nanofiltration processes depended primarily on the Donnan exclusion but the size effect also played an important role. For single salts, the rejection was observed to decrease with increasing valency of the counter-ion. Similar to the concentration effect presented in previous work (Jiang, 1999), bivalent ions (Mg^{2+}), compared to monovalent ions (Na^{+}), provides higher shielding to the fixed negative charges on the membrane and make it easier for co-ions (Cl^{-}) to pass through the membrane. As a result, the rejection of Mg^{2+} is expected to be lower than that of Na^{+}.

The difference in free solution diffusivity between Na^{+} and Mg^{2+} could be a factor affecting their rejections. The diffusion coefficient is 1.33×10^{-9} m^2/s for Na^{+} and 0.71×10^{-9} m^2/s for Mg^{2+} (Lide, 1996). These numbers are applicable in free solution. The ion diffusivity in a membrane is generally different due to hindrance and electrostatic interactions between the mobile ions and the fixed charges of the membrane. The difference in diffusion coefficient suggests that Na^{+} diffuses faster than Mg^{2+} in dilute solution. However, for the polyelectrolyte highly filled membranes in this work, this effect should be smaller than the Donnan exclusion effect. For example, if the difference in diffusivity were the main effect, the net effect should have led to a lower rejection of single NaCl than single $MgCl_2$. This is not observed in Figure 2.

Mixed solute system

The rejection and flux results for mix solute systems are given in Figure 3. In the mixed salt system, NaCl and $MgCl_2$, with a co-ion in common, the difference in separation performance between Na^{+} and Mg^{2+} is related to the change in valence of the competing cations, i.e., the selectivity of one ion is affected by the presence of the other competing ion (Xu, 1997). The rejection results with mixed solutes stand in marked contrast to the behavior of these membranes with single salts, Figure 2. For the mixed salt solutions containing Na^{+} and Mg^{2+}, the rejection of Na^{+} is lower than that of Mg^{2+}, Figure 3. The permeability of the monovalent ions (Na^{+}) through the cation-exchange membrane is higher than Mg^{2+}. This can be understood in terms of the charge neutrality and Donnan exclusion. Because of the higher interactions between the bivalent ions (Mg^{2+}) and fixed charges, the Donnan exclusion prefers to attract Mg^{2+} into the membrane from solution but to repel co-ions (Cl^{-}). Due to the charge neutrality, the transport of counter-ions through the membrane must be accompanied by co-ions (Cl^{-}). The transport of the bivalent Mg^{2+} requires twice amount of the co-ions (Cl^{-}) than the monovalent Na^{+}. However, the Donnan exclusion restricts the transport of Cl^{-}. Thus, the monovalent counter-ions (Na^{+}) are forced to permeate preferentially comparing to the bivalent counter-ions (Mg^{2+}). Hence, a lower rejection is observed for monovalent Na^{+} than bivalent Mg^{2+} in the mixed salt system.

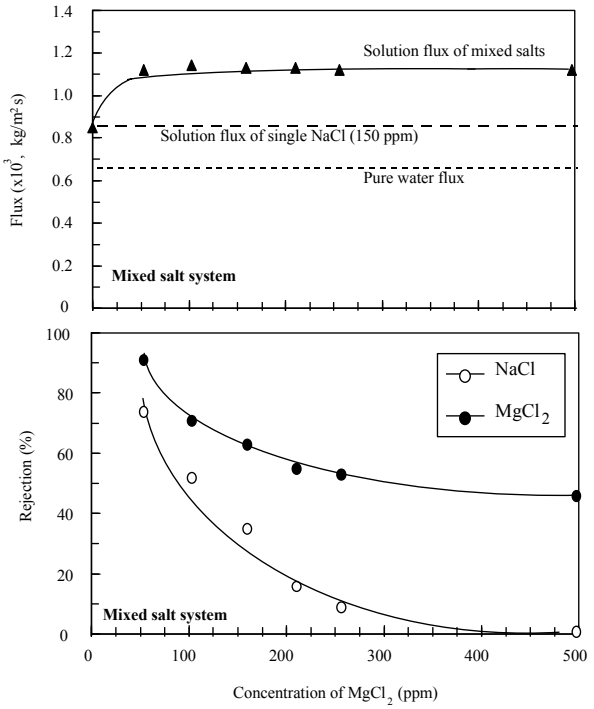

Figure 3. Flux and rejection as a function of concentration of $MgCl_2$ the mixed salt system was NaCl/$MgCl_2$; the concentration of NaCl was kept at 150 ppm; 2000 kPa pressure at 25°C.

Pressure effect

The results of flux and rejection as a function of applied pressure for a mixed solute system are given in Figure 4. The observed relationship of flux *versus* Pressure was not linear through the origin. A linear relationship is common in RO/NF membranes. Similar to the finding of Mika et al. (1995, 1999), who reported the results of pressure effect on separating salts in NF using polyvinylpyridine-filled membranes, a non-linear relationship was observed. The non-linear relationship

is likely due to that the highly swollen crosslinked polyelectrolyte gels are deformable by the ion flow through the membrane. When a solution flows through pores filled with swollen polyelectrolyte gels, the solution penetrates into a certain depth limit of the gel and perturbs the equilibrium. An increase in solution flow forces the polyelectrolyte chains to realign along the flow field. This alignment forces charged neighboring chains closer together resulting in an increase in excluded volume interactions and a lower solution flux (Kim, 1991; Levie, 1996). For example, Levie (1996) used a simplified polyelectrolyte-grafted brush model to developed mathematical equations that were in good agreement with the experimental nanofiltration results obtained by Mika (1995).

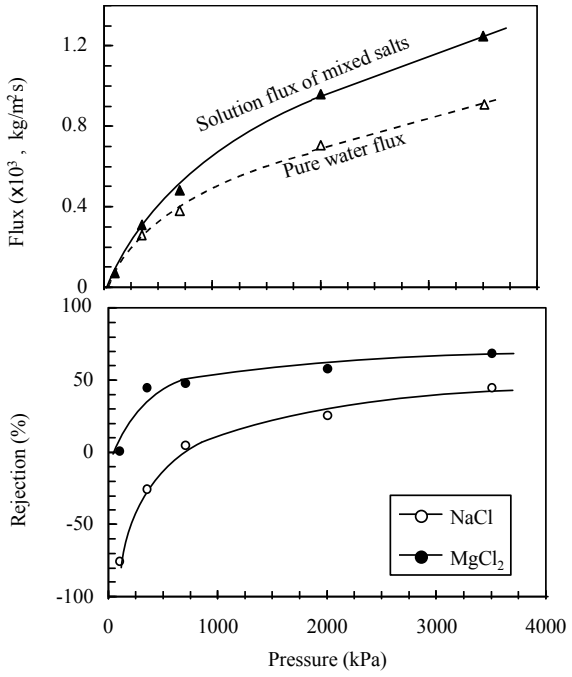

Figure 4. Flux and rejection as a function of pressure for a mixed solute system; the feed contains 110 ppm of NaCl and 55 ppm of $MgCl_2$.

Negative rejection

From Figure 3, the rejection of Na^+ was found to decrease with increasing the concentration ratio of Mg^{2+}/Na^+. Negative rejections of Na^+ were found in the mixed $NaCl/MgCl_2$ system, Figure 4. A negative rejection, calculated by equation 1, means that the ion is more concentrated in the permeate than in the feed. In the literature, negative rejections were observed and various reasonable explanations had been used to understand this phenomenon. Recently, Tsuru (1991) and Bardot (1995) had reported similar findings to the results shown in Figure 2 and Figure 3 for the same system of mixed salts using a sulfonated poly(2,6-dimethylphenylene ether) ion-exchange membrane and using negatively charged, commercial membranes, respectively. Tsuru's explanation was based on partial association of the counter-ion (Mg^{2+}) of the higher valency within the fixed charges in the membrane. Bardot interpreted ion separation by the convective and diffusive fluxes caused by the addition of counter-ions of different mobilities.

In this study, negative cation rejection has been observed with multi-cationic solutions using the pore-filled cation-exchange membranes. For instance, for in the mixed ion system, Figure 3, when the pressure was decreased from 3500 kPa to 100 kPa, the rejection of decreased from 43% to -75% for Na^+. But at the time, the rejection of Mg^{2+} did not go negative, ie., from 70% to nearly 0%. Tap water and a synthetic mixed solute solution containing 2.0×10^{-3} M of NaCl and 1.0×10^{-3} M of $MgCl_2$ were used as the feed with two similar pore-filled cation-exchange membranes prepared previously (Jiang, 1999) under the conditions (350 kPa, 25°C). The results are presented in Table 3. As can be seen, the results obtained from the two pore-filled membranes are consistent. Negative rejections were observed with both tap water and the synthetic solution. For instance, with tap water, the rejection of Na^+ was negative (-29%) while the rejections for Mg^{2+} and Ca^{2+} were positive. Tap water is a complex system and concentration of all ionic species present was not measured. Thus, a simple synthetic mixture ($NaCl/MgCl_2$) was also examined and again the rejection was negative for Na^+ (-25%) and positive for Mg^{2+}. When a single cationic solution was used in the experiments, only positive rejections for the cation were observed irrespective of the charge of the cation due to electroneutrality. The rejection of a monovalent cation (Na^+) could be negative only in the presence of ions with competing ions, such as multi-valent cations (Mg^{2+} or Ca^{2+}). This is good for water softening, eg., Na^+ is concentrated in the permeate while most of hard Mg^{2+} and Ca^{2+} ions are removed. The pressure affected the negative rejection significantly in pressure-driven separation processes. As can be seen in Figure 4, negative rejections of Na^+ were observed when the pressure was low (low flux), ie., at 100 kPa and 350 kPa. This was probably due to the Donnan exclusion and charge neutrality.

Modelling studies are helpful to understand the membrane performances. For example, Nielson et al. (1994) found in their data that computed negative rejections up to 1000% could be obtained at low pressures. The results of the reductions in negative rejections (more negative) obtained from modelling studies seemed to be consistent with the experimental results in this work. However, the model developed by Yaroshchuk (1995) based on irreversible thermodynamics had failed to analyze the transport properties of macroscopically homogeneous gels. Though some mathematical model successfully fitted

the performance of the commercial nanofiltration membranes, these models failed to fit the performance of the pore-filled cation-exchange membranes prepared in this study. Some models could qualitatively but not quantitatively describe the salt rejections as a function of the salt concentrations, based on the data shown in Figures 2, 3 and 4.

Table 3. Rejection of Inorganic Ions Using Pore-filled Cation-exchange Membranes [a]

Ion	Na^+	Mg^{2+}	Ca^{2+}	Cl^-	SO_4^{2-}
			Tap water [b]		
Ion concentration in feed (ppm)	23	7	30	21	30
Rejection (%)	-29	21	23	16	26
			Synthetic solution [c]		
Ion concentration in feed, ppm (*×10³, M*)	42 (*2.0*)	23 (*1.0*)	-	140 (*4.0*)	-
Rejection (%)	-25	45	-	58	-

[a] Pressure = 350 kPa at 25°C.
[b] Membrane #1: ion-exchange capacity = 2.2 meq/g, mass increase = 83%, crosslinking = 2.5%, ion-exchange concentration = 3.3 eq/kg, flux = 0.31×10^{-3} kg/m^{2}s.
[c] Membrane #2: ion-exchange capacity = 1.9 meq/g, mass increase = 80%, crosslinking = 2.5%, ion-exchange concentration = 3.3 eq/kg, flux = 0.33×10^{-3} kg/m^{2}s.

Conclusion

This paper has presented the results of evaluation of pore-filled cation-exchange membranes using a pressure-driven separation process. These membranes were found to be capable of rejecting single and mixed solute systems in pressure-driven processes. The flux and rejection were studied. Negative rejections for counterions were observed in mixed salt solutions in this study. The degree of negative rejection is affected by concentration ratio of the competing mobile ions, primarily depending on membrane ion-exchange concentration (Donnan exclusion). As we have previously shown the new class of pore-filled ion-exchange membranes are unique in that they can function effectively under pressure-driven pressures. The observation of negative separations of counterions is very important in the context of this study. The pore-filled cation-exchange membranes are able to concentrate mono-valent ion and reject bivalent ions. Thus, this allows the treatment of a water stream by removing bi-valent ions, e.g., Ca^{2+} and Mg^{2+}, and replacing them by mono-valent ions, such as Na^+.

The work was supported by the Natural Sciences and Engineering Research Council of Canada (NSERC) and Materials and Manufacturing Ontario (MMO), Canada. The donation of the substrate polyethylene membrane by the 3M Company is gratefully acknowledged.

Corresponding to (Current address):
Wayne Jiang
National Food Safety and Toxicology Center Michigan State University
East Lansing, Michigan 48824-1302, USA
Telephone: 517-432-3100
Fax: 517-432-2310
E-mail: jiangw@cvm.msu.edu

References

Bardot C, Gaubert E, Yaroshuk A. Unusual mutual influence of electrolytes during pressure-driven transport of their mixtures across charged porous membranes. J Membr Sci 1995;103:11-8.

Hoffer E, Kedem O. Hyperfiltration in charged membranes: The fixed charged model. Desalination 1967;2:25-9.

Hoffer E, Kedem O. Negative rejection of acids and separation of ions by hyperfiltration. Desalination 1968;5:167-72.

Hayashita T, Takagi M, Ueno K. Negative rejection of group IB metal cyanide complexes in the hyperfiltration by cellulose acetate membranes. Donnan membrane effect. Sep Sci Tech 1983;18:461-6.

Jiang W. Preparation and characterization of pore-filled cation exchange membranes, Ph.D. Thesis, McMaster University, Hamilton, Ontario (1999).

Jiang W, Childs RF, Mika AM, Dickson JM. Pore-filled cation-exchange membranes containing poly(styrenesulfonic acid) gel, Desalin-ation (In press 2003).

Kim JT, Anderson JL. Diffusion and flow through polymer-lined micropores. Ind Eng Chem Res 1991;30:1008-14.

Komkova EN, Mika AM, Childs RF. Gas separation device, Canadian Patent, CA 2428280 (2003).

Levie CJ. Investigation into the permeation behavior of filled-pore membranes: Modelling the transport of solvent in chemical valve membranes. M. Eng. Thesis, McMaster University, Hamilton, Ontario, Canada (1996).

Lide DR. editor, CRC Handbook of chemistry and physics, 77th edition (1996-1997), CRC Press, Boca Raton, Florida. 1996, Chapter 5, page 98.

Mehdizadeh H. Modelling of transport phenomena in reverse osmosis membranes, Ph. D. Thesis, McMaster
University, Hamilton, Ontario, Canada (1990).

Mika AM, Childs RF, Dickson JM, McCarry BE, Gagnon DR. A new class of polyelectrolyte-filled microfiltration membranes with environmental controlled porosity. J Membr Sci 1995;108:37-56.

Mika AM, Childs RF, Dickson JM. Ultra-low pressure water softening: a new approach too membrane construction. Desalination 1999;121:149.

Mika AM, Childs RF, Dickson JM. Microporous membranes and uses thereof Canadian Patent, CA 2268955 (1999).

Nielsen DW, Jonsson G. Bulk-phase criteria for negative ion rejection in nanofiltration of multicomponent salt solutions. Sep Sci Tech 1994;29(9):1165-82.

Rilling K, Dickson JM, Childs RF, Gagnon DR. Interfacial polymerization in a porous substrate and substrates functionalized with photochemical groups, U.S. Patent 2099727 (1999).

Peeters JMM, Boom JP, Mulder MHV, Strathmann H. Retention measurements of nanofiltration membranes with electrolyte solutions. J Membr Sci 1998;145:199.

Sourirajan S. Reverse Osmosis, Academic Press, New York. 1970.

Tsuru T, Nakao S, Kimura S. Calculation of ion rejection by extended Nernst-Planck equation with charged reverse osmosis membranes for single and mixed electrolyte solutions. J Chem Eng Japan 1991;24(4):511-7.

Xu J, Xing X, Yamamoto S, Tanji Y, Unno H. Effect of ion adsorption on its permeation through nanofiltration membranes. J Chem Eng Japan 1997;30(5):806-12.

Yaroshchuk A. Osmosis and reverse osmosis in fine-porous charged diaphragms and membranes. Adv Colloid Interface Sci 1995;60:1.

Mouse Osteoblast Cell Sensitivity to the AC Magnetic Field at 14 Hz

Hsien-Chiao Teng*, Shen Cherng**

* Department of Electrical Engineering, Chinese Military Academy, Fengsang, Taiwan (HCT), R O C;
** Department of Electrical Engineering, Cheng Shiu University, Niau Sung, Taiwan (SC), R O C,
scteng@cc.cma.edu.tw; cherngs@csu.edu.tw.

Abstract: Since the surface electrical current of the attached mouse osteoblast cell monolayer in a culture plate could induce magnetic fluctuation, power density spectrum of the geomagnetic fluctuation (GF) recorded at the sample rate 2000 times per second illustrated the signal to noise ratio (SNR) spectrum in a frequency interval (0 ~ 60 Hz) for the mouse osteoblast cells system. In contrary to the background, 14±2 Hz was an intrinsic signal within cells. We exposed cells into a constant extremely low frequency (ELF) magnetic field (~ 50 m Gauss) at 14 Hz for 60 minutes, 20% modulation of the gap junction intracellular communication (GJIC) within mouse osteoblast cells was observed from the analysis of Lucifer yellow fluorescence microscopic image while comparing with the control group. Cellular response, GJIC modulation caused by the ELF magnetic field applied through ac function generator and solenoid coil was relied on the resonance within cells at intrinsic frequency. [Nature and Science 2003;1(1):27-31].

Key words: power sensitive spectrum, signal to noise ratio, GJIC

Introduction

The attention of the reaction of ELF magnetic field for biological system has been discussed a lot. Researches have focused on two major concerns for twenty years. The first one is public concern about hazard and health effect. The other one is the scientific interest, which goes further to answer if biological system reacts to ELF magnetic field; even ELF provides less energy than thermal motion (Adair, 1991; 1992; 1994). However, no clinical evidence has shown any human health effect by ELF magnetic field and no mechanism can clearly explain every observed biological effect for the biological system under ELF magnetic field (Takebe, 1999; Adair, 1994; EPRI, 1994). In addition, some experimental observations reported in a laboratory cannot be duplicated in another laboratory. The confliction of the unduplicated experimental observations makes the study of biological effect under ELF magnetic field more difficult. Nevertheless, if ELF magnetic field influences the cell membrane surface electrical current, the form of the reaction of the biological system under ELF magnetic field can be electrical signals. Eugene recognizes deterministic, stochastic, fractal and chaotic signals (Eugene, 2001) as four different type biological signals. A deterministic signal is one whose values in the future can be predicted if enough information about its past is known. Stochastic signals are signals for which it is impossible to predict an exact future value even if one knows it's entire past history. Fractal signals have the property that they look very similar at all levels of magnification, which is referred as scale-invariance. Chaotic signals are deterministic signals with sensitive dependence on some conditions that cannot be predicted exactly in the future. Therefore, we assume the signals from cells induced membrane surface electrical current can affect geomagnetic fluctuation B(t). In addition, we can measure B(t) by using the probe of gauss-meter, transform it to oscilloscope voltage as V(t) and digitally record it at the rate of 2000 times in a second. Mathematically, we write it as follows:

$V(t) = \{ V_1, V_2, \ldots\ldots\ldots V_{N-1}, V_N \}$

Take the autocorrelation coefficients of V(t)

$$R_q = \left(\frac{1}{N}\right)\sum_{p=1}^{N} V_p V_{p+q}$$

Perform the Fourier expansion of R_q

$$S_k = \sum_{q=1}^{N} R_q e^{\frac{i2\pi kq}{N}}$$

S_k is the component at frequency k and the unit of is watt per frequency.

$\omega_k = \frac{2\pi}{N}$ k (fundamental frequencies) for V_p ; $i = \sqrt{-1}$.

If N~ ∞,

$$S(\omega) = \int_{-\infty}^{\div\infty} R(\tau) e^{-i\omega\tau} d\tau \qquad (1)$$

$$R(\tau) = \frac{1}{2\pi}\int_{-\infty}^{+\infty} S(\omega) e^{-i\omega\tau} d\omega \qquad (2)$$

$R(\tau) = \langle V(t+\tau)V(t) \rangle$, τ is the time interval and S(ω) is the average power for V(t). Equations (1) and (2) are the Fourier transform pairs and V(t) is a stationary process which means changing the original point of V(t) will not affect the statistical characteristics. Contrarily, $\int_{-\infty}^{+\infty} S(\omega)d\omega$ is the total energy of the system, the power of the signal can be calculated from power density spectrum and the SNR of the intrinsic signal can be calculated. In this report, we take N=2000 and calculate the SNR spectrum of the mouse osteoblast cells system from 5 to 60 Hz. Relying on surface electrical current distribution induced within cells, ELF magnetic field may cause gap junctional intracellular communication (GJIC) modulation (Hart, 1996). Since GJIC is affiliated with many pathological endpoints (Trosko, 1990, 2001; Upham, 1998), we use GJIC as a factor to evaluate the ELF magnetic field reaction for mouse osteoblast cell system. Scrape loading dye transfer of Lucifer yellow is used to measure gap junction intracellular communication (GJIC) modulation under the exposure of ELF magnetic field. The intrinsic resonance detected in SNR spectrum of the mouse osteoblast cells system is very likely to be a chaotic signal, which is not fully predictable.

Materials and Methods

For the diameter of the culture dish used was 3.5 cm, we used a simple 5-cm radius helical coil, which is wrapped with 200 turns 0.45-mm diameter cooper string around a plastic cylinder tube connected to the function generator for input ELF signals. The whole system was placed in an incubator. The incubator controlled the environment at 5% CO_2 at 98% relative humidity. Another sham field chamber was exactly same as the ELF incubator only with no exposure to the ELF. The cell culture dishes were placed perpendicular to the input ELF. The function generator generated the ELF signal through the solenoid applied to the cells located in the center of the solenoid for sixty minutes.

Cell Culture

Mouse osteoblastic MC3T3-E1 cell line was obtained from: D.T. Yamaguchi, Research Service and Geriatrics Research, Education, and Clinical Center, VAMC, West Los Angeles, California, USA. It was cultured in D-medium (Formula 78-5470EF, GIBCO, Grand Island, NY), supplemented with 5% fetal bovine serum (GIBCO) and 50 µg/ml gentamicin. The cells were incubated at 37˚C in a humidified atmosphere containing 5% CO_2 and 95% air and were fed or split every two to three days. Upon confluency, the osteoblastic cells could be induced to differentiate by the addition of 50 g/ml ascorbic acid alone or ascorbic acid plus 7 mM ß-glycerophosphate (ß-GP) to the medium for 1 month.

Detection SNR of Intrinsic

We used a probe of Gauss-meter to measure the $B_{cigf}(t)$, which is the coupled fluctuation of geomagnetic field and cells induced magnetic fields. The probe was located vertically 10^{-4} meter to the mono-layer of the cells attached at the culture dish. The Gauss-meter was manufactured by F.W. Bell Company (series of 9550) in Florida, USA. Oscilloscope transformed $B_{cigf}(t)$ to electrical voltages as $V_{cigf}(t)$. The oscilloscope was manufactured by Agilent Company (54621A). By using the software also provided by Agilent Company, we collected the digital $V_{cigf}(t)$ from the oscilloscope. In contrast, $V_{gf}(t)$ and $V_{migf}(t)$ were also measured. V_{gf} was only earth magnetic fluctuation and m V_{migf} was the magnetic fluctuation of the medium in culture plate without cells. Matlab and Fortran computer languages were used for power density spectrum analysis. The sample rate was taken 2000 times in a second. The following steps identified intrinsic frequency and its SNR:

Let ω = {1 Hz, 2 Hz, …20 Hz, 21 Hz, 22 Hz……58 Hz, 59 Hz} denote the set of frequency ω_i of the given test signal. Sine(ω_it), simulated by Matlab software, from 1 Hz to 59 Hz, where ω_1 = 1 Hz, ω_2 = 2 Hz, ω_3 = 3 Hz,….. ω_{50} = 50 Hz, …ω_{59} = 59 Hz, respectively.

1. Take the maximum V_{max} from $V_{gf}(t)$
2. Add sine(ω_it) with amplitude V_{max} to $V_{gf}(t)$ and name the result as $V_{gftest}(t)$.
3. Perform autocorrelation and Fourier transform to get the power density spectrum (PDS) of $V_{gftest}(t)$.
4. Calculate the SNR, which can be represented as $S_{max}(\omega_i)$ for each ω_i from PDS of $V_{gftest}(t)$ to get SNR spectrum. Be noted that (a) the power of the signal is defined as the area under the frequency at ω_i, and (b) the power of the noise is defined as the total power of the $V_{gf}(t)$, and (c) the SNR is defined as the power of the signal divided by the power of the noise.
5. Repeat step 2, step 3 and step 4 with the amplitudes 0.7 V_{max}, 0.4 V_{max}, 0.03 V_{max}, respectively for the given test signal at every frequency ω_i to get $S_{0.7}(\omega_i)$, $S_{0.4}(\omega_i)$ and $S_{0.03}(\omega_i)$.
6. Assume $pX^2 + qX + r = 0$, using square curve for fitting data,
   $pS_{0.7}(\omega_i)^2 + q\ S_{0.7}(\omega_i) + r = 0$
   $pS_{0.4}(\omega_i)^2 + q\ S_{0.4}(\omega_i) + r = 0$
   $pS_{0.03}(\omega_i)^2 + q\ S_{0.03}(\omega_i) + r = 0$

Since there are three unknowns p, q and r, with three known equations, we can easily calculate the value of r,

which is the SNR of the intrinsic frequency ω_i at the amplitude of test signal ω_i equals to zero. After we found the intrinsic frequency, we expose cells at intrinsic frequency provided by function generator in the center of solenoid. We used the same steps to calculate the SNR of intrinsic for the observations of $V_{cigf}(t)$ and $V_{migf}(t)$.

Bioassay of GJIC

The scrape load/dye transfer (SL/DT) technique was used to measure GJIC. After exposure to either sham or ELF, the cells were rinsed with phosphate buffered saline (PBS), and a PBS solution containing a small molecular weight fluorescent dye, 4% concentration Lucifer yellow fluorescence dye is injected into the cells by a scrape using a scalpel blade. Afterwards the cells were incubated for 3 min and extra cellular dye was rinsed off and fixed with 5% formalin. We then measured the area of the dye migrated from the scrape line using digital images taken by an epifluorescent microscope and quantitated with Nucleotech image analysis software (Upham, 1998) for the GJIC images.

Results

Figure 1 is the figure of V_{cigf}. Figure 2 has shown the correlation between the SNR and the amplitude of the test signal while fitting curves for V_{cigf}, V_{migf} and V_{gf}. The intercept of the curve was at 0.005, which is the intrinsic SNR value for the test signal at 14 Hz. Therefore, if 14 Hz modulates GJIC, GJIC modulation can work as an index to find the biological effect at intrinsic ELF. We demonstrated the GJIC fluorescent image in Figure 3 and Figure 4. Since the GJIC in cells was quantified with the measurement of the average distance of dye migration, GJIC was reported as a fraction of the control (FOC) in Figure 5. An FOC value equals to 1.0 indicates normal GJIC. The FOC value less than 1.0 indicates inhabitation. All experiments were done at least triplicate and the results were reported as mean ± standard deviation at the 95% confidence interval. When the 14 Hz ELF was applied vertically to the cell, we observed 20% inhibition of the GJIC within cells.

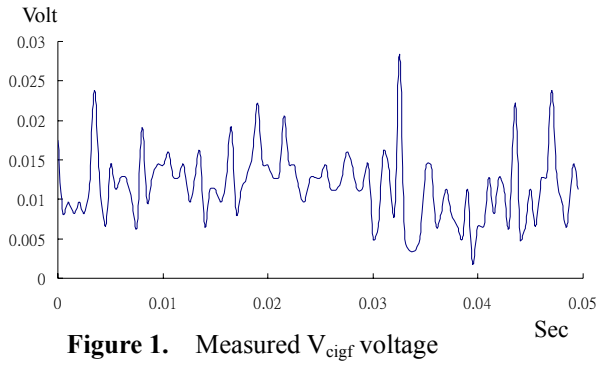

Figure 1. Measured V_{cigf} voltage

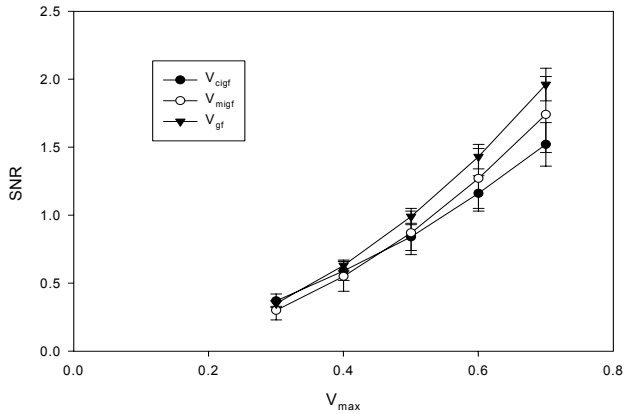

Figure 2. The signal to noise ratio fitting curve of the applied ELF test signal at 14 Hz. The intercept of the fitting curve is at 0.005 for V_{cigf}.

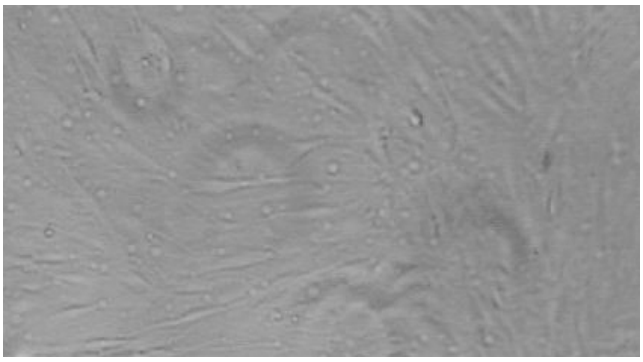

Figure 3a. The monolayer of the mouse osteoblast cells.

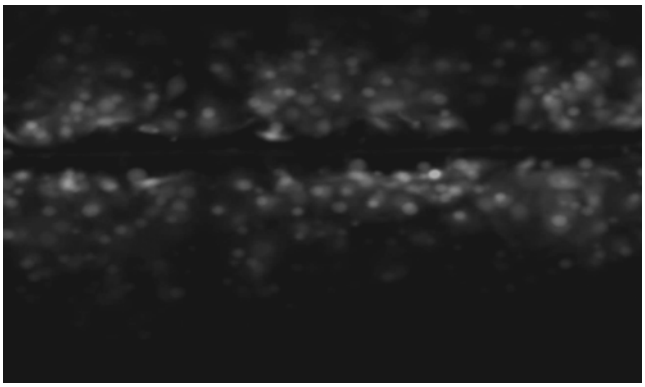

Figure3b. Fluoresce image of the GJIC of the cells in control.

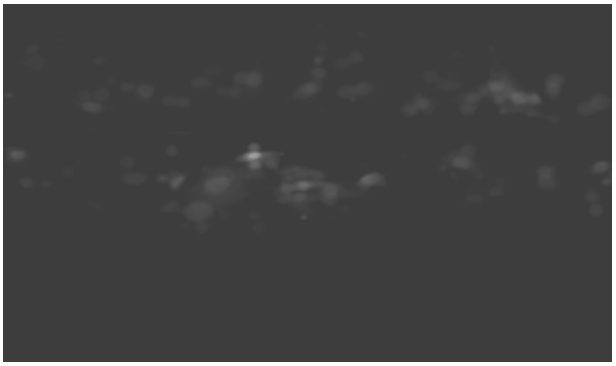

Figure 4. Fluoresce image of the GJIC of the cells under the exposure of 14 Hz ELF magnetic field.

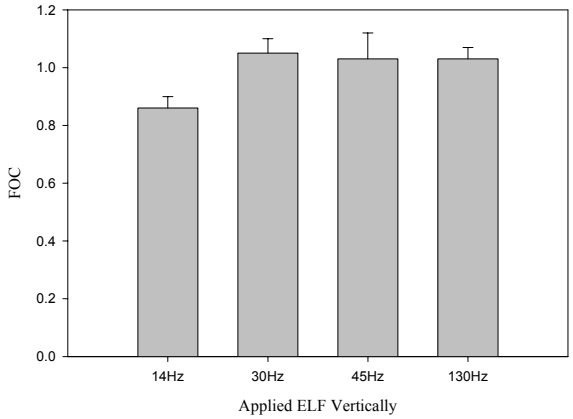

Figure 5. The FOC result of the GJIC Assay at 14 Hz ELF Exposure.

Discussion

The cell-induced current density in a 3.5 cm diameter cultured dish is proportional to the geomagnetic fluctuation, which fluctuates between 20 mGauss and 100 mGauss. The calculated intracellular/intercellular electrical current within a 3.5 cm diameter cell culture dish with confluent cells is about 10^{-9} Amp (Hart, 1996) under geomagnetic fluctuation. This report demonstrates test signals with defined amplitudes for detecting the signals buried in the V_{cigf} (t) and V_{migf} (t) providing evidence that V_{cigf} (t) affected the GJIC within cells. This study therefore, shows the mouse osteoblast cells could be a nonlinear system that can sense ELF signals and the intrinsic ELF signal is about 300 times less than the noise, which is ambiguous to obtain from direct measurement but can be detected by the help of V_{cigf} (t) with GJIC assay. Furthermore, Gap Junctional Intracellular Communication can be a target in which ELF acts on to cause the cell system responded. It is linked PDS to the degree modulation of GJIC within mouse osteoblast cells by using the amount of Lucifer yellow dye transfer area to indicate the modulation of GJIC due to the presence and absence of the ELF. The present results then indicated that the SNR analysis of the ELF signals buried in V_{cigf} can refer to the degree of modulation of GJIC within cells in the culture dish. Particularly, ELF at 14 Hz in cell system might be linked to ion cyclotron resonance (Liboff, 1991) and the calcium oscillation hypothesis (Fewtrell, 1993; Glaser, 1998).

Conclusion

We concluded that the cell induced electrical surface current on mouse osteoblast cells monolayer membrane attached to the cell culture plate under the influence of geomagnetic fluctuation created specific V_{cigf} (t). If we exposed the mouse osteoblast cells into intrinsic ELF at 14 Hz, it would modulate the GJIC within cells. Therefore, ELF 14 Hz is one of the intrinsic frequencies within mouse osteoblast cell system. Even though Adair (1991) criticized the resonance mechanisms, using the ion cyclotron resonance hypothesis, parametric resonance, electromagnetic coupling hypothesis, and the stochastic resonance mechanism may still validated to explain our experimental and calculated results. The major concern for this report, not only was the geomagnetic fluctuation affected cell system, but also we observed that the SNR of the intrinsic frequency, which power was so low as 200 to 300 times less than noise at 14 Hz. Since we exposed intrinsic frequency buried in the V_{cigf} and used the scrape load/dye transfer (SL/DT) technique to obtain the corresponding degree of modulation of GJIC, geomagnetic fluctuation and intrinsic ELF played the roles of adjusting GJIC within cells. Even we still question how cells can find the optimization between the V_{cigf} and the applied ELF signal that we see the GJIC modulation for cell system, we recognize geomagnetic fluctuation affected the intrinsic frequencies within the cells as well.

Correspondence to:
Shen Cherng, P.E., M.D., Ph.D.
Associate Professor
Department of Electrical Engineering
Cheng Shiu University,
840 Cheng Ching Road, Niau Sung
Kaohsiung, Taiwan 833
Email: cherngs@csu.edu.tw; cherng@msu.edu

References

Adair RK. Constraints on biological effects of weak extremely low frequency electromagnetic field. Physical Rev A 1991;43:1039-48.

Adair RK. Criticism of Lednev's mechanism for the influence of weak magnetic fields on biological systems. Bioelctromagneics 1992;13:231-5.

Adair RK. Biological responses to weak 60 Hz electrical and magnetic fields must vary as the square of the field strength. Proc Natl Acad Sci 1994;91:9422-5.

EPRI. Biology and electric and magnetic fields: biological

mechanisms of interaction. Printed by Gradint Corporation, Cambridg, Massachusetts, USA. 1994.

Eugene N. Biomedical signal processing and signal modeling. A Wiley-Interscience Publication, John Wiley & Sons, Inc. New York, NY, USA. ISBN 0-471-34540-7.

Fewtrell C. Calcium oscillation in non-excitable cells. in Ann Rev of Physiology, Editor Hoffman JF, Annual Review, Inc. Palo Alto. 1993;55:427-54.

Glaser R, Michalsky M, Schamek R. Is the Ca^{+2} transport of human erythrocytes influenced by ELF- and MF-electromagnetic fields? Bioelectrochemistry and Bioenergetics, 1998;47:311-8.

Hart F. Cell culture dosimetry for low frequency magnetic fields. Bioelectromagnetics 1996;17:48-57.

Kaiser F. External signals and internal oscillation dynamics: biophysical aspects and modeling approaches for interactions of weak electromagnetic fields at the cellular level. Bioelectrochemistry and Bioenergetics 1996;41:3-18.

Liboff AR, Parkinson WC. Search for ion cyclotron resonance in an Na^{+}- transport system. Bioelectromagnetics, 1991;12:77-83.

Takb H, Shiga T, Kato M, Masada E. Biological and Health effects from exposure to power line frequency electromagnetic fields – confirmation of absence of any effects at environmental field strengths. IOS Press, Ohmsha, ISBN 4-274-90402-4C3047, 1999.

Trosko JE, Chang CC, Madhukar BV. Modulation of intercellular communication during radiation and chemical carcinogenesis. Radiation Research 1990;123:241-51.

Trosko JE, Chang CC. Role of stem cells and gap junctional intercellular communication in human carcinogensis. Radiation Research 2001;155:175-80.

Upham BL, Deocampo ND, Wurl B, Trosko JE. Inhibition of gap junctional intracellular communication by perfluorinated fatty acids is dependent on the chain length of the fluorinated tail. Int J Cancer 1998;78:491-5.

Extraction, Purification and Detection by Liquid Chromatography−Electrospray-Ionization Mass Spectrometry of Tetrahydrofolate Metabolites in *Arabidopsis thaliana*

Zhenzhan Chang, Douglas A. Gage

MSU/NIH Mass spectrometry Facility, Department of Biochemistry and Molecular Biology, Michigan State University, East Lansing, MI 48824, USA, changz@pilot.msu.edu

Abstract: The interconversions of C1-substituted folates form the core of plant one carbon metabolism. An analytical method for extraction, purification and liquid chromatography−electrospray-ionization mass spectrometry detection of low level, labile tetrahydrofolate monoglutamates from *Arabidopsis thaliana* was developed in this study. Under gold fluorescent light, folates were extracted by homogenizing the leaves in extraction buffer and heating the homogenate. A portion of leaf homogenate was incubated with crude preparation of rat plasma conjugase to remove the polyglutamate tails in order to simplify the mixture for analysis. The resulting extract containing the monoglutamyl folates was then applied to an agarose affinity column containing folate binding protein which was purified from milk whey. After elution from the affinity column, the folates were separated and identified by liquid chromatography−electrospray-ionization mass spectrometry on a 150×0.32 mm Symmetry 300 C18 column using isocratic elution with mobile phase (0.1% formic acid/95% acetonitrile, containing 0.1% formic acid, 88:12) at a flow rate of 0.3 µl/min. In positive ion mode, ions representing 5-methyl-tetrahydrofolic acid, 5-formyl-tetrahydrofolic acid and 5,10-methenyl-tetrahydrofolic acid were detected and identified. It is concluded that this folate extraction procedure, combined with folate binding protein affinity column purification is applicable to liquid chromatography−electrospray-ionization mass spectrometry and this method is appropriate for analysis of tetrahydrofolate metabolites in plant leaf tissues. [Nature and Science 2003;1(1):32-36].

Key words: liquid chromatography−electrospray-ionization mass spectrometry; rat plasma conjugase; folate binding protein; affinity column; tetrahydrofolate metabolites; *Arabidopsis thaliana*

1. Introduction

One-carbon (C_1) metabolism is essential to plants. Many C_1 transfers are mediated by the coenzyme tetrahydrofolate (THF). C_1 derivatives of THF are interconverted between different oxidation states, ranging from 10-formyl-tetrahydrofolate (10-HCO-THF) through 5,10-methenyl-tetrahydrofolate (5,10-CH^+-THF) and 5,10-methylene-tetrahydrofolate (5,10-CH_2-THF) to 5-methyl-tetrahydrofolate (5-CH_3-THF). These interconversions of C_1-substituted folates form the core of plant C_1 metabolism (Hanson, 2000). The parent compound, folic acid, is synthesized *de novo* in bacteria and plants, but *id* a dietary requirement in humans and animals. The molecules of THF metabolites consist of pterine ring, para-aminobenzoate that is conjugated to polyglutamyl tails of variable length (typically 5-8) (Konings, 2001).

Analysis of THF metabolites in plant tissues is challenging because of their low level, complexity and general instability (sensitivity to light, oxidation and extremes of pH). We ever employed HPLC method for quantifying the content of THF metabolites in spinach and *Arabidopsis thaliana* by fluorescence detection (Chang, 2003). Our objective in this study is to develop a reliable method for extraction, purification and detection by liquid chromatography−electrospray-ionization mass spectrometry (LC/ESI-MS) of THF metabolites in plant leaf tissues, in preparation for an investigation on folate flux through the metabolic pathway in the C1 metabolism engineered plants (Roje, 1999).

Materials and Methods

Rat plasma conjugase and folate binding protein (FBP) affinity columns were prepared by following the procedure described previously (Chang, 2003).

1. Extraction of Folates from *Arabidopsis* Leaves

The *Arabidopsis thaliana* plants (ecotype Columbia) were grown on soil with 16-h-light/8-h-dark fluorescent illumination at 21°C in growth chamber. Leaves from one month-old plants were collected, covered with foil as 1.0 gram per portion and soaked into liquid Nitrogen. One portion of frozen leaves was homogenized in a mortar containing liquid Nitrogen then transferred into a 15 ml centrifuge tube containing 8 ml extraction buffer (50 mM Hepes-50 mM Ches, containing 2% ascorbic acid and 10 mM 2-mercaptoethanol, pH 7.85). The tube was flushed with N_2 gas then kept in boiling water bath for 10 minutes to inhibit the endogenous enzymes and finally in ice-water bath for 3 minutes. The homogenate was adjusted to pH 7.0 with 4 M HCl before one portion of crude rat plasma conjugase preparation (1.0 ml) was

added. The tube was flushed with N_2 gas and incubated for 4 hours in 37°C water bath. The deconjugation reaction was quenched by keeping the tube in boiling water bath for 5 minutes. After kept in ice-water bath for 3 minutes and centrifuged at 4,800×g, 4°C for 30 minutes, the supernatant was transferred into a clean 15 ml centrifuge tube; The residue was suspended in 2 ml extraction buffer and centrifuged, the supernatant was combined with that previously collected and flushed with N_2 gas.

2. FBP Affinity Chromatography Purification

All FBP affinity purification steps were performed at 4 ° C, the flow rate was controlled as about 0.3 ml/min. FBP Affi-Gel 10 column (covered by foil) was Rinsed with 5 ml 0.1 M potassium phosphate buffer (pH 7.0). Folate extract was applied onto the FBP column for 2~3 rounds. After washing with 5 ml 0.025 M potassium phosphate (pH 7.0) containing 1.0 M NaCl and with 5 ml 0.025 M potassium phosphate (pH 7.0), folates were eluted into 5 mL volumetric flask containing 40 µl 25% ascorbic acid solution, 5 µl 2-mercaptoethanol and 18.4 µl 600g/l KOH with elution buffer (0.02 M trifluoroacetic acid-0.2% sodium ascorbate, pH 2.0). The elute was saved in 1.5 ml dark centrifuge tubes, flushed with N_2 gas.

3. LC/ESI-MS Analysis

LC/ESI-MS analysis of THF metabolites in *Arabidopsis thaliana* was accomplished using the Waters CapLC system (Waters Corp., Milford, MA) coupled to an LCQ DECA quadrupole ion trap mass spectrometer (ThermoFinnigan, San Jose, CA, USA) through the picoview nanospray source (New Objective, Cambridge, MA, USA). The chromatographic conditions were modified as to be compatible with analysis by the electrospray ion trap instrument. A 10 µl aliquot of purified sample solution was injected on a 150×0.32 mm Symmetry 300 C18 column. The folates were then eluted from the column using isocratic program of 88% A and 12% B in 30 min at a flow rate of 3 µl/min. Mobile phase A consisted of 0.1% formic acid while mobile phase B consisted of 0.1% formic acid in a 95:5 acetonitrile/water solution. Diode array detector (DAD) was set at 290 nm. The Picofrit column made electrical contact through a precolumn ZDV titanium union, and terminated in a 15 µm tip i.d. outlet spray needle. The mass spectrometer was operated in positive mode and spray voltage was 2.75 KV.

Results and Discussions

1. Extraction and Purification

Extraction and purification are the key steps for successful analysis of folic acid and THF metabolites from plant tissues. Folates are generally not stable. The chemical reactivity of some folates results in losses of folates during extraction and purification. Oxidative degradation enhanced by O_2, light and heat is responsible for a major part of those losses. This extraction and purification procedure was performed under gold fluorescent light or subdued light. Solutions containing folates were deaerated by flushing with N_2 gas and stored at –80°C in dark tubes. Pfeiffer et al and Vahteristo et al mentioned the superiority of combination of ascorbic acid and 2-mercaptoethanol as antioxidants during the extraction (Pfeiffer, 1997; Vahteristo, 1997). In our study, ascorbic acid and 2-mercaptoethanol were employed as antioxidants in the Hepes/Ches extraction buffer. Dithioerytritol (DTE) or dithiothreitol (DTT) which is usually used as antioxidants in elution buffer (Konings, 2001; Pfeiffer, 1997), was replaced by sodium ascorbate and 2-mercaptoethanol in our analysis.

Different extraction procedures were employed to extract folates from different type of samples (Engelhardt, 1990). Tri-enzyme extraction method (using conjugase, α-Amylase and protease) is the most commonly used method for extraction of folates from food stuff which containing much protein, starch and carbohydrate matrixes (Konings, 2001; Pfeiffer, 1997; Martin, 1990). Konings at al found that for the vegetable extracts, potatoes and meals, no statistically significant increase in folate amounts was observed after addition of protease and amylase (Konings, 2001). Our extraction method was established for analysis of folates from fresh leafy tissues which do not contain much protein and starch matrixes. We applied conjugase only for enzymatic deconjugation of polyglutamates.

Folate extracts which may contain many interfering compounds with identical chemical and/or chromatographic properties have to be purified and/or concentrated. FBP affinity chromatograph was employed in recent years for cleanup and concentration of folate extracts (Konings, 1999, 2001; Pfeiffer, 1997). In our experiment, FBP affinity columns were prepared by following the procedure of Konings (Konings, 1999). The folate binding capacity was determined as 5.4 µg folate /column by adding more and more folic acid spiked with ^{3}H folic acid to one FBP column until the breakthrough point. When FBP affinity columns were used for actual samples, it is critical that the folate content in the sample be not more than 30% of the capacity of the column. Pfeiffer et al and Konings mentioned sample folate loading should not exceed 25% of the capacity because of the low 5-formyl-tetrahydrofolate (5-HCO-THF) recoveries (Pfeiffer, 1997; Konings, 1999). This is important because there is competition among folate species for the folate binding sites. If folate content is more than 30% of the capacity, the less avidly bound species would not be adequately retained, thus the content of those species and the total folate content would be underestimated.

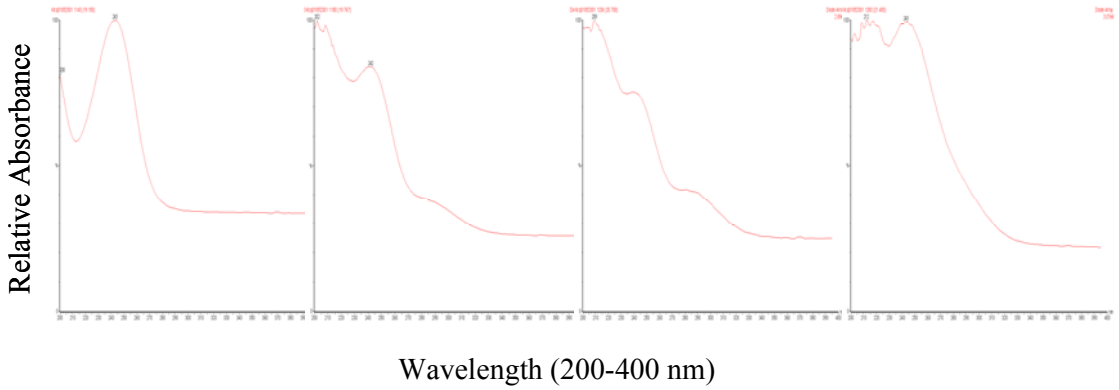

Figure 1. LC/ESI-MS analysis of THF metabolites in *Arabidopsis thaliana* extract. The diode array spectra showing elution of 5- CH_3-THF at 290 nm. The retention time from left to right: 19.15, 19.77, 20.70, 21.48 minute.

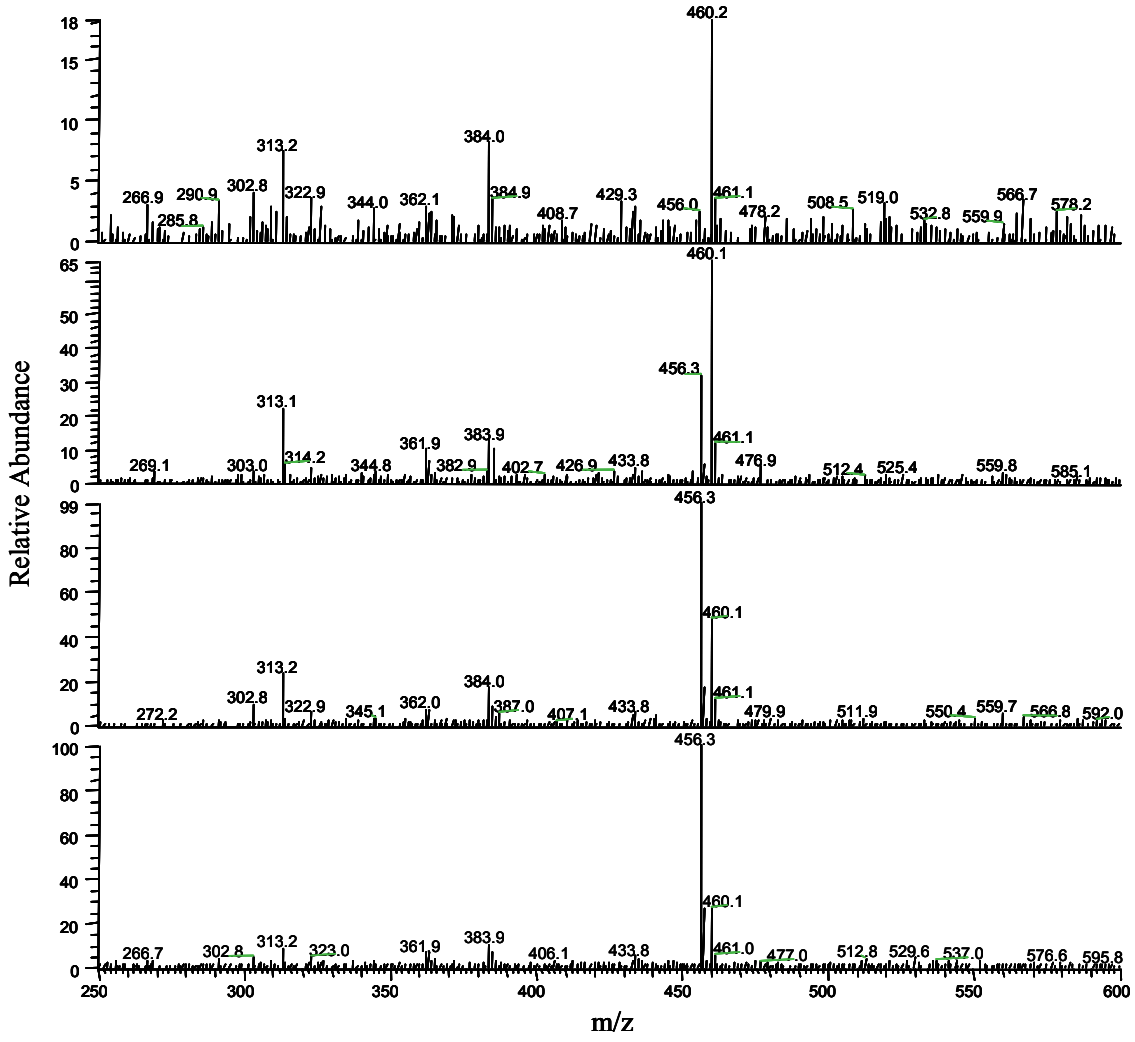

Figure 2. LC/ESI-MS analysis of THF metabolites in *Arabidopsis thaliana* extract. The MS spectra illustrating the sequential detection of 5-CH_3-THF (m/z 460) and 5,10-CH^+-THF (m/z 456). The retention time from top to bottom: 22.10, 22.17, 22.24, 22.32 minute.

Table 1. Maximum Wavelengths (λmax), Retention Time (t_R) on Selected ion Chromatograms, Molar Mass (M), ms (MH^+) for THF Metabolites in *Arabidopsis thaliana* Extract

Folates	λmax (nm)	t_R (min)	M	MH^+ (m/z)
5-CH_3-THF	290	22.17	459.4	460.1
5-HCO-THF	285	25.88	473.5	474.4
5,10-CH^+-THF	352	22.32	456.4	456.3

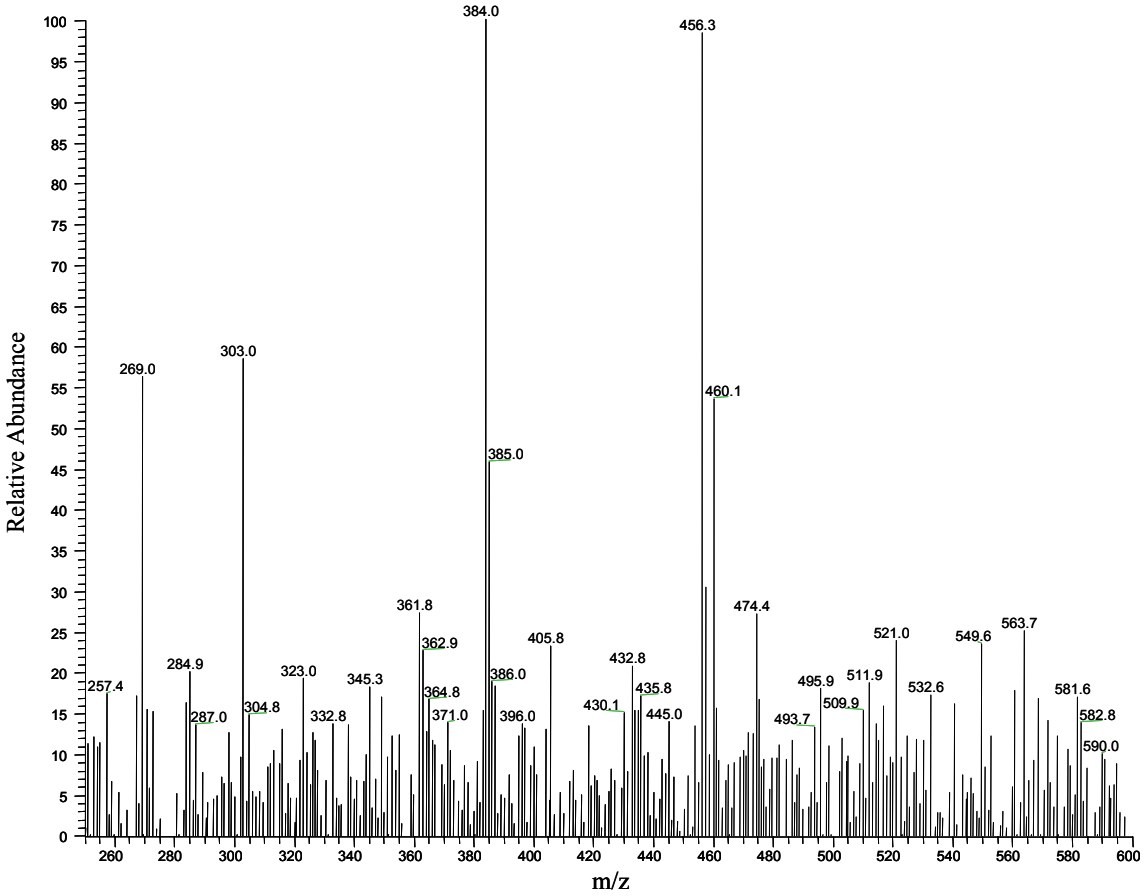

Figure 3. Positive electrospray mass spectrum of THF metabolites from *Arabidopsis thaliana* extract at retention time of 22.58 minute.

2. LC/ESI-MS Analysis

LC/ESI-MS analysis of THF metabolites in *Arabidopsis thaliana* extract was accomplished using 150×0.32 mm Symmetry 300 C18 column, eluted (isocratic program) at a flow rate of 3 µl /min. Figure 1 showed the diode array spectra of elution of 5-CH_3-THF at 290 nm with retention time 19.15, 19.77, 20.70, 21.48 minute, respectively (from left to right). In positive ion mode, ions representing 5-CH_3-THF, 5,10-CH^+-THF and a small amount of 5-HCO-THF were detected (Table 1, Figure 2, Figure 3). Figure 2 illustrated the MS spectra of the sequential detection of 5-CH_3-THF (m/z 460) and 5,10-CH^+-THF (m/z 456) with retention time 22.10, 22.17, 22.24, 22.32 minute, respectively (from top to bottom). The peak at m/z 313 represented the degraded product of folic acid ([M-HOOC-CH_2-CH-CH-COOH]$^+$). Figure 3 showed the positive ion electrospray mass spectrum (mass range: m/z 250~600) of THF metabolites in *Arabidopsis thaliana* extract at retention time of 22.58 minute. m/z 456, 460, 474 represented protonated molecules of 5,10-CH^+-THF, 5-CH_3-THF, 5-CHO-THF, respectively. A variable mixture of cationized species including their sodium adduct (m/z 496, 5-CHO-THF +H+ Na), potassium adducts (m/z 512, 5-CHO-THF + H +K; m/z 494, 5,10-CH^+-THF +K) and sodium-potassium adduct (m/z 521, 5-CH_3-THF+H+Na+K) were also detected.

Conclusion

This paper describes an analytical procedure for the extraction, purification and detection by LC/ESI-MS of THF metabolites in plant leaves. The amount of fresh plant tissues used for folate extraction is as low as 1.0 gram. Liquid chromatography provided separation of folate species using a mobile phase that is compatible with positive ion electrospray mass spectrometric detection. This procedure is suitable for analysis of the naturally occurring THF metabolites in plant tissues. However, it is poorly suited to identification and quantification of 10-HCO-THF and 5,10-CH_2-THF because 10-HCO-THF convertes to 5-HCO-THF during heat treatment (Pfeiffer, 1994), while 5,10-CH_2-THF readily dissociates to THF and formaldehyde at physiological pH even with presence of antioxidants (Horne, 2001). Our experiment results indicate that liquid chromatography directly combined with electrospray-ionization mass spectrometry can be used to selectively separate and detect C_1 metabolism relevant folates (5-CH_3-THF, 5-HCO-THF and 5,10-CH^+-THF) in plant extracts. The combination of folate extraction procedure with FBP affinity chromatography purification and with LC/ESI-MS detection could eventually lead to the development of a quantitative method for selective identification and sensitive quantification of C_1 metabolism relevant folates in plant leaf tissues.

These studies were supported by the National Science Foundation Grant BES 9902875 (to Professor Douglas A. Gage).

Correspondence to:
Zhenzhan Chang, Ph.D.
6195 Biomedcal Physical Sciences Building
Department of Microbiology & Molecular Genetics
Michigan State University
East Lansing, MI 48824, USA
Fax: 517-353-8957

References

Chang Z, Gage DA. J Agric Food Chem 2003; In press.
Engelhardt R, Gregory JF. J Agric Food Chem 1990;38:154-8.
Hanson AD, Gage DA, Shachar-Hill Y. Trends in Plant Sci 2000;5:206-12.
Horne DW. Analytical Biochemistry 2001;297:154-9.
Konings EJM. J AOAC Int 1999;82:119-27.
Konings EJM., Roomans HHS, Dorant E, Goldbohm RA, Saris WHM, van den Brandt PA. Am J Clin Nutr 2001;73:765-66.
Martin JI, Landen WO, Jr Soliman AG, Eitenmiller RR. J Assoc Off Anal Chem. 1990;73:805-8.
Pfeiffer C, Diehl JF, Schwack W, Z Ernarungswiss 1994;33:85-119.
Pfeiffer C, Gogers LM, Gregory JFJ. Agric Food Chem 1997;45(2):407-13.
Roje S, Wang H, NcNeil SD, Raymond RK, Appling DR, Shachar-Hill Y, Bohnert HJ, Hanson ADJ. Biol Chem 1999;274:36089-96.
Vahteristo LT, Ollilainen V, Varo P. Journal of AOAC International 1997;80(2):373-8.

Paulownia serrata - a New Species from China

Dali Fu

Paulownia Research and Development Center, The Chinese Academy of Forestry, Zhengzhou, Henan 450003, China, fudali@pntfrc.com

Abstract: A new species of *Paulownia, Paulownia serrata* D. L. Fu et T. B. Zhao , sp. nov., was described in this paper. The species appears to be similar to *P. kawakamii* Ito, but it has some particular characteristics which can be distinguished with *P. kawakamii* Ito and other species of *Paulownia*. The main distinguishing features are that the margin of leaf is irregularity serrate, the inflorescent conical triplicate-ternate-cymes, the cyme 1~3-flowers generally 1-flower sine peduncles, the flower white, and there are sparse verruciform, cyathiform or acetabuliform glands on leaf, petiole and the inflorescent ramifications. The species was found and collected on April 25, 1999 in Zhuzhou, Hunan Province of China by Da-Li Fu. The holotype is kept at Henan Agricultural University, No. 199904251. [Nature and Science 2003;1(1):37-38].

Key words: *Paulownia*; *P. serrata* D. L. Fu et T. B. Zhao; New species; China

***Paulownia serrata* D. L. Fu et T. B. Zhao, sp. nov.**
Plate I

Species *P. kawakamii* Ito. similis, sed ramulis foliisque juvenilibus et petiolis dense pilis longi-glandulosis et glandulis mastoideis, breviter pilis glandulosis sparse villis rare dendro-pilis. foliis cordatis margine irregulariter serraturis interdum supra medium minute integris undulatis vel integris inter sparse serraturas vel (3~)~5 lati-trianguste lobis, margine dense ciliis longi-glandulosis rare stellato-pilis et villis fortuito longe stipitatii dendrociliis. foliis petiolisque cum rami-inflorescentiis sparse verrucis glandulosis, glandibus cyathiformibus et glandibus acetabuliformibus. inflorescentiis coniciformibus triplicato-ternati-cymis; cymis 1~3-floribus, generaliter 1-flore, sine pedunculis; pedicellis et calycibus floribus extus dense flavo-brunnei-dendro tomentosis. floribus albis minute purpurascentibus, labellis et extus tubis dense minute pubescentibus, densio-pilis glandulosis rare dendro-pilis, tubis in ventralibus 2-plicis longitudinalibus valde elevatis 4~5 mm altis, striis purpureis vel 20~23-striis in interrupte purpureis inter flavidos; calycibus fructibus patelliformibus, lobis planis apice mucronibus inflexis extus glabris.

Arbor decidua, 8 m alta. ramuli grossi pallide brunnei, lenticellis expresse elevatis, juveniles virides dense pili longi-glanduliferi, pili-glanduliferi papillati et breviter pili glandulosis sparse villi et stellato-pili longi-stipitati. Folia cordata vel late triangusti-cordata 8~20 cm longa 10~17 cm lata supra atro-viridia sparse breviter pili glandulosa et pubescentes rare stellato-pila, costis et nervis lateralibus densioris pilis glandulosis, pilis glandulosis papillatis rare pilis et pilis dendro-brevi-stipitatis, subtus viridula densiora pilia, breviter pili-glandulosa et stellato-pila rare dendro-pili brevi-stipitata et villi, costis et nervis lateralibus expresse elevatis dense pilis longe glandulosis, pilis glandulosis, pili-glanduosis papillatis rare villis et verrucis glandulosis, glandulis cyathiformibus et glandulis acetabuliformibus, fortuito dendro-pilis, apice acuminata vel acuta basi cordata margine irregulariter serratura interdum supra medum minute undulati-integra, integra inter sparse serraturas vel (3~)~5 lati-trianguste lobis, dense cilis longe glandulosis rare stellato-pilis et villis fortuito dendro-cilis; petioli 7~14 cm longi viriduli interdum minute pallide purpurascentes dense breviter pilis glandulosis et pilis glandulosis papillatis rare villis glandulosis et dendro-pilis. Inflorescentiae coniciformes triplicato-ternati-cymae; ramuli inflorescenti brunnei glabri, in juvenile pilis et glandulosis cum ramulis juvenilibus; cymis 1~3-floribus, generaliter 1-flore, sine pedunculis. Alabastra ob-ovoidea dense dendro-tomentosa flavo-brunnea apice obtusa basi ob-trianguste conica 5-lobis lobis triangulatis suturis expressis, pedicellis 8~12 mm longis supra medium ampliatis dense tomentosis flavo-brunneis; calycibus ob-trianguste infundibuliformibus basi conicis 5-lobis extus dense flavo-dendro-tomentosis brunneis; flores albi minute purpurascentes, corollis 4.2~5.0 cm longis tubis 2.5~3.0 cm longis diam. ca. 1.5 cm apice 5-lobis fauce diam. 4.0~4.5 cm, labellis ca. longitudinem 1/3 tubi partes aequanlibus, supra 2-labellis semiorbiculatis erectis vel minute posticis margine irregulariter rotundi-serratis dense minute glanduli-cilis et dendro-cilis, tubis labellisque extus dense minute pubescentibus, pilis densioribus glandulosis, intus labellis minute pubescentibus, intus tubis glabris, tubis in ventralibus 2-plicis longitudinalibus valde elevatis 4~5 mm altis, striis purpureis vel 20~23-striis interrupte purpureis inter flavidos; stamina 4 aequilonga antheris flavidis glabris filamentis 1.2~1.5 cm longis basi curvatis sparse breviter pilis glandulosis; ovariis viridulis ovoideis

dense glandibus papillatis, stylis 1.2~1.5 cm longis sparse glandibus papillatis. Capsulae ovoideae 1.5~2.5 cm longae diam. 1.2~1.8 cm, apice acutae apiculis ca. 3 mm longis basi rotundatae cinerei-brunneae; calycibus fructibus patelliformibus 5-lobis planis fortuito reflexis lobis apice mucronibus inflexis extus glabris. Florescentiae Apr., Fructus maturatione Aug.

Hunan: Zhuzhou, 25. 04. 1999. D. L. Fu, No. 199904251(holotype, HNAC); ibidem. 28. 05. 1999. D. L. Fu, No. 199905281.

Plate 1 ***Paulownia serrata*** **D. L. Fu et T. B. Zhao**
1-3. leaf; 4. inflorescent; 5. flower buds, flowers and corolla; 6. ramification of inflorescent; 7. capsules

Influence of the Different NO_3^-/NH_4^+ on mRNA of NR in Sugar Beet

Yue Zhao, Zimin Wei, Fengming Ma

Life Science College, Northeast Agricultural University, Harbin, Heilongjiang 150030, China,
weizm691120@163.com

Abstract: In sugar beet seedling period and sugar accumulation period, the quantity of NR-mRNA raised with the rate of nitrate nitrogen and ammonium nitrogen raised, and the activity of NR raised also, that was the quantity of NR-mRNA of NO_3^-/NH_4^+ —4:0 was the highest. In phyllome formation period and root growth period, the quantity of NR-mRNA of NO_3^-/NH_4^+—3:1 was the highest, and its activity was the highest and that of NO_3^-/NH_4^+—4:0 was the second, that was because these periods were peak of absorbing nitrogen. The results showed that nitrate nitrogen regulated NR in transcriptional level. [Nature and Science 2003;1(1):39-41].

Key words: different NO_3^-/NH_4^+; mRNA of NR; sugar beet

1. Introduction

Nitrate reductase (NR) is a key enzyme involved in the first step of nitrate assimilation in plants, and it is also found in bacteria and fungi. Although in these different organisms it catalyzes a similar reduction of nitrate, the enzyme displays a variety of structures and dissimilarities. In *Escherichia coli* the enzyme is a heterotrimer bound to the bacterial membrane (Calza, 1997) and in *Chlorella* it is anhomotetramer (Howard, 1992) found in the pyrenoid. In plants the enzyme is a homodimer possibly interacting with the chloroplast outer membrane. Apart from NADH, the three other cofactors involved in the reduction of nitrate by NR are FAD, cytochrome b557 and the molybdenum cofactor. The NR from several plant species has been purified to homogeneity (Redinbaugh, 1995) shown to catalyze, apart from nitrate reduction, other reactions, such as the reduction of ferricion (Campbell, 1995), which may be of physiological significance. The subunits of these plants' NR have a molecular weight close to 110 kDa.

The regulation of NR activity in plants appears to be rather complex and many studies have been devoted to the description of this regulation (Huang, 1999). For instance, the catalytic process of nitrate reduction takes place in the leaves of numerous plant species, but it can also occur exclusively in the roots of other species such as white lupin. Molecular tools have been using to study more deeply the features of these regulations, for instance, NR monoclonal antibodies have been available, and the isolation and characterization of a cDNA encoding more than 50% of the tobacco NR mRNA is presented. For the basis of studying sugar beet NR mRNA, the methods of Northern and Southern are complex, and the polymerase chain reaction (PCR) technology is simple and it can analyze the micro-DNA. In this study we used PCR technology to quantitatively analyze NR mRNA of sugar beet that controlled by different nitrogen source. We engineered NR genes to improve utilization rate of nitrogen fertilizer and culture top quality and high yield sugar beet in practice.

2. Materials and Methods

***Materials*:** The present leading variety in Heilongjiang Province of China — Tian Yan 7 was used in this study.

***Plant Culture*:** The gravel culture was used and the nutrient solution was improving Hoagland. A nutrient solution containing mixed nitrogen-ammonium nitrogen and nitrate nitrogen (total nitrogen source is 8.0 mmol/L) was used. The nitrogen were used as the different rate: NO_3^-/NH_4^+ 4:0, 3:1, 2:2, 1:3, 0:4, respectively. The nutrient solution was changed every 7 days and regulated the pH every 3 days to keep it neutrality. From seedling stage sampling was done from 8 to 10 o'clock in sunny morning per 20 days. Functional leaves were sampled to measure NR activity.

***Measurement of NR*:** Sulfanilamide colorimetric method.

***Quantity of NR-mRNA*:** Extracted total RNA (according to a procedure of Trizol kit) and got intact RNA → purified RNA → inverse transcription (according to a procedure of Promega inverse transcription kit, first strand cDNA was synthesized from total RNA using primers P_1 5'GAA CAC AGC TTC CAA GAT CAT CCA 3', P_2 3'GTTATGATGTCACCAATATACCCT 5') → PCR [with 40 cycle of 94℃ (30') denaturation, 60℃ (1') annealing, 72℃ (2') extension]. PCR products were resolved in 2% agarose gels and were visualized by ethidium bromide staining, then scanned by CS-930 chromato-scanner (made in Japan).

3. Results

Extraction and Selection of Total RNA from Sugar Beet: Total RNA was extracted from sugar beet leaf tissues according to a procedure in Trizol kit. The sample was determined in λ_{260nm}, λ_{280nm}, λ_{230nm} differently (Table 1). The results showed that OD_{260}/OD_{280} of RNA was 1.932 and it was in the middle of 1.8- 2.0. Electrophoresis was carried out. The electrophoretogram (Figure 1) showed that the products 23sRNA, 28sRNA and 5sRNA were obtained. It was intact and it could be done RT-PCR (reverse transcription- polymerase chain reaction).

Table 1. Quality Determination of RNA

OD	OD_{260}	OD_{280}	OD_{230}	OD_{260}/OD_{280}	OD_{260}/OD_{230}
RNA	0.398	0.206	0.197	1.932	—

Figure 1. Electrophoretogram of Sugar Beet Total RNA

Table 2. The Effect of Different NO^-_3/ NH^+_4 on the Activity of NR in Endogenoussubstrate (μ gNO^-_2/gFWh)

Control NO_3^-/NH_4^+	Date of Sampling						
	6.14	6.25	7.15	8.01	8.17	9.13	9.25
CK	0.446	4.057	8.728	1.424	4.289	2.673	1.879
4:0	2.101	5.779	16.134	1.784	6.097	4.105	2.348
3:1	1.734	6.893	17.556	2.026	7.381	4.029	2.189
2:2	1.619	5.274	15.931	1.706	5.788	4.096	2.102
1:3	0.904	4.969	11.642	1.498	4.403	3.028	1.884
0:4	0.716	3.986	10.958	1.349	4.039	2.952	1.904

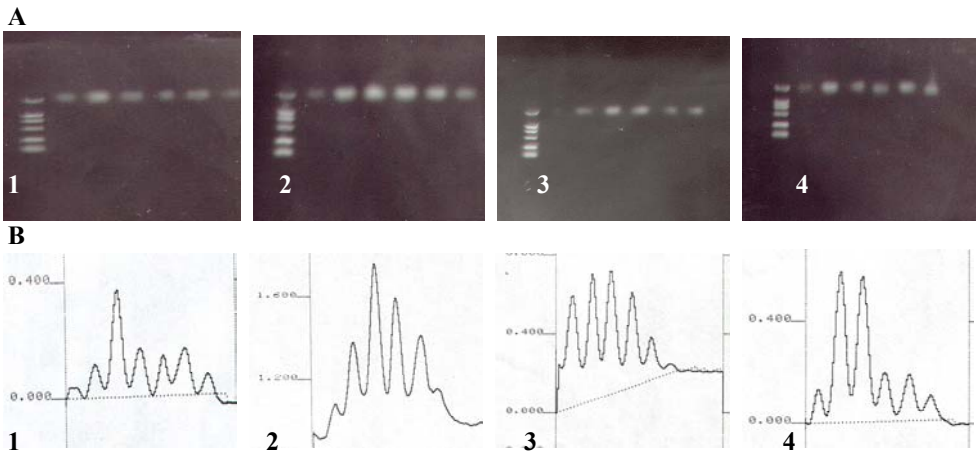

Figure 2. Quantity of NR-mRNA from Sugar Beet in Different Growth Period. (A1-4) Electrophoretogram of RT-PCR product on NR-mRNA. The bands were mark, ck, 4:0, 3:1 ,2:2, 1:3, 0:4 in proper order from left to right. (B1-4) chromatogram of electrophoretogram of RT-PCR product on NR-mRNA. (1) seedling period. (2) phyllome formation period. (3) sugar accumulation period. (4) root growth period.

The Measurement of NR Activity and Quantity of NR-mRNA from Sugar Beet Leaves. In sugar beet seedling period and sugar accumulation period, the quantity of NR-mRNA raised with the rate of nitrate nitrogen in mixed nitrogen sources raised, and the activity of NR raised also. In the quantity of NR-mRNA of NO_3^-/NH_4^+—4:0 was the highest. In phyllome formation period and root growth period**,** the quantity of NR-mRNA of NO_3^-/NH_4^+—3:1 was the highest, and its activity was the highest and that of NO_3^-/NH_4^+—4:0 was the second. This showed that adding small amount of NH_4^+-N under the circumstance of NO_3^-–N was abundant to improve the NR-mRNA transcriptional quantity and raise the NR activity same time. But in every growth period with the rate of ammonium nitrogen in mixed nitrogen sources raised the quantity of NR-mRNA and NR activity was decreased deeply (Table 2, Figure 2). We know that NH_4^+-N could inhibit the NR activity, but in the periods of absorbing nitrogen peak, NH_4^+-N could stimulate the NR-mRNA also. The results showed that the NR activity was controlled at the transcriptional level and nitrate nitrogen regulated NR at the transcriptional level.

4. Discussion

We know that NO_3^-–N could induce the NR activity, but in period of uptaken nitrogen peak of sugar beet – that is NH_4^+-N could improve NR activity also. Because this was in the period of uptaken nitrogen peak, NH_4^+-N could improve the utilization rate of NO_3^--N and improve transcriptional quantity of NR-mRNA. The rate of NH_4^+-N was increased in mixed nitrogen source, and the NR-mRNA level was decreased. NH_4^+-N can stimulate the GS activity and improve Gln. But, as the reference showed (Xiao, 2000) a negative correlation between NR-mRNA level and increasing Gln, and the NR-mRNA level decreased sharply when Gln was improved to plants. This paper showed that we could control NR activity of sugar beet at the transcriptional level. So, we may engineer NR genes by molecular biological technology to improve NR-mRNA level and increase NR activity. We could improve utilization rate of nitrogen fertilizer and culture top quality and high yield sugar beet in practice.

The financial support provided by the National Natural Science Fund (39770434).

Correspondence to:
Yue Zhao
Wood Street 59
Gongbin Road, Xiangfang District
Harbin, Heilongjiang 150030, China.
Telephone: 01186-451-5519-1377
Cellular phone: 01186-13845081249
E-mail: weizm691120@163.com

References

Calza R. Cloning of DNA fragments complenentary to tobacco nitrate reductase mRNA and encoding epitopes common to the nitrate reductases from higher plants. Mol Gene 1997;209:552-62.

Campbell WH, Redinbaugh MG. Ferric-citrate reductase activity of nitrate reductase and its role in iron assimilation by plants. J Plant Nutr 1995;7:799-806.

Howard WD, Solomonson LP. Quatrnaty structure of assimilatory NADH: nitrate reductase from Chlorella. J Biol Chem 1992;257:10243-50.

Huang Q, Yin L, Chai X, et al. Influence of nitrogen sources on glutamine synthetase in wheat seeding [J]. Acta Botanica sinica 1999;37(11):856-62.

Xiao K, Zhang S, Zuo D, et al. The effect of different nitrogen nutrition forms on photosynthetic characteristics in wheat leaves [J]. 2000;26(1):53-8.

Mating System and Outcrossing Rates of Four *Bruguiera Gymnorrhiza* Populations of Mangrove, China

Jingping Ge*, Baiyan Cai**, Peng Lin***

* College of Life Science, Heilongjiang University, Harbin, Heilongjiang 150080, China; ** College of Dongfang, Harbin, Heilongjiang 150080, China; *** Xiamen University, Xiamen, Fujian 361005, China.
gejingping@0451.com, gejingping9178@hotmail.com

Abstract: Using polymorphic loci of allozyme as genetic marker and horizontal sliceable gel electrophoresis as method to examine the genotypes of 4 *Bruguiera gymnorrhiza* populations in Fugong of Fujian (24°24′), Futian of Guangdong (22°32′), Shankou of Guangxi (21°28′) and Dongzhai Harbor of Hainan (19°51′), China. The mating system was also decided by Multi Locus Testing. The polymorphic loci selected for analyzing were different in these four areas: *Mdh*-1, *Mdh*-2, and *Me*-1 in Fugong, Guangxi and Hainan as well as *Mdh*-1, *Mdh*-2, *Aat*-1, *Aat*-2 in Shenzhen. The results showed that the difference between outcrossing rates of polymorphic loci were quite obvious, that of Fugong was the biggest, which was 0.845 and that of Hainan was the smallest, which was 0.267. The different value between outcrossing rates of polymorphic loci and the mean of outcrossing rates of monomorphic loci in these four areas were vary, which showed that the mating system of Fugong, Guangxi and Hainan were slightly biaparental inbreeding and that of Guangxi was at random. *Bruguiera gymnorrhiza* was mixed-mating species and its mating system was mainly outcrossing. This was influenced by factors such as plant population density and structure, the adaptability of pollinator and whether it's self-incompatibility or not. [Nature and Science 2003;1(1):42-48].

Key words: mangrove; mating system; *Bruguiera gymnorrhiza*

1. Introduction

Mating system is determinant for genetic differentiation of inter-population and intro-populations (Brown, 1989; Brown, 1989; Hamrick, 1989). As a bridge connecting two generations, mating system also determines the genotype distribution and population dynamic of offspring populations（Hamrick, 1982）. Many researchers have emphasized the functions of mating system on gene flow, genetic structure of populations and potential evolution of plant population (Brown, 1979; Hamrick, 1979; Loveless, 1984). Recently, the studies involved plant mating systems have been thought a lot of. For example, in the article of Barrett and Eckert (1990), 129 plants' mating systems have been concerned. Polymorphic loci are useful for estimating plant mating systems (Brown, 1978; Hamrick, 1989), these have been affirmed in recent studies (Moran, 1989; Sampson, 1989; Warwick, 1989; Morgan, 1990; Watkins, 1990; Sun, 1998), and have provided rapid and efficient methods for studying genetic diversity of plant populations. There are many models used for estimating mating system, and the classical one is Mixed Mating Model (Fyffe, 1951). On the basis of above, Shaw et al. (1982) and Ritland (1981) published Multi Locus Testing (MLT) Model, which is the most popular procedure used in estimating outcrossing rate. In this study, we also use this MLT.

Mangroves are woody plant communities growing in tropical and subtropical areas along seashore and widely distributed in Guangdong, Guangxi, Hainan, Fujian and Taiwan Provinces, China. They have distinct characteristics such as vivipary, salinity-resistance and similar living habitats. All of these made them far different from terrestrial plant communities. Although the energy ecology, physiology ecology and pollution ecology of mangroves have much been studied since 1980s, the studies on mating system are not much concerned.

Several examples of mating system of mangroves were used, such as characteristic that the hypocotyls still stay in the mother trees after they maturated, so it is easy to observe the offspring separation rate. For example, the outcrossing rates of *Rhizophora mangle* (Lowenfeld, 1992; Klekowski, 1994) and *Kandelia candel* (Chen, 1996) were estimated by observation of chlorophyll-deficient heterozygotes of offspring. Recently, allozymic polymorphic loci were used as genetic markers to estimate mating system of *Kandelia candel* by Sun et al. (1998). In this study, *Bruguiera gymnnorrhiza*, which is widespread species in mangrove, was used as materials to study mating system through MLT procedure. Upon this study, genetic diversity and genetic differentiation will be much better understood.

2. Materials and Methods

2.1 Sampling Sites

Bruguiera gymnorrhiza is widespread thermophile (Lin, 1984), pollinated by birds or butterflies, hermaphrodite, which is naturally distributed along seashore in Guangdong, Guangxi, Hainan, Fujian and Taiwan

Provinces, China. Five sampling sites were selected in these areas according to limited conditions. Climate, chemical and physical characteristic of soils in sampling sites were shown in Table 1.

Table 1. Climate and Chemistry-Physic Characteristic of Soils in Research Sites of *Bruguiera gymnorrhiza* Populations

Items	Fugong	Shenzhen	Guangxi	Hainan
Latitude	24°24′	22°32′	21°28′	19°51′
Longitude	117°55′	114°05′	109°43′	110°24′
annual mean temperature℃	21.0	22.0	22.6	23.8
annual temp. difference℃	16.7	14.0	15.2	11.3
rainfall mm	1365.1	1926.7	1796.8	1697.8
Organism%	2.67	3.62	4.94	7.38
total N%	0.54	0.53	0.50	0.55
total P（P_2O_5%）	0.018	0.021	0.009	0.011
total salinity%	0.821	0.844	1.590	5.921
content of Cl^-%	13.280	4.195	6.938	7.266
PH	6.92	6.55	3.16	3.01

Fugong site is located in Longhai Mangrove Protect Area, Guoxia Village, Fugong Town, Longhai, Fujian Province. This protected area is in the entrance of Jiulong River, where belongs to subtropical climate. Several species of mangroves are natural growing, which includes *Aegiceras corniculatum*, *Avicennia marina*, *Acanthus ilicifolius* and *Acanthus xiamenensis*.

Shenzhen site is located in Futian National Mangrove Protect Area, northeast to Shenzhen Bay, Guangdong Province, where is 11 km long and 10 to 200 m wide. This area is close to subtropical sea, belongs to subtropical monsoon climate. The main species are *Kandelia candel*, *Aegiceras corniculatum* and *Avicennia marina*, and secondly are *Bruguiera gymnorrhiza*, *Acanthus ilicifolius* and *Excoecaria agallocha*, sum up to five families, six genera and six species. Semi-mangrove species such as *Acrostichum aureurm*, *Thespesia populnea* and *Pluchea indica* also exist.

Guangxi site is located in Shankou National Mangrove Ecological Nature Protect Area, Yingluo bay, Hepu county, southeast of Guangxi district, where is located in the marginal terrain between north torrid zone and south sub-torrid zone, belongs to north monsoon torrid zone. Mangrove in Yingluo bay lies in high tide beach, which is 86.67 hm^2 large. *Kandelia candel* and *Aegiceras corniculatum* live at the edge of the zone, accompanying with scattered *Avicennia marina*. *Bruguiera gymnorrhiza* is a small community near to seashore.

Hainan site is located in Dongzhai Harbor National Mangrove Protect Area, Qiongshan, Hainan. Mangrove species are quite lot more here and sum up to 12 families, 14 genera and 18 species. Furthermore, another 8 species were introduced. *Bruguiera gymnorrhiza* is natural and pure forest, accompanying by *Bruguiera sexangula*, *Ceriops tagal* and *Kandelia candel*.

2.2 Sample Collecting and Treating

2.2.1 Sample Collecting

Five to eight trees, used as mother family arrays, were selected at random in each site when hypocotyls were mature. Five to eight hypocotyls were sampled on each tree as progeny arrays. Took these hypocotyls back to lab and planted them in fresh water washed sand. Hypocotyls in the same mother family arrays should be planted in the same pot. When leaves grew up, sampled fresh leaves according to progeny arrays.

2.2.2 Sample Treating

Fresh young leaves were taken into analysis. The leaves were cut into small pieces, and put into mortars. Suitable Tris-HCl extracted buffer were added, and the leaves were ground. All of these above processes would be on the ice bath. When the leaves were ground into even pasty, 4×7 mm wicks were used to absorb even pasty liquid (i.e. crude enzyme extracted solution). Loading sample and running with horizontal sliceable gel electrophoresis. Those enzymes must be analyzed as quickly as possible. As mangroves are full of tannin (Lin, 1984), the enzyme-extracted buffer was slightly modified according to Tris-HCl extracted solution (Wang, 1996; Chen, 1997).

2.3 Electrophoresis and Analysis of Zymogram

Horizontal sliceable starch gel electrophoresis (SGE) was used to detect the genotypes of progeny and parent. Hydrolyzed potato starch made by Sigma (s-5691) was used and its concentration was 12.75%, the corresponding gel buffer system was Tris-Boric Acid-EDTANa_4 （#10）（pH8.6）(Wang, 1996).

The enzyme systems, E.C. No., numbers of loci and buffer systems used in this study were show in Table 2. Locus and their numbers were different in each site (Table 3).

Table 2. The Enzyme Systems, E.C.No., Numbers of Loci and Buffer Systems of *Bruguiera gymnorrhiza* Populations

Enzyme system (Abbreviation in parentheses)	E.C.No.	Type of gel (buffer in parentheses)	numbers of loci
Malate dehydrogenase (MDH)	E.C.1.1.37	SGE（#10）	3
Malic enzyme (ME)	E.C.1.1.40	SGE（#10）	1
Aspartate (AAT)	E.C.2.6.1.1	SGE（#10）	2

Table 3. Loci of *Bruguiera gymnorrhiza* Populations Used in Mating System

Locus	Fugong	Shenzhen	Guangxi	Hainan
Mdh-1	+	+	+	+
Mdh-2	+	+	+	+
Me-1	+		+	+
Aat-1		+		
Aat-2		+		

2.4 Estimating Methods of Outcrossing Rates

Mating system of *Bruguiera gymnorrhiza* populations were estimated by MLT-1（Ritland, 1990）. This procedure also can estimate maternal plant genotype and pollen pool allelic frequencies at the same time. The included estimation parameters were shown as follows:

tm－multiloci outcrossing rate

ts－mean of single locus outcrossing rate

tsa－outcrossing rate of each locus using MLT

tm-ts－difference between tm and ts. If tm-ts is bigger than zero, which indicated that the parents are inbreeding. The estimation of tm, ts, tsa is through the comparison between maternal genotype and progeny genotype. Computer was used to do all of these estimations. Estimating the multiloci will have much priority because all of the results are on the base of all loci, which avoid some problems in using single locus (Green, 1980; Shaw, 1982), such as affected by selection or random mating（Ritland, 1981）.

3. Results

3.1 Allelic Frequencies of Hypocotyls, Maternal Plants and Pollen Pool in Each *Bruguiera gymnorrhiza* Population

Allelic frequencies of hypocotyls, maternal plants and pollen pool of four populations were shown in Table 4. The results showed that there were certain difference in these three items at different loci and different populations. In Shenzhen population, allelic frequencies difference between pollen pool and hypocotyls were small, but that between pollen pool and maternal plants were quite large. Same phenomenon also existed in other three populations. This might be due to the different pollen amounts produced by different mature individual. In addition, tree ages might also affect pollen amounts. There were some reports on this problem in conifer (Muller, 1984). Both limited spreading of pollen and selecting function of gamete can result in allelic frequencies difference of pollen pool and maternal plants (Apsit, 1989). Except for some alleles in certain loci, such as *Aat*-1C in Shenzhen population, *Mdh*-1A in Guangxi population, *Me*-1B in Hainan population and *Mdh*-1A in Fugong population，there were slight difference between pollen pool and maternal plant, which showed that the pollen contribution of maternal plant to this allele was equal.

3.2 Outcrossing Rates of Each *Bruguiera gymnorrhiza* Population

The outcrossing rates of each population estimated by MLT and those of single locus were shown in Table 5-8. The results showed that tm in each population differed quite big. tm in Fugong population was the biggest, which was 0.845 and that in Hainan population was the smallest, which was 0.267. tm in Guangxi population was similar with that in Fugong population, which was 0.820, while tm in Shenzhen population was 0.561. The tm of *Kandelia candel* population was 0.697 (Sun, 1998), that is in the same family with *Bruguiera gymnorrhiza*. tm in Guangxi and Fugong were little higher while that in Shenzhen and Hainan was little lower.

Except for Guangxi population, the tm-ts of other three populations were positive which showed that these three populations were slightly inbreeding while Guangxi population was random mating. Reasons for these might be focus on different population structures.

Outcrossing rates of each locus were also estimated by MLT using single locus. The results showed that the mean of single locus outcrossing rates differed not too much in Guangxi (0.817), Shenzhen (0.816) and Fugong (0.812). But that in Hainan was much lower (only 0.502). There was some difference on the estimated value at each locus of each population. The significance of locus outcrossing rates of each population by χ^2 tests showed that the difference in

Table 4. Allelic Frequencies of Seeds, Maternal Plant and Pollen Pool of *Bruguiera gymnorrhiza* Populations (standard errors in parentheses)

Locus	Allele	Fugong			Shenzhen			Guangxi			Hainan		
		Maternal	pollen pool	*hypo-cotyles	Maternal	pollen pool	Hypo-cotyles	Maternal	Pollen pool	Hypo-cotyles	Maternal	pollen pool	Hypo-cotyles
Mdh-1	A	0.917	0.984	0.971	0.750	0.930	0.934	0.900	0.989	0.974	0.583	0.351	0.489
		(0.079)	(0.013)	(0.020)	(0.125)	(0.025)	(0.028)	(0.095)	(0.009)	(0.018)	(0.142)	(0.135)	(0.052)
	B	0.083	0.016	0.029	0.250	0.070	0.066	0.100	0.011	0.026	0.417	0.649	0.511
		(0.079)	(0.013)	(0.020)	(0.125)	(0.025)	(0.028)	(0.095)	(0.009)	(0.018)	(0.142)	(0.135)	(0.052)
Mdh-2	A	0.833	0.903	0.914	0.750	0.955	0.934	0.800	0.971	0.950	0.833	0.979	0.957
		(0.108)	(0.041)	(0.034)	(0.354)	(0.021)	(0.028)	(0.126)	(0.009)	(0.024)	(0.108)	(0.007)	(0.021)
	B	0.167	0.097	0.086	0.250	0.045	0.066	0.200	0.029	0.050	0.167	0.021	0.043
		(0.108)	(0.041)	(0.034)	(0.354)	(0.021)	(0.028)	(0.126)	(0.009)	(0.024)	(0.108)	(0.007)	(0.021)
Me-1	A	0.583	0.487	0.529				0.200	0.064	0.064	0.333	0.586	0.404
		(0.142)	(0.085)	(0.060)				(0.126)	(0.030)	(0.028)	(0.136)	(0.138)	(0.051)
	B	0.417	0.513	0.471				0.300	0.581	0.462	0.417	0.404	0.574
		(0.142)	(0.085)	(0.060)				(0.145)	(0.107)	(0.056)	(0.142)	(0.138)	(0.051)
	C	0.000	0.000	0.000				0.500	0.355	0.474	0.083	0.010	0.021
		(0.000)	(0.000)	(0.000)				(0.158)	(0.104)	(0.057)	(0.080)	(0.004)	(0.015)
Aat-1	A				0.333	0.233	0.263						
					(0.136)	(0.102)	(0.051)						
	B				0.500	0.639	0.579						
					(0.144)	(0.113)	(0.057)						
	C				0.167	0.128	0.158						
					(0.108)	(0.049)	(0.042)						
Aat-2	A				0.417	0.380	0.382						
					(0.142)	(0.136)	(0.056)						
	B				0.583	0.620	0.618						
					(0.142)	(0.136)	(0.056)						

* The reproductive organ of *Bruguiera gymnorrhiza* is hypocotyl but not seed

Table 5. Outcrossing Rates of Fugong *Bruguiera Gymnorrhiza* Population (standard errors in parentheses)

Locus	Tsa	Tm	Ts	tm-ts
Mdh-1	0.643（0.454）	0.845（0.276）	0.740（0.162）	0.104（0.138）
Mdh-2	0.476（0.193）			
Me-1	1.318（0.141）			
Mean	0.812			
$\chi^2=\Sigma$ Ii（ti-t）^{2}=2.468 df=2 p>0.05				

Table 6. Outcrossing Rates of Shenzhen *Bruguiera gymnorrhiza* Population （tandard errors in parentheses）

Locus	Tsa	Tm	Ts	Tm-ts
Mdh-1	0.511（0.182）	0.561（0.154）	0.530（0.131）	0.032（0.063）
Mdh-2	0.751（0.096）			
Aat-1	0.001（0.086）			
Aat-2	1.999（0.007）			
mean	0.816			
$\chi^2=\Sigma$ ii（ti-t）^{2}=208.21 df=3 p<0.001				

Table 7. Outcrossing Rates of Guangxi *Bruguiera gymnorrhiza* Population （standard errors in parentheses）

Locus	Tsa	Tm	Ts	Tm-ts
Mdh-1	0.744（0.088）	0.820（0.100）	0.835（0.109）	-0.015（0.025）
Mdh-2	0.774（0.088）			
Me-1	0.932（0.187）			
Mean	0.817			
$\chi^2=\Sigma$ Ii（ti-t）^{2}=0.155 df=2 p>0.05				

Table 8. Outcrossing Rates of Hainan *Bruguiera gymnorrhiza* Population （standard errors in parentheses）

Locus	Tsa	Tm	Ts	tm-ts
Mdh-1	0.001（0.000）	0.267（0.010）	0.242（0.100）	0.025（0.025）
Mdh-2	0.764（0.230）			
e-1	0.741（0.472）			
Mean	0.502			
$\chi^2=\Sigma$ Ii（ti-t）^{2}=0.900 df=2 p<0.05				

Guangxi and Fugong was not too much while that in Hainan and Shenzhen was quite large. The lower outcrossing rates in Hainan and Shenzhen might be due to the lopsided distribution of outcrossing rates between each locus in populations. At the same time, ts-ta also differed quite large in different populations. The estimated outcrossing rate of single locus was easily affected by irregular distribution of individual in natural population. Chen (1997) has obtained the similar conclusion when studying *Cyclobalano glauca* populations.

4. Discussion

The outcrossing rates of different *Bruguiera gymnorrhiza* populations differed quite large. The outcrossing rates of Fugong population was the biggest, which was 0.845 and that of Hainan population was the smallest, which was 0.267. The discrepancy was 0.578. Hainan, Shenzhen and Fugong populations were slightly inbreeding and Guangxi population was random mating from the ts-tm. As a result, it can be inferred that *Bruguiera gymnorrhiza* was mix-mating system, mainly outcrossing. Kondo et al. （1987） also found that *Bruguiera gymnorrhiza* and *Rhizophora mucronata* might be outcrossing and inbreeding, which had the same results with Tomlinson （1986）.

Species in *Bruguiera* were pollinated by birds and butterflies through the study on anadem biology by Tomlinson et al. （1979） and Tomlinson （1986）. Moreover, the mating systems of entomoplily are generally outcrossing (Barrett, 1990). So the mating system of *Bruguiera gymnorrhiza* gives priority to outcrossing. The similar conclusion was obtained when studying another mangrove—*Kandelia candel* (Sun, 1998; Chen, 1996). Chen et al.（1996） found that the outcrossing rates of *Kandelia candel* in Fugong and Zuta was 0.197 and 0.177, respectively, using chlorophyll-deficient mutants. Sun et al.（1998）found the tm was 0.679 and 0.797 in two *Kandelia candel* populations, Hongkong. As a result, *Kandelia candel* also gives priority to outcrossing due to its characteristic of entomoplily.

At the same time outcrossing rates between multiloci differed quite large. It was a common phenomenon in mix-mating species that there were difference in

outcrossing rates between populations（Schoen, 1982）. Though Lande and Schemske （1985） had pointed out that significant outcrossing and inbreeding might exist in equilibrium populations, environment factors and statistic error might disrupt such equilibrium and brought distinct outcrossing rates. Some genetic factors also have functions to certain extend (Brown, 1989), such as pollination types, pollinator adaptability, anadem structure, population size and density, inbreeding incompatibility and genetic controlling, etc.

Similarly, outcrossing rates differences between *Bruguiera gymnorrhiza* populations were also affected by plant density, population structure, pollinator adaptability and activity as well as whether they were inbreeding incompatibility or not.

First, the larger the population density, the higher outcrossing level between relatives, owing to the large connection between plants. *Bruguiera gymnorrhiza* is inbreeding compatibility （Tomlinson, 1986）. The opportunity of outcrossing and inbreeding for inbreeding compatibility species is much more when population density is lower. Thereby the outcrossing rates decreases. In Shenzhen site, individual of *Bruguiera gymnorrhiza* population scattered distributed while the density was low. This caused the individuals to accept small amount pollen offered by off-relativities. Chen （1995） also found that outcrossing rates was positive correlation with plant density when he studied *Cyclobalano glauca* population, a kind of inbreeding compatibility species. However, the relationship between outcrossing rates and plant density was relatively complex according to entomoplily, sometimes it was positive and sometimes it was negative. For example, outcrossing rates and plant density was negative correlated in *Phloxdrum moradii*, which was inbreeding incompatibility. Watkin et al. （1990） argued that the plant density was lower and the pollinator activity distance was longer, so they could contact off-relativities, and outcrossing happened.

Population structure is the most important factor on mating system when estimating the outcrossing rates or inbreeding rates. Using single locus to estimate outcrossing rates is not quite right because this is including real outcrossing and inbreeding. However, theoretically, multiloci estimation was slightly affected by consanguinity mating, and could commendably estimate inbreeding. In this study, Shenzhen, Hainan and Fugong population were slightly parental inbreeding according to tm-ts.

Pollinator adaptability and active ability also have effect on mating system, particularly entomoplily. An example is *Banksia cuneata*. Schemske and Lande （1985） showed that pollinator activity might cause outcrossing rates varied in some kinds of entomoplily. *Bruguiera gymnorrhiza* is entomoplily, big flower, pollinated by birds (Tomlinson, 1986). Thus the lower outcrossing rates in Hainan population might be affected by bird's activity to some extent, which include looking for foods, suckling and changing in bird's population structure.

The financial support provided by the Natural Science Fund of China, No. 39670135.

Correspondence to:
Jingping Ge
74 Xuefu Road
Nangang District
College of Life Science, Heilongjiang University
Harbin, Heilongjiang 150080, China
Telephone: 01186-451-86608586 (Office)
01186-451-86609178 (Home)
Mobile phone: 01186-13836002907
E-mail: gejingping@0451.com or
gejingping9178@hotmail.com

References

Apsit VJ, Nakamura RR, Wheeler NC. Differential male reproductive success in Douglas fir. Theoretical Application Genetic 1989;77:681-4.

Barrett SCH, Eckert CG. Variation and evolution of mating systems in seed plants. In: Kawano S ed. Biological Approaches and Evolutionary Trends in Plants. Academic Press, London, Britain. 1990:229-54.

Brown AHD. Enzyme polymorphism in plant populations. Theoretical Population Biology 1979;15:1-42.

Brown AHD. Genetic characterization of plant mating system. In: AHD Brown, MT Clegg, AL Kahler eds. Plant Population, Genetics, Breeding and Genetic Resources. Sinauer Associates, Sunderland, Britain 1989:145-62.

Brown AHD, Zohary D, Nevo E. Outcrossing rates and heterozygosity in natural populatons of Hordeum spontaneum Koch in Israel. Heredity 1978;41:49-62.

Brown AHD, Byrdon JJ, Jarosz AM. Isozyme analysis of plant mating systems. In: Soltis DE, Soltis PS eds. Isozyme in Plant Biology. Dioscorides Press, Oregon, Portland. 1989:73-86.

Chen XY, Song YC. Mating system and inbreeding depression of Cyclobalanopsis glauca Diaoqiao of Huangshan. Acta Ecologica Sinica 1997;17(5):463-8.

Chen XY, Lin P, Lin YM. Mating systems and spontaneous mutation rates for chlorophyll-deficiency in populations of the mangrove *Kandelia candel*. Hereditas 1996;125:47-52.

Fyfe JL, Baily NT. Plant breeding studies in leguminous forage crops, 1, Natural crossbreding in winter beana. Journal of Agriculture Science 1951;41:371-8.

Green AG, Brown AHD, Oram RN. Determination of outcrossing rate in a breeding population of Lupinus albus L (White Lupin). Journal of Pflanzenzuchtg 1980;84:181-91.

Hamrick JL. Plant population genetics and evolution. American Journal of Botany 1982;69(10):1685-93.

Hamrick JL. Isozymes and the analysis of genetic structure in plant populations. In: Soltis DE, Soltis PS eds. Isozyme in Plant Biology. Dioscorides Press, Oregon, Portland. 1989:66-70.

Hamrick JL, Linhart YB, Mitton JB. Relationship between history characteristics and electrophoretically detectable genetic variation in plants. Annual Review of Ecology System 1979;10:173-200.

Klekowski EJ, Lowenfeld R, Hepler PK. Mangrove genetics Ⅱ. Outcrossing and lower spontaneous mutation rates in Puerto Rican *Rhizophora*. International Journal Plant Science 1994;155:373-81.

Kondo K, Nakamura T, Tsuruda K. Pollination in Bruguiera gymnorrhiza and Rhizophora mucronata in Ishigaki Island, the Ryukyu Islands, Japan. Brotropica 1987;19:377-80.

Lande R, Schemske DW. The evolution of self-fertilization and inbreeding. 1. Genetic Models. Evolution 1985;39:24-40.

Lin P. Mangrove. Ocean Press, Beijing, China. 1984;16-35.

Loveless MD, Hamrick JL. Ecological determinants of genetic structure in plant populations. Annual Review of Ecology System 1984;15:65-95.

Lowenfeld REJ, Klekowski JR. Mangrove genetics. I. Mating system and mutation rates of *Rhizophora mangle* in Florida and San Salvador Island. Bahamas. International Journal of Plant Science 1992;155:373-81.

Moran CL, Muona O, Bell JC. Breeding systems and genetic diversity in Acacia auriculiformis and A. Crassicarpa. Biotropica 1989;21:250-6.

Morgan MT, Barrett SCH. Outcrossing rates and correlated mating within a population of Erchornia paniculata (Pontederiaceae). Heredity 1990;64:271-80.

Muller-Starck G, Iiehe M. Reproductive systems in conifer seed orchards. 3. Female and male fitness of individual's cones realized in seeds of Pinus sylvestris L. Theoretical Application Genetic 1984;69:173-7.

Ritland K, Jain SK. A model for the estimation of outcrossing rate and gene frequencies using n independent loci. Heredity 1981;47:35-52.

Ritland K. A series of FORTRAN computer programs for estimating plant mating system. Journal of Heredity 1990;81:235-7.

Sampson JF, Hopper SD, James SH. The mating system and population genetic structure in a bird pollinated mallee, Eucalyptus rhodantha. Heredity 1989;63:383-93.

Schemske DW, Lande R. The evolution of self-fertilization and inbreeding depression in plants. 2. Empirical observations. Evolution 1985;39:41-52.

Schoen DJ. The breeding system of Gilia achilleifolia: variation in floral characteristics and outcrossing rate. Evolution 1982;36:596-613.

Sun M, Wong KC, Lee JSY. Reproductive biology and population genetic structure of Kandelia candel (Rhizophoraceae), a viviparous mangrove species. American Journal of Botany 1998;85 (11):1631-7.

Tomlinson PB, Bunt JS. Preliminary observations on floral biology in mangrove Rhizophoraceae. Biotropica 1979;11:256-77.

Tomlinson PB. The botany of mangroves. Cambridge University Press, London, Britain. 1986:399-404.

Wang ZR. Allozyme Analysis in Plants. Science Press, Beijing, China. 1996;23-65.

Warwick SI, Thompson BK. The mating system in sympatric populations of Carduus nutana, C. acanthoides and their hybrid swarms. Heredity 1989;63:329-38.

Watkins L, Levin DA. Outcrossing rates as related to plant density in Phlox drummordii. Hetedity 1990;65:81-90.

Magnolia cathayana - a New Species from China

Dali Fu*, Tianbang Zhao**

* Non-timber Forestry Research and Development Center, The Chinese Academy of Forestry, Zhengzhou, Henan 450003, China; ** Henan Agricultural University, Zhengzhou, Henan 450002, China,
fudali@pntfrc.com

Abstract: A new species of genus *Magnolia* L., *Magnolia cathayana* D. L. Fu et T. B. Zhao, sp. nov. was described in this paper. The species was found and collected on April 26, 1999 in Zhuzhou, Hunan Province of China by Dali Fu and Tianbang Zhao. The type is kept at Henan Agricultural University of China, No. 199904261 (flos). [Nature and Science 2003;1(1):49].

Key words: *Magnolia* L.; *M. cathayana* D. L. Fu et T. B. Zhao; New species; China

***Magnolia cathayana* D. L. Fu et T. B. Zhao, sp. nov.**
Plate I

Species *M. officinalis* Rehd. & Wils. et *M. officinalis* Rehd. & Wils. var. *bilobae* Rehd. & Wils. similis, sed foliis patentibus ante 20~30 dies apertis. Foliis et alabastris cum floribus tepalisque omnino conspicue parvioribus. Ramulis juvenilibus praeter sub cicatrici-stipulas sparse pubescentibus albis post glabris. Gemmis juvinilibus apice xerampelini-vel albo-villosis vel glabris. Alabastris extus glabris dense verruculosis. Pedicellis praeter sub cicatrices spathacei-bracteae villosis albis cetero glabris. Staminibus candidis; 4~8-ovulis in quoque disjuncte simplici-pistillo.

Arbor decidua. Ramuli hornotini purpureo-brunnei nitidi in juventute viriduli nitidi primo sub stipuli-cicatrices annulatis manifestis sparse pubescentibus albis denique glabris. Gemmae juveniles apice albi-vel xerampelini-villosae vel glabrae. Folia veris saepe 6~9 in veris ramulo conferta, crasse chartacea anguste elliptica 10~20.5 cm longa 4.5~9.0 cm lata apice saepe emarginata vel obtuse cum acumine basi cuneata margine integra supra virida nitida glabra costis minute recavis glabris subtus pallide viridula sparse pubescentia, costis et nervis lateralibus conspicue elevatis sparse albi-vel xerampelini-villosis vel glabris; petiole 1.8~3.1 cm longi flavo-virentes primo villosi post glabri vel interdum villosi; stipulis dense villosis albis vel xerampelinis, cicatricibus stipularum longitudinem 1/3~1/2 petiolorum partes aequantibus. Folia alterna parva ovata in ramulis aestivis autumnalibusque. Alabastra terminalia ovoidea in ramulis veris 2.5~4.3 cm longa diam. 2.0~2.5 cm, apice obtusa prope basin cylindrica (4~6 mm longa); bractea spathacea una coriacea nitidi glabra extus dense verrucosa; pedicelli grossi 1.0~1.2 cm longi diam. 4~6 mm nitidi viriduli glabri, praeter sub cicatrice spathaceos albi-vel xerampelini-villosis. Flores bisexuals; tepala 11 rare 10 extra 3 rare 2 in florescentia reflexa, tenuiter coriacea spathuli-elliptica vel oblongi-spathulata 6.5~8.0 cm longa 4.5~5.0 cm lata extra viridula interdum minute purpureo-rubella apice obtusa basi truncata 1.0~1.2 cm lata, interna 8 candida elliptici-spathulata vel anguste elliptici-spathulata 5.5~7.5 cm longa 2.5~5.0 cm lata apice obtusa vel mucronata basi cuneata ad anguste cuneata. Stamina ca. 130, 1.4~1.6 cm longa candida filamentis ca. 3 mm longis antheris 1.0~1.2 cm longis introrsi-longitudinalibus dehiscentibus connectives apice triangulate mucronatis; Gynoecia ovoidea 3.2~3.5 cm longa diam. 1.1~1.3 cm virida glabra; disjuctis simplici-pistillis ca. 100, glabris, stylis et stigmatibus 3~4 mm longis apice revolutis minute purpurascenti-rubis; 4~8-ovulis in quoque simplici-pistillo. Pedicelli glabri infra cicatrices spathacei-bractearum villosis. Syncarpia ignoti.

Hunan: Zhuzhou. 26.04.1999. D. L. Fu et T. B. Zhao, No. 199904261 (flos). Typus in Herb. HNAC.

Plate 1 *Magnolia cathayana* D. L. Fu et T. B. Zhao
1. Branch and leaves; 2. Leaves of long branch: base caespitose, above-media alternate; 3. A: leaf of *M. cathayana*, B: leaf of *M. offficinalis* var. *biloba*; 4. Tepals type and gynandrium; 5. Flower bud, leaves and branch; 6. Flower and leaves.

GIS Based AGNPS Assessment Model in a Small Watershed

Yongsheng Ma, Jon Bartholic

Institute of Water Research, Michigan State University, Michigan 48823, USA,
ysma66@yahoo.com.cn, yongshengma@hotmail.com

Abstract: AGNPS, which is an agricultural non-point source pollution model, was used in combination with GIS tools to assess the feasibility of water quality effluent trading for phosphorus, in Morrow Lake sub-watershed, Kalamazoo, Michigan, USA. GIS software packages (Arc/Info and ArcView) were used to prepare data input for the model and post process the results. The sensitivity of AGNPS parameters was evaluated to determine which most influenced phosphorus sediment loading. Evaluations were conducted to determine whether calculation processes could be simplified for rapid pollution forecasts. The results showed that pollution could be predicted by varying temporary model data (i.e. precipitation etc.) in the AGNPS model. Lastly, parameter sensitivity showed that phosphorus sediment is most sensitive to soil texture while sediment loss is most sensitive to the SCS curve number. [Nature and Science 2003;1(1):50-56].

Key words: watershed; AGNPS model; phosphorus; sedimentation; Michigan

1. Introduction

Agricultural non-point source (NPS) pollution has risen to the leading cause of surface water degradation due to agricultural pollution in last few decades. NPS pollution from agricultural activities contributed to 72% of the impaired stream miles in 48 states reporting sources (Yagow, 1999). Morrow Lake watershed was studied using Arc/Info 7.0 and ArcView 3.0 to generate cell data, and using AGNPS 5.0 to integrally analyze water and nutrients runoff and sediment of the watershed.

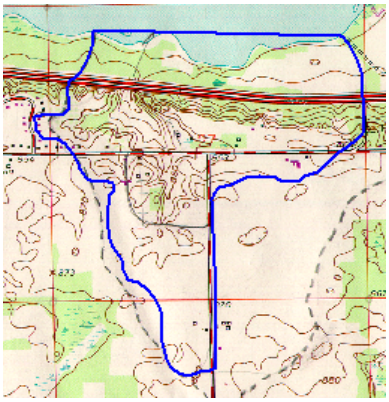

Figure 1. Morrow Lake Watershed Map

Figure 2. Kalamazoo Watershed

Symbol	Soil Name	Group
KaA	Kalamazoo Loam, 0 to 2 percent slopes	B
KaB	Kalamazoo Loam, 2 to 6 percent slopes	B
KaC	Kalamazoo Loam, 6 to 12 percent slopes	B
CoB	Coloma loamy sand, 0 to 6 percent slopes	A
CoC	Coloma loamy sand, 6 to 12 percent slopes	A
CoD	Coloma loamy sand, 12 to 18 percent slopes	A
OsB	Oshtemo sandy loam, 1 to 6 percent slopes	B
OsC	Oshtemo sandy loam, 6 to 12 percent slopes	B
OsD	Oshtemo sandy loam, 12 to 18 percent slopes	B
OsE	Oshtemo sandy loam, 18 to 35 percent slopes	B
SpB	Spinks loamy, 0 to 6 percent slopes	A
SpC	Spinks loamy, 0 to 6 percent slopes	A
SpD	Spinks loamy, 0 to 6 percent slopes	A

Table 1. Soil Types in Morrow Lake Watershed.

Morrow Lake Watershed (Figure 1) is located in southwest corner of the state of Michigan, and has an area of 400 acres. It belongs to Kalamazoo phosphorus trading project (Figure 2). The surface water flows from south to north and then leads to the lake. The soil in the watershed is composed of Kalamazoo loam; Coloma loam sand; Spinks loamy sand and Oshtemo sandy loam (Table 1).

In the watershed, the land is primarily cultivated with pasture, corn, soybean, alfalfa, hay and wood. There is a village located in western area of the watershed, and a horse yard feedlot (30 horses) in the eastern area of watershed. Freeway 94 passes through the watershed from east to west. Due to steep land slopes over of 8%, and combines with agricultural activities, the soil erosion and fertilizer runoff pollution problems are very significant.

AGNPS model was developed at United State Department of Agriculture – Agricultural Research Service (USDA – ARS) for evaluation of alternative agricultural management. AGNPS is a grid-based model where spatial variability is a function of cell size. AGNPS has characteristics of multipurpose use and strong calculating functions with three basic components: hydrology, soil erosion, and nutrients.

The hydrology component of AGNPS uses the Curve Number method that developed by USDA Soil Conservation Service (SCS) to compute the runoff for each cell. The runoff equation (Kang, 1998) is:

The nutrient components of AGNPS are based on Pollutant Loading (PL) computer model. The PL's predicted are: (1) water; (2) sediment by particle size class & source of erosion; and (3) chemicals-nitrogen, phosphorus, organic carbon, & pesticides. PL's are generated from land areas (cells) and routed through stream systems on a daily basis. Special land use components such as feedlots, gullies, field ponds, and point sources are included (USDA/AGNPS, 2001).

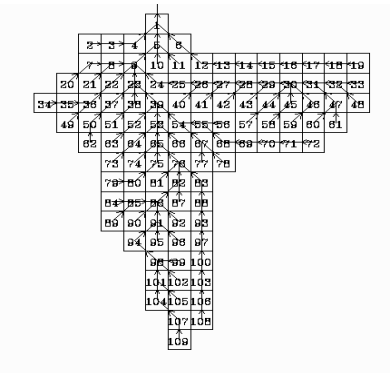

Figure 3. The AGNPS Model Grid Layout and Flow Net

$$Q = (P - I_a)^2 / (P - I_a) + S \quad \text{or} \quad Q = (P - I_a)^2 / (P + 0.8\,S) \quad (\text{when } I_a = 0.2S) \qquad (1)$$

Where: S = *potential maximum retention after runoff begins, (in)*

$$S = 1000 / CN - 10 \qquad (2)$$

Q = *runoff, (in),*
P = *rainfall, (in), and*
I_a = *initial abstraction, (in).*

The erosion and sediment component of AGNPS adopted the Universal Soil Loss Equation (USLE) model for calculating on-site soil erosion, in equation (3) (Kang, 1998):

$$A = RKLSPC \qquad (3)$$

Where:
A = *annual soil loss*
R = *rainfall factor*
K = *soil erosion factor*
L = *field slope length factor*
S = *field slope factor*
P = *supporting practice factor*
C = *cover and management factor*

Geographic Information System (GIS) is "an organized collection of computer hardware, software, geographic data, and personnel designed to efficiently capture, store, update, manipulate, analyze, and display all forms of geographically referenced information." (US Army Corps of Engineers, 2000). In this study, GIS tools are used to divide Morrow Lake watershed into 109 cells as grid data format, each cell area equaling 3.2 acres. GIS generated flow net, soil, and pollution loading provides input data for the model.

2. AGNPS Model Input Data

2.1 Input Data Preparation

The AGNPS 5.00 is designed for watersheds where over land flow dominates. The input data are composed of initial data of whole watershed and each cell.

The initial data are general information that are required for the whole watershed, including Area of each cell, Cell Number, Precipitation and Storm type. Storm type (there are 4 classes of storm type: I, IA, II, III) is used to calculate the peak discharge at a location in the watershed and also to determine the Energy Intensity (EI) for a storm to calculate sediment yield. Michigan is in the Type IA region. The value of Energy Intensity (EI) is the rainfall erosion index for the storm event used in universal soil loss equation (USLE).

There are 22 input data required for each cell. In the project, the watershed is divided into 109 grid cells**.**

The flow-net, flow direction, land slope and slope length are generated by means of Arc/Info and ArcView.

- The **SCS Curve Number** is hydrologic soil-cover complex number, is selected by III (wet land) adjusted curve numbers since Michigan is in Great Lake wet moisture condition.

- **K factor** is soil erosion factor, **C factor** is the cropping management factor and **P factor** is the conservation practice factor that all are used in **the universal soil loss equation** (USLE) and can be found in USDA Agricultural Handbook 537.

- The **Surface Condition Constant** is a value based on land use at the time of the storm to make adjustments for overland flow velocity.

- The **Chemical Oxygen Demand (COD)** factor is a value for the COD concentration in runoff, based on the land use in the cell.

- **Overland Manning's Coefficient** is the roughness coefficient for the predominant surface condition within the cell at the time of the storm, is selected according to AGNPS User Manual attached Table.

- The data of **Fertilizer** are input by two Steps: 1) the user puts a **Fertilizer Indicator** 0 or 1 to indicate whether fertilizer has been applied to the cell. 1) 0 indicates no fertilization (such as water or marsh) while 1 indicates fertilization being applied. 2) When the user puts 1, Fertilizer Level screen appears. The user should input a fertilizer level in the screen. The **Fertilizer Level** is a single digit (a value of 1 - 4) indicating the level of fertilization on the field. The number to be input and the associated levels are shown in fertilizer level screen. If user puts a value of 1 – 3 for a fertilizer level, the appropriate Nitrogen and Phosphorus application levels appear. If there is not a fertilization level that fits the amount of fertilization that has actually been applied in the cell. The user can put 4 and then input the amount of Nitrogen and Phosphorus that has actually applied in the cell. In the project, the general fertilizer application levels in Michigan have been considered. In order to test the sensitivity of fertilization level to Nitrogen and Phosphorus in sediment and runoff outputs, two additional trial levels of fertilizer were used. A low level (10% less than normal fertilizer level) and a high level (10% more than normal fertilizer level) have been tested.

- The **Point Fertilizer Source:** in the project**,** there is only one feedlot, horse yard, with 30 horses. Because the main objectives of the project were assessing of soil and phosphorus sediment, the other analyses such as pesticide were not emphasized.

2.2 AGNPS Data Input Model

AGNPS is a GIS based model. The data must be prepared for all cells of the watershed. It will be difficult to input data by hand for a large watershed. In this study, a data input model - **AGDAT** has been developed. The model can directly utilize AGNPS formatted data from GIS generated database. Figure 4 shows the flow chart of the input data model.

AGDAT can read "*.GIS" files. The files are groups of data that are digitized with GIS methods

and surrounded by **Negative Numbers,** such as
Table 2.

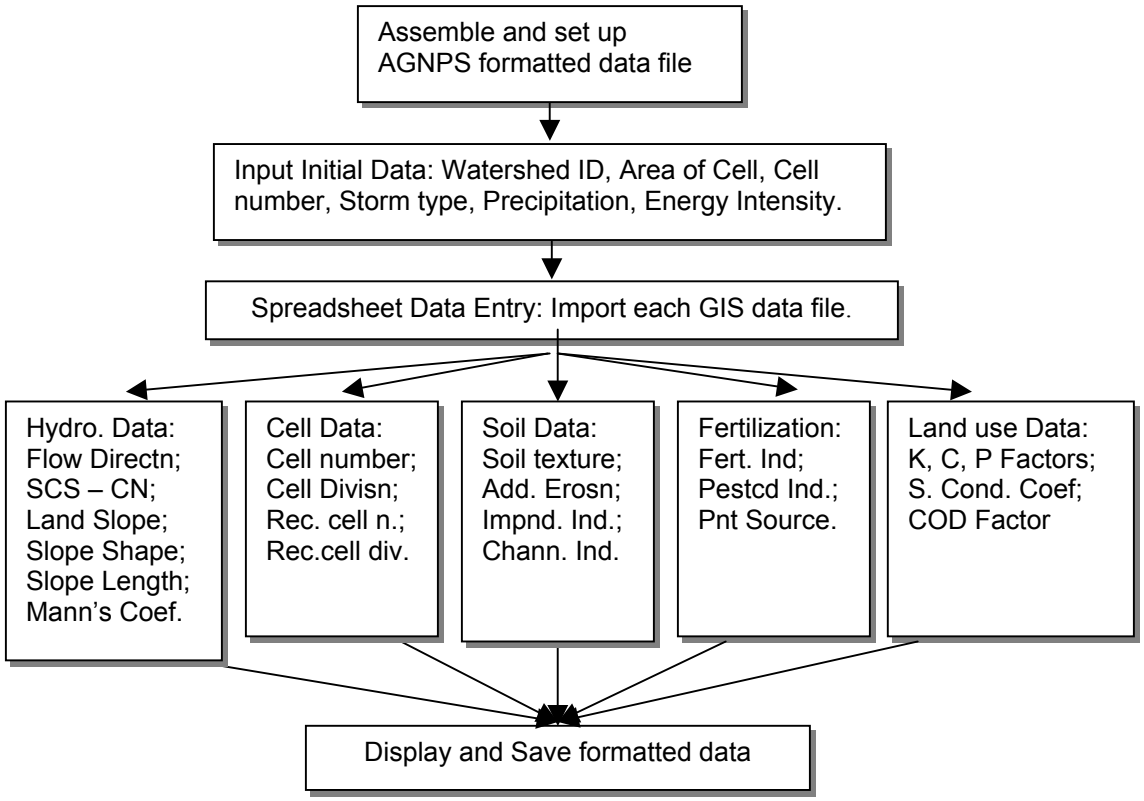

Figure 4. AGDAT Flow Chart

```
ncols         15
nrows         17
xllcorner     527774.5
yllcorner     526522.5
cellsize      373
NODATA_value  -9999
 -9999 780 780 780 780 780 780 780 780 780 780 -9999
 -9999 790 789.12 784.54 780.12 781.58 780 780 780 782.48 82.77 83.73 784.51 -9999
 -9999 814.78 813.07 794.24 804.07 803.00 792.78 792.37 789.54 791.08 788.81 789.83 794.49 792.25 -9999
 -9999 850 850 835.96 811.93 841.93 824.81 820.83 813.30 808.81 807.46 805.97 806.00 807.36 813.85 -9999
 -9999 859.04 850 840 837.30 823.78 822.76 855.86 860 860 858.78 843.75 842.80 842.68 829.17 843.15 -9999
 -9999 860 859.37 860 839.60 830.52 843.77 850 860 864.50 870 870 867.17 868.53 -9999
 -9999 870 870 870 846.88 860 856.59 862.29 865.80 870 870 870 -9999
 -9999 880 870 860 859.81 879.79 880 -9999
 -9999 871.64 870 870.51 877.67 876.19 -9999
 -9999 870 870 860 861.79 872.87 -9999
 -9999 877.15 870 866.04 870 869.61 -9999
 -9999 868.62 869.99 871.31 872.10 -9999
 -9999 869.43 873.78 874.58 -9999
 -9999 869.32 876.24 877.06 -9999
 -9999 873.65 878.69 879.54 -9999
 -9999 880 880 -9999
 -9999 880 -9999
```

Table 2. Arc/Info digitized Contour line data

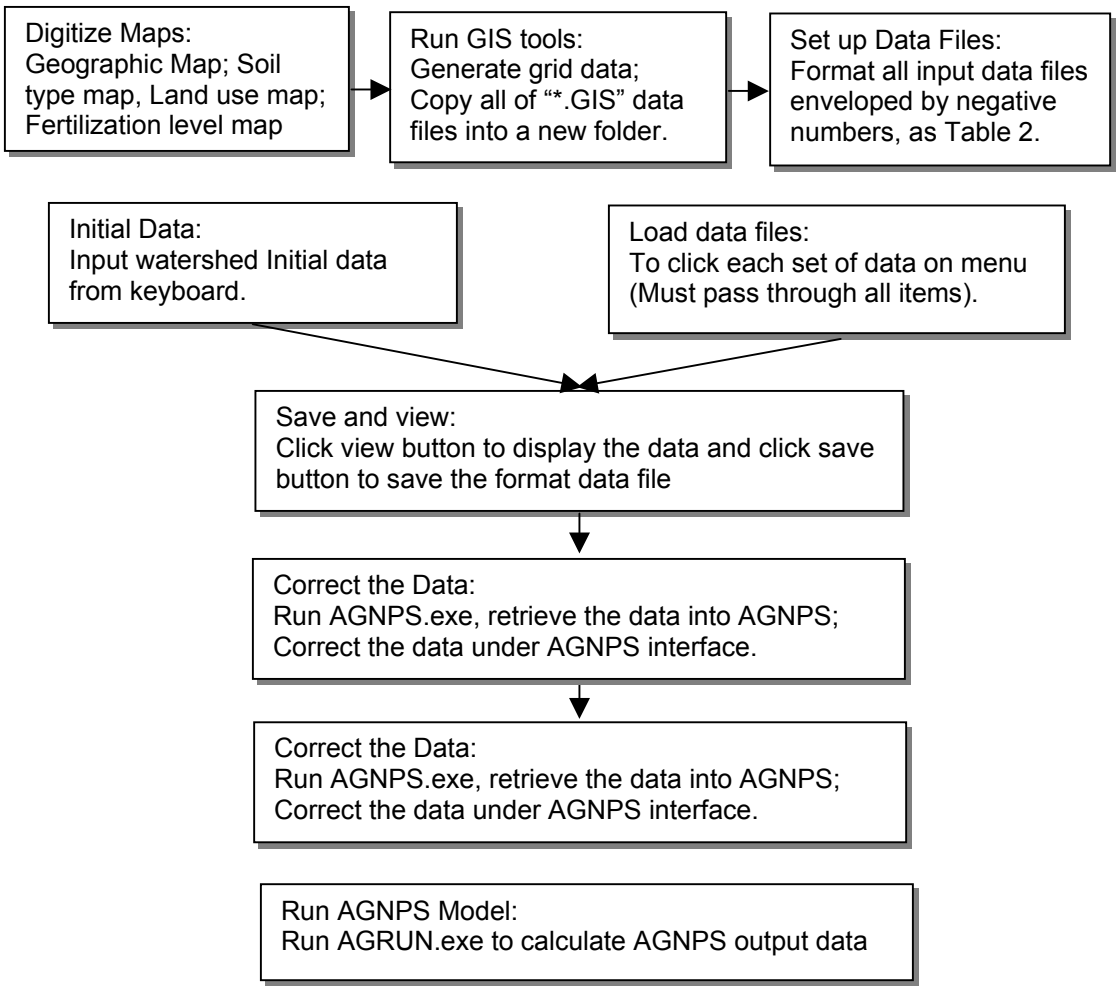

Figure 5. The procedure of running AGNPS

For running the model AGDAT, the user should set up a new folder and copy all of "*.GIS" files into the folder. The process steps are shown in Figure 5.

3. Watershed AGNPS Results

The AGNPS study of Morrow Lake Watershed has been carried out for several conditions. An examination of several model outputs is discussed below.

Phosphorus Concentration and Sediment: As stated in the previous sections, the main problems of Morrow Lake Watershed are nutrient and sediment runoff. The phosphorus in runoff water occurs due to residual P in soil and P fertilizer applications (Figure 6). Phosphorus sediment loss generated within a cell depends on the total mass of soil erosion, soil phosphorus concentration and enrichment ratio (Baker, 1995).

In Figure 7, there are two zones with high phosphorus sediment. The first zone is located in Cells 51, 52 and 63 (farmland and village). The flow with fertilizer contaminants will converge to the outlet of these cells. The second zone is in cells 46, 60 and 61. This is due to horse yard pollution.

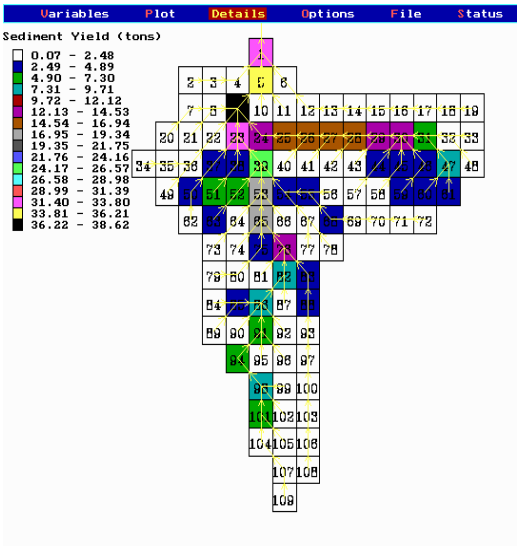

Figure 6. Sediment Yield (tons)

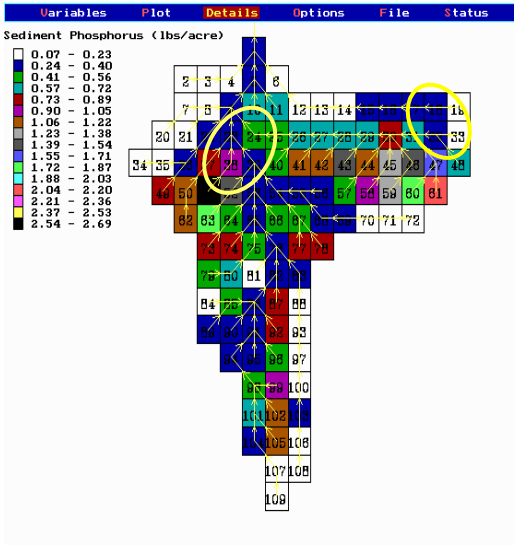

Figure 7. Sediment Phosphorus (lbs/acre)

4. Sensitivity Test and Discussion

In general, AGNPS software can calculate water quality, soil erosion and non-point pollution. However, the reasonableness of calculated results needs to be investigated. Also, simplifying the calculation process of AGNPS input data (i.e. AGDAT) for fast pollution forecasts is another focus in this paper. In order to further analyze AGNPS application for non-point source pollution assessment, several trials with different AGNPS parameters were conducted.

4.1 Soil Sediment and Phosphorus Change Following Precipitation

Both soil and phosphorus sediment increases rapidly with increasing rainfall values. The curves in Figure 8 show that rainfall is a factor strongly effecting soil and phosphorus sediment. The curves are taken in cells 1, 5 and 9 (the out flow cells of the watershed). The curves look like an exponential function. The three curves increase in value following rainfall increases. In Cell 1, phosphorus sediment increases more slowly because there was interval flow added which diluted phosphorus concentration.

4.2 The Sensitivity Test of AGNPS Parameters

In order to test the sensitivity of AGNPS parameters, it is important to re-test following parameter changes. Eight parameters that related to soil and phosphorus sediment including K factor (KFc), C factor (CFc), P factor (PFc), COD (COD), Fertilizer application level (Fert), SCS curve number (SCS), Soil texture (SlTx) and Surface condition constant (Surf) have been tested respectively.

Phosphorus sediment is affected by K, C, P factors, SCS curve number and soil texture (SlTx). It is most strongly affected by SITx, as shown in Figure 9.

Soil sediment yield is calculated in AGNPS model with the Universal Soil Loss Equation (USLE). In formula (3), the soil loss is the function of rainfall, soil erodibility, field slope, and land use. It is most

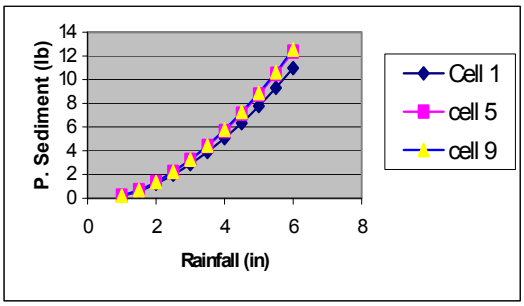

Figure 8. P. Sediment in Different Rainfall (lbs)

sensitive to the SCS curve number (Figure 9).

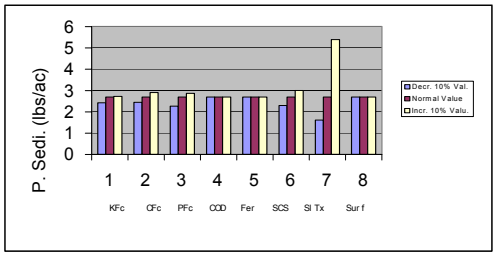

Figure 9. The sensitivity test of P. sediment vs. Parameters change (in Cell #51)

4.3 Establishing a NPS Forecast System

The variables of AGNPS may be divided into 3 categories: 1. Long term data (topography, land scope, soil types), will not change annually. 2. Seasonal data (crops, fertilizer application level, land use) will change according to human activities and will rarely change during a season. 3. Temporary data (precipitation) will change frequently according to rainfall and weather variations.

The evaluations were conducted to determine whether calculation process could be simplified to meet pollution forecasts. The results determined that pollution forecast could be predicted by utilizing temporary variables (i.e. precipitation etc) in the AGNPS model.

5. Conclusions

Non-point source pollution has been identified as the major pollution of water and soil resources environment. Although many efforts have been initiated to reduce agricultural NPS pollution, it remains a problem. The AGNPS model is designed for assessing agricultural non-point source pollution. It can be used to predict water resources runoff, NPS pollution and soil erosion within and from watersheds. AGNPS is a cell-based model for which it is difficult to prepare input data. This study developed an input model AGDAT for AGNPS 5.0. It can directly convert GIS format data into AGNPS data. This study used AGNPS for estimating NPS pollution on Morrow Lake watershed. In order to analyze how the watershed NPS change in different Situations and conditions, several trials with different precipitation values have been calculated. All of computations provided reasonable results. The results showed that pollution forecast could be predicted by varying temporary variables (i.e. precipitation etc) in the AGNPS model.

Correspondence to:
Yongsheng Ma
School of conservancy and civil engineering
Northeast Agricultural University
Harbin, Heilongjiang 150030, China
Telephone: 01186-451-5511-7878
Fax: 011-86-451-5191502
Email: ysma66@yahoo.com.cn
yongshengma@hotmail.com

Yongsheng Ma is presently working in the School of Conservancy and Civil Engineering, Northeast Agricultural University, Harbin, Heilongjiang 150030, China.

References:

Dressing SA. Non-point Source Management System Software: A Tool for Tracking Water Quality and Land Treatment, U.S. Environmental Protection Agency, Washington DC, 1999; http://www.epa.gov/owow/watershed/proceed/dressing.htm.

Joubert L. Watershed Non-point Assessment and Nutrient Loading Using the Geographic Information System – Based MANAGE Method, University of Rhode Island, Natural Resources Science, Kingston, RI, 1999; http://ww.epa.gov/owow/watershed/proceed/joubert.html.

Kang YT. A Watershed Based Optimization Approach For Agricultural Non-point Source Pollution Management, Institute of Water Research, Michigan State University, East Lansing, MI, 1998;24-30.

Patwardhan AS. Modeling Nutrients From The Minnesota River Watershed, Publication of Environmental Protection Agency, 1999; http://www.epa.gov/owow/watershed/proceed/patwardh.htm.

US Army Corps of Engineers. Geographic Information Systems (GIS) Definition, 2000; http://www.nww.usace.army.mil/gis/definition.htm.

USDA, National Sedimentation Laboratory AGNPS- Pollutant Loading (PL) Computer Model, 2001; http://www.sedlab.olemiss.edu/AGNPS.html.

Yagow G. Procedures for Indexing Monthly NPS Pollution Loads from Agricultural and Urban Fringe Watersheds, Publication of Environmental Protection Agency, 1999;http://www.epa.gov/owow/watershed/Proceed/yagow.htm.

Young RA. Agricultural Non-point Source Pollution Model, Version 5.00 AGNPS User's Guide, USDA-Agricultural Research Service, 1994:1-5.

Zhang Y, et. al. Nitrogen Transformation, Transport and Leaching in Drained Land, China university of geo-sciences, Wuhan, China, 1997:45-8.

Applying PPE Model Based on RAGA in the Investment Decision-Making of Water Saving Irrigation Project

Qiang Fu, Hong Fu

School of Water Conservancy & Civil Engineering, Northeast Agricultural University, Harbin, Heilongjiang 150030, China, fuqiang100@371.net

Abstract: Through applying PPE model based on RAGA in the investment decision-making of water saving irrigation project, this study turns multi-dimension data into low dimension space. So the optimum projection direction can stand for the best influence to the collectivity. Thus, the value of projection function can evaluate each item good or not. The PPE model can avoid jamming of weight matrix in the method of fuzzy synthesize judgement, and obtain better result. The authors want to provide a new method and thought for readers who engaged in investment decision-making of water saving irrigation and other relative study. [Nature and Science 2003;1(1):57-61].

Key words: RAGA; PPE; water saving irrigation; investment; decision-making

1. Introduction

At present, more and more water-saving irrigation demonstration items have been developed broadly in many areas. Through carrying out these items, we can spread some water saving irrigation techniques according to local conditions, and use the water resource continually. In China, government has invested some items. So, many units compete to bid. Which unit should be chosen by decision-making to investing will be influenced by many factors. And that, many factors can't be quantitative change entirely. Thus, how to making a scientific decision is very important (Yan, 2000). At present, the method of fuzzy synthetic judgement has been applied broadly. But this method is short of the best criterion of system evaluation, and it will appear many errors or give us abnormal result. The method of giving weight subjectively and gray system evaluation has definite artificial factors. The evaluated method based on entropy calculates the weight of each index according to the mutation degree among indexes. This method can avoid the shortcoming of giving weight subjectively in a certain extent. But in fact, each weight will have the average value or the same value (Jin, 2000). The essential of synthetic evaluation is to handle with high dimension data. That is to reduce the dimension number. The weight matrix given by experts is corresponding to the projection value in low-dimension space of each index. The evaluation will be run in low-dimension space. But we can't ensure whether the weight matrix is the best projection in low-dimension space. Thereby, the author put forward a new technique named projection pursuit (PP) to reduce the dimension number. Because it is very difficult to optimize many parameters at one time, the author applies genetic arithmetic (GA) that is fit for optimizing the multi-dimension and total scope to combine with PP model. Through optimizing the parameters at the same time with GA, the author can complete the decision process of water saving irrigation investment.

2. Projection Pursuit Evaluation (PPE) Model

2.1 Brief Introduction of PP Model

The main characteristics of PP model are as follows. Firstly, PP model can handle the difficulty named dimension disaster, which has been brought by high-dimension data. Secondly, PP model can eliminate the jamming, which are irrespective with data structure. Thirdly, PP model provides a new approach to handle high-dimension problem using one dimension statistics method. Fourthly, PP method can deal with non-linearity problem (Fu, 2003; Jin, 2000; Zhang, 2000).

2.2 Step of PPE Modeling

The step of building up PPE model includes 4 steps as follows (Fu, 2003; Jin, 2000; Zhang, 2000):

Step 1: Normalizing the evaluation indexes set of each sample. Now, we suppose the sample set is $\{x^*(i,j)|i=1\sim n, j=1\sim p\}$. $x^*(i,j)$ is the index value of j and sample of i. n ——the number of sample. p ——the number of index. In order to eliminate the dimension influence and unite the change scope of each index value, we can adopt the following formulas to

The financial support provided by National "863" High-Technique Programme (No. 2002AA2Z4251-210041).

normalize the data.

$$x(i,j)=\frac{x^*(i,j)-x_{min}(j)}{x_{max}(j)-x_{min}(j)} \quad (1—a) \text{ or:}$$

$$x(i,j)=\frac{x_{max}(j)-x^*(i,j)}{x_{max}(j)-x_{min}(j)} \quad (1—b)$$

In formula: $x_{max}(j)$ and $x_{min}(j)$ stand for the max and the min of j index value. $x(i,j)$ is the index list after moralization.

Step 2: Constructing the projection index function $Q(a)$. PP method is to turn p dimension data ($\{x^*(i,j)|j=1\sim p\}$) into one dimension projection value $z(i)$ based on projection direction a.

$$a=\{a(1),a(2),a(3),\cdots,a(p)\},$$

$$z(i)=\sum_{j=1}^{p}a(j)x(i,j) \qquad (i=1\sim n) \quad (2)$$

Then, we can classify the sample according to one-dimension scatter figure of $z(i)$. In formula (2), a stand for unit length vector.

Thus, the projection index function can be expressed as follows:

$$Q(a)=S_z D_z \quad (3)$$

In formula: S_z ——the standard deviation of $z(i)$, D_z ——the partial density of $z(i)$.

$$S_z=\sqrt{\frac{\sum_{i=1}^{n}(z(i)-E(z))^2}{n-1}} \quad (4)$$

$$D_z=\sum_{i=1}^{n}\sum_{j=1}^{n}(R-r(i,j))\cdot u(R-r(i,j)) \quad (5)$$

In formula (4) and (5), $E(z)$ ——the average value of series $\{z(i)|\,i=1\sim n\}$; R ——the window radius of partial density, commonly, $R=0.1S_z$. $r(i,j)$ ——the distance of sample, $r(i,j)=|z(i)-z(j)|$; $u(t)$ ——a unit jump function, if $t\geq 0$, $u(t)$ =1,if $t<0$, $u(t)$ =0.

Step 3: Optimizing the projection index function. When every indexes value of each sample have been fixed, the projection function $Q(a)$ change only according to projection direction a. Different projection direction reflects different data structure characteristic. The best projection direction is the most likely to discovery some characteristic structure of high-dimension data. So, we can calculate the max of $Q(a)$ to estimate the best project direction.

Function: $Max: Q(a)=S_z\cdot D_z \quad (6)$

Restricted condition: $s.t:\sum_{j=1}^{p}a^2(j)=1 \quad (7)$

Formula (6) and (7) are a complex non-linearity optimization, which take $\{a(j)|\,j=1\sim p\}$ as optimized variable. Traditional method is very difficult to calculate. Now, we adopt RAGA to handle the kind of problem.

Step 4: Classification. We can put the best projection direction a^* into formula (2), then we can obtain the projection value of each sample dot. Compare $z^*(i)$ with $z^*(j)$, if $z^*(i)$ is closer to $z^*(j)$, that means sample i and j are trend to the same species. If we dispose $z^*(i)$ from big to small, we can obtain the new sample list from good to bad.

3. Real Coding Based Accelerating Genetic Algorithm (RAGA)

3.1 Brief Introduction of GA

Genetic algorithm has been put forward by Professor Holland in USA. The main operation includes selection, crossover and mutation (Jin, 2000; Zhou, 2000).

3.2 Eight Steps of RAGA The coding mode of traditional GA adopted binary system. But binary system coding mode has many abuses. Through consulting the literature (Jin, 2000; Fu, 2003), the author put forward a new method named real coding based accelerating genetic algorithm (RAGA). RAGA includes 8 steps as follows. For example, we want to calculate the following best optimization problem.

Max : f(X)

s.t. : $a_j \leq x_j \leq b_j$

Step 1: In the scope of $[a_j,b_j]$, we can create N group uniformity distributing random variable $V_i^{(0)}(x_1,x_2,\cdots x_j,\cdots x_p)$. $i=1\sim N$, $j=1\sim p$. N——the group scale. p ——the number of optimized parameter.

Step 2: Calculate the target function value. Putting the original chromosome $V_i^{(0)}$ into target function, we can calculate the corresponding function value $f^{(0)}(V_i^{(0)})$. According to the function value, we dispose the chromosome from big to small. Then, we obtain $V_i^{(1)}$.

Step 3: Calculate the evaluation function based on order expresses as $eval(V)$. The evaluation function gives a probability for each chromosome V. It makes the probability of the chromosome be selected to fit for the adaptability of other chromosomes. The better the adaptability of chromosome is, the much easier it will be selected. Now, if parameter $\alpha\in(0,1)$, the evaluation function based order can be expresses as follows:

$$eval(V_i)=\alpha(1-\alpha)^{i-1},\ i=1,2,\cdots,N$$

Step 4: Selecting operation. The course of selecting is based on circumrotating the bet wheel N times. We can select a new chromosome from each rotation. The bet wheel selects the chromosome according to the adaptability. We obtain a new group $V_i^{(2)}$ after selecting.

Step 5: Crossover operation. Firstly, we define the parameter P_c as the crossover probability. In order to ensure the parent generation group to crossover, we can repeat the process from $i=1$ to N as follows. Create random number r from [0，1]. If $r<P_c$, we take V_i as parent generation. We use $V_1^{'},V_2^{'},\cdots$ to stand for male parent that is selected. At the same time, we divide the chromosome into random pair based on arithmetic crossing method. That is as follows:

$X=c\cdot V_1^{'}+(1-c)\cdot V_2^{'}$ $\quad$ $Y=(1-c)\cdot V_1^{'}+c\cdot V_2^{'}$

c ——a random number from (0,1).

We can obtain a new group $V_i^{(3)}$ after crossover.

Step 6: Mutation operation. Define the P_m as mutation probability. We select the mutation direction d randomly from R^n. If $V+Md$ isn't feasible, we can make M a random number from 0 to M until the value of $V+Md$ is feasible. M is an enough big number. Then, we can use $X=V+Md$ replace V. After mutation operation, we obtain a new group $V_i^{(4)}$.

Step 7: Evolution iteration. We can obtain the filial generation $V_i^{(4)}$ from step 4 to step 6, and dispose them according to adaptability function value from big to small. Then, the arithmetic comes into the next evolution process. Thus, the above steps have been operated repeatedly until the end.

Step 8: The above seven steps make up of standard genetic arithmetic (SGA). But SGA can't assure the whole astringency. The research indicates that the seeking optimization function of selecting and crossover has wear off along with the iteration times increasing. In practical application, SGA will stop to working when it is far away from the best value, and many individuals are conformed or repeated. Enlightening by the reference (Xiang, 2000), we can adopt the interval of excellence individual during the course of the first and the second iteration as the new interval. Then, the arithmetic comes into step 1, and runs SGA over again to form accelerate running. Thus, the interval of excellence individual will gradually reduce, and the distance is closer to the best dot. The arithmetic will not stop until the function value of best individual is less than a certain value or exceed the destined accelerate times. At this time, the currently group will be destined for the result of RAGA.

The above 8 steps make up of RAGA.

3.3 PPE Model Based on RAGA

Take projection function $Q(a)$ as the most target function in the PPE model and the projection $a(j)$ of each index as optimized variable. Through running the 8 steps of RAGA, we can obtain the best projection direction $a^*(j)$ and projection value $z(i)$. To compare the $z(i)$ each other, we can obtain the evaluated result. At the same time, if we build PPE model about the soil grade evaluation standard according to the above steps, we will obtain the best projection value $Z(i)$. Then, through comparing the distance between $z(i)$ and $Z(i)$, the smallest distance between any two samples, then, the number i is the soil sample grade.

4. Application Example

Now, we use the data of Yan (2000) and Fu (2002) to give an example. The evaluated indexes about cost and benefit indexes are investment, self-investment, economy benefit, water saving rate, internal yield, benefit-cost ratio, years of investment and repayment, and so on. The factors that will influence the decision-making in the demonstration item of water saving irrigation are shown in the follows. These are degree of lacking water, measure of water saving, crop, society benefit, difficulty of construction, demonstrate function, construction enthusiasm and so on (Table 1, Table 2) (Yan, 2000; Fu, 2002).

Table 1. The Economy Evaluated Indexes in the Item of Water Saving Irrigation

County Name	1	2	3	4	5	6
investment per hectare（yuan/hm^2）	22800	11325	19200	6750	37950	3450
self-investment（yuan/hm^2）	5700	4650	7200	3450	9300	2700
economy benefit（yuan/hm^2）	5250	3450	4800	1800	6300	2250
water saving rate（%）	42	18	30	10	35	10
internal yield（%）	15	17	14	12	12.5	21
benefit-cost ratio	1.5	1.8	1.9	1.7	1.1	1.9
investment and repayment years（year）	8.6	6	7.8	5.5	8.8	4
project life（year）	20	10	15	8	16	5

Table 2. The Result After Handling the Evaluated Indexes in the Item of Water Saving Irrigation

	County Name	1	2	3	4	5	6
1	investment per hectare	0.4391	0.7717	0.5435	0.9043	0	1.0
2	Self-investment	0.4545	0.2955	0.6818	0.1136	1.0	0
3	economy benefit	0.7667	0.3667	0.6667	0	1.0	0.1
4	water saving rate	1.0	0.25	0.6250	0	0.0556	1.0
5	internal yield	0.3333	0.5556	0.2222	0	0.0556	1.0
6	Benefit-cost ratio	0.5	0.875	1.0	0.75	0	1.0
7	investment and repayment years	0.0417	0.5833	0.2083	0.6875	0	1.0
8	project life	1.0	0.3333	0.6667	0.2	0.7333	0
9	degree of lacking water	0.9	0.8	0.6	0.8	0.4	0.5
10	measure of water saving	0.6	0.5	0.8	0.4	0.3	0.7
11	Crop	0.8	0.6	0.9	0.7	0.6	0.9
12	society benefit	0.8	0.6	0.7	0.8	0.8	0.7
13	difficulty of construction	0.8	0.6	0.8	0.5	0.6	0.9
14	demonstrate function	0.8	0.7	0.6	0.8	0.6	0.6
15	Construct enthusiasm	0.8	0.7	0.6	0.8	0.9	0.6

Now, we can build up PPE model based on the data in the Table 1 and Table 2. During the course of RAGA, the parent generation scale is 400 ($n=400$). The crossover probability is 0.80 (p_c =0.80). The mutation probability is 0.80 (p_m =0.80). The number of excellence individual is 20 (α =0.05). Through accelerating 12 times, we can obtain the best projection value and it is 0.2618. The best projection direction: a^*=（0.0558 ,0.4213 ,0.3816 ,0.4150 ,0.1199 ,0.1080 , 0.0459 , 0.4881 , 0.1117 , 0.2700 , 0.1677 , 0.1803 , 0.1715 ,0.1535 ,0.1903）. Putting a^* into formula (2), we can obtain the projection value of each county. It is $z^*(j)$=（2.4845，1.5680，2.2254，1.1283，2.0254，1.2504）. If we arrange $z^*(j)$ in big or small, we can know which county is the best. The result is P1>P3>P5>P2>P6>P4. Now, the synthetic benefit of P1 county is the best. P3 county and P5 county are the next. P2 county and P6 county are the following. P4 county is in the end. The PPE model has the same as literature (Jin, 2000), which applied fuzzy synthetic evaluation.

We can analyze the influence degree of each evaluated index according to the best projection direction. We arrange the a^* in big to small, then, the order numbers are 8，2，4，3，10，15，12，13，11，14，5，9，6，1，7. They are project life, self-investment, water saving rate, economy benefit, measure of water saving, construct enthusiasm, society benefit, difficulty of construction, crop, demonstrate function, internal yield, degree of lacking water, benefit-cost ratio, investment per hectare, investment and repayment years.

It is obvious that the PPE result can reflect the practical condition basically. The contribution rate is consistent with the weight in fuzzy synthetic evaluation. The relation among the samples and the best projection direction see also to Figure 1 and Figure 2.

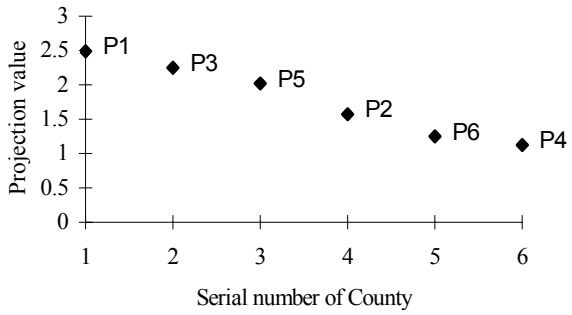

Figure 1. The Spread of Projection Value for Each County

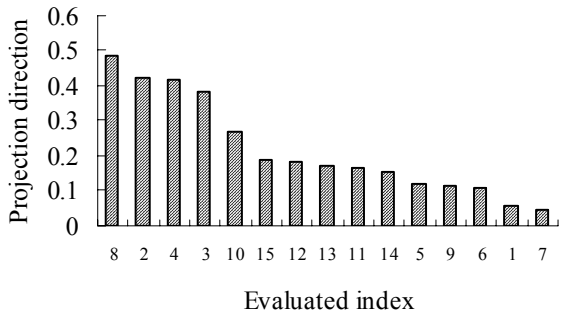

Figure 2. The Compositor of Projection Direction for Each Index

5. Conclusions

(1) The authors improved on SGA, and put forward a new method named RAGA. Through reducing the interval of excellence individual we accomplished the accelerate process. The method of RAGA can realize quick convergence and seek the best result in the whole

scope.

(2) Combing RAGA with PPE model, through using RAGA to optimize the many parameters in the PPE model, we can obtain the best projection direction of evaluation index of each county. The process of PPE modeling has been predigested. PPE model can be used in many other fields.

(3) Through applying the PPE model based on RAGA to the investment decision-making in the item of water saving irrigation, the authors do not only know which county is the best, but also obtain the important degree of each evaluated index. The result is good. Furthermore, the PPE model based on RAGA can be applied on some other research field about classification and evaluation.

Correspondence to:
Qiang Fu
School of Water Conservancy & Civil Engineering
Northeast Agricultural University
Harbin, Heilongjiang 150030, China
Telephone: 01186-451-5519-0298
Cellular phone: 01186-13936246215
E-mail: fuqiang100@371.net

References

Fu Q, Liang C. Modeling and optimize technique of water saving irrigation system. Sichuan Technology Publishing Company, Chengdu, Sichuan, China. 2002:149-150

Fu Q, Xie YG, Wei ZM. Application of projection pursuit evaluation model based on real-coded accelerating genetic algorithm in evaluating wetland soil quality variation in the Sanjiang Plain, China. Pedosphere. 2003;13(3):249-56.

Jin J, Ding J. Genetic arithmetic and its application to water science. Sichuan University Publishing Company, Chengdu, Sichuan, China. 2000:42-7.

Xiang J, Shi J. The statistics method of data processing in the non-linearity system. Science Publishing Company, Beijing, China. 2000:190-2.

Yan L. Applying fuzzy synthetic evaluation model on the investment decision-making in the item of water saving irrigation. Water Saving Irrigation 2000;4:11-3.

Zhang X. Projection pursuit ant its application to water resources. Sichuan University Publishing Company, Chengdu, Sichuan, China. 2000:67-73.

Zhou M, Sun S. The theory of genetic arithmetic and its application. National Defense Industry Publishing Company, Beijing, China. 2000:4-7, 37-8.

Theory and Methods of Drought System Analysis

Zhenmin Zhou, Zhiliang Wang

North China College of WRHP, Zhengzhou, Henan 450045, China, zzm1022@yahoo.com.cn

Abstract: Based on analysis on statistic parameters including mean, coefficient of variation and serial correlation of drought, the foresaid parameters on drought duration and severity were studied. The extreme drought duration and severity expressions were developed. Taking Dongzhou Reservoir as an example, the related design parameters were calculated. [Nature and Science 2003;1(1):62-66].

Key Words: drought frequency; drought duration; drought severity; truncated level

1. Introduction

Droughts have attracted the much attention in different areas at the present. The sequences of the rainfall or stream flow that are used to characterize droughts are known as drought variables. In general, droughts are measured in terms of deficiency in the rainfalls or streams flows below a predefined reference level. The cumulative deficit during a drought spell is known as the severity, the reference level for identification of the droughts, or for quantifying the severity. It is termed the truncation level and is taken to be equal to the long-term mean of the sequence of the drought variable.

From the point of view of creating provisions for meeting the exigencies during a drought spell, the most important parameters of concern are the longest duration and the largest severity for a desired return period of T years, and are termed as extreme duration and severity in this paper. The sequence representing the drought could be distributed normally or may have a skewed distribution. The simple type of pdfs used for modeling the annual rainfall and runoff sequences are normal, log-normal and gamma, all with two parameters. Likewise, the simplest kind of dependence is Markovian, represented by the lag-one serial correlation coefficient ρ. For a given place or a basin the reliable statistics available for annual rainfall and stream flow are mean, coefficient of variation and lag-one serial correlation coefficient. One might wish to know the answers to the following questions based on the above readily available information. (1) How does the coefficient of variation affect the extreme duration and severity characteristics? (2) How do the skewness (pdf of the drought variable sequence) and the dependence (ρ) influence the extreme values of the aforesaid parameters? (3) Is there any formula terms of the largest severity and the return period that may appear parallel to the flood frequency formula, commonly cited in the hydrological texts? The flood frequency formula is used for design of the runoff handling structure. The drought frequency formula should be usable for the design of water storage structures for the drought periods. Therefore, based on statistic theory and analysis methods, the research was carried out on above problems.

2 Stochastic Analysis of Extreme Drought Duration and Severity

2.1 Evaluation of Drought Probability Quantile Q

If a time-series x_i (modular form, mean=1 and standard deviation=σ_χ) is truncated at the mean level x_m=1, then the event of excesses ($x_i > x_m$) and deficits ($x_i < x_m$) would emerge along the time axis. The truncation level can be assigned a probability quantile as q=P ($x_i \leqslant x_m$=1), where q is the probability of drought corresponding to the truncation level x_m=1 and P(…) stands for the notation of probability. For normal pdf, the relationship between q and the truncation level can be obtained by standardizing the sequence x_i into z_i (z_i has mean=0 and σ_z=1 and a standard normal distribution). Thus, for the normal pdf (coefficient of skewness, C_s=0) the value of z_i (corresponding to x_m=1) is 0, and q=p($x_i \leqslant 1$)=P($z_i \leqslant 0$)=0.5 is obtained straightforwardly from the standard normal probability tables or through the following standard normal probability integral

$$q = p(z \leq z_m) = \frac{1}{\sqrt{2\pi}} \int_{-\infty}^{z_m} \exp(-0.5 z^2) dz \quad (1)$$

The value of z_i corresponding to x_m=1 for normal pdf is referred to as z_m(=0) in the text.

For the log-normal distribution, the value of the truncation level z_{ml}, equivalent to the mean of the sequence x_m=1, can be worked out using the following explanation. If x_i is log-normal variate with a mean x_m and standard deviation σ_χ (coefficient of variation=C_v), ln(x_i) is normal with a mean μ_1 and standard deviation σ_1. The x_i sequence can be standardized as $u_i = (x_i - x_m)/\sigma_x$, where the U_i sequence has mean=0 and standard deviation=1.

Therefore x_i can be expressed in terms of mean (x_m) and coefficient of variation (C_v) as follows

$$x_i = x_m (1 + C_v \cdot u_i) \quad (2)$$

As the variate $\ln(x_i)$ can also be standardized, the new normal standardized variate (designated as Z_i) can be expressed as

$$z_i = \frac{\ln(x_i) - \mu_1}{\sigma_1} = \frac{\ln[x_m(1 + c_v \cdot u_i)] - \mu_1}{\sigma_1} \quad (3)$$

At the mean level of x_i sequence, $u_i = 0$, hence z_i, designated as z_{ml}, can be expressed using equation (3) as

$$z_{ml} = \frac{\ln(x_m) - \mu_1}{\sigma_1} \quad (4)$$

It is known that moments of x_i and $\ln(x_i)$ are related by the following relationships

$$\mu_1 = \ln(x_m) - 0.5\sigma_1^2 \quad (5)$$

$$\sigma_1^2 = \ln(1 + C_v^2) \quad (6)$$

Using equations (5) and (6), equation (4) can be simplified as

$$z_{ml} = \frac{\ln x_m - (\ln x_m - 0.5\sigma_1^2)}{\sigma_1}$$

$$= 0.5\sigma_1 = 0.5[\ln(1 + C_v^2)]^{0.5} \quad (7)$$

Note the modular form, hence $x_m=1$ in all the above relationships. Since z_{ml} is a standard normal variate, the value of the probability quantile of the equation $q = P(z_i \le z_{ml})$ can be obtained from the standard normal probability tables or computed by the numerical integration of the standard normal function shown in equation (1) with z_m replaced by z_{ml}. Looking at the structure of equation (7), it is obvious that z_{ml} is great than 0 for the mean of the sequence x_i (i.e. $x_m=1$). The value of q for the log-normally distributed sequence will always be greater than 0.5 and is dependent on the C_v of the sequence. The effect of skewness is implicitly included in C_v. As for the log-normal pdf, C_s and C_v are functionally related through the following relationship

$$C_s = 3C_v + C_v^3 \quad (8)$$

The same analysis can be extended to the two-parameter gamma distribution. If γ_i is the standardized gamma variate [$\gamma_i = (x_i - 1)/C_v$], then z_i, i.e. the standardized normal variate, is related approximately to γ_i through the following linkage relationship

$$z_i = \frac{6}{c_s}\left[(0.5C_s \cdot \gamma_i + 1)^{0.333} - 1\right] + \frac{C_s}{6} \quad (9)$$

For a two-parameter gamma variable $C_s = 2C_v$, equation (9) can be reduced to

$$z_i = 3C_v^{-1}\left[x_i^{0.333} - 1\right] + 0.333C_v \quad (10)$$

Therefore, a modular gamma variate can be transformed into a standard normal variate using equation (10) and at the mean level, $x_m = 1$, $z_{m\gamma} = 0.333\ C_v$. Note the value of z_i is designated as $Z_{m\gamma}$ for $x_i=1$. That is, if the drought variable is gamma distributed, at the truncation level equal to the mean of the sequence the equivalent standard normal variates $Z_{m\gamma}$ will be 0.0666, 0.1332, 0.2098, 0.2664 and 0.333 for C_v values of 0.2, 0.4, 0.6, 0.8 and 1, respectively. For a normally distributed drought variable all of them will be equal to 0, regardless of the C_v. Therefore, the probability quantile for a gamma-distributed drought variable could be worked out for the desired value of C_v by consulting the standard normal probability tables or through integration of equation (1), replacing z_m by $Z_{m\gamma}$. Note here again that $Z_{m\gamma} > 0$ for $x_m=1$. For example, for a gamma-distributed drought variable with $C_v=0.4$, $Z_{m\gamma} = 0.13$ and q = 0.55 at the level of truncation equal to the mean level of the sequence, against 0.5 for a normally distributed drought variable, and 0.58 for a log-normally distributed variable. Values of q for normal, two-parameter gamma and log-normal pdfs for various C_v values are shown in Table 1.

2.2 Modeling Extreme Drought Duration

Any uninterrupted sequence of deficits can be regarded as a drought length (duration) equal to the number of deficits in the sequence, designated by L (L=1, 2, 3, ... , j). Each drought duration is associated with deficit sum D, i.e. the sum of the individual deficits, d_1, d_2, d_3, ... , in the successive epochs of the spell. This deficit sum is termed as drought standardized sequence of the drought variable. The actual severity (D) is functionally related to the standardized severity (S) through the relationship $D = \sigma_X \cdot S$ (Guven, 1983). The term S/L is termed the drought intensity or magnitude. One can expect n (n=0, 1, 2, 3, ... , i) drought spells (runs) over a period of "T" years and correspondingly there will be n values of severities designated as D_1, D_2, D_3 .... or S_1, S_2, S_3 .... , in the standardized terms.

A designer is interested in the longest values of L, designated as L_T, and the largest value of S, designated as S_T. The period "T" means a sample size of T (T = 10, 20, ..., 100) years and can be regarded as equivalent to a return period of "T" years. The probabilistic relationship for L_T can be obtained by applying the theorem of extreme of random number of random variables. The computations for drought durations and form does not affect the magnitude of the duration (L)

Table 1. Values of Q and R at the Mean Level for Different Probability Distributions

Model	For all c_v	c_v =0.2		c_v =0.4		c_v =0.6		c_v =0.8		c_v =1.0		Remarks
Distribution	n	γ	ln	γ	ln	γ	ln	γ	ln	γ	ln	
q ρ =0	0.5	0.53	0.54	0.55	0.58	0.58	0.61	0.61	0.64	0.64	0.66	n :normal γ :gamma ln : log
Different ρ 、 c_v and r value												
ρ =0.1	0.53	0.56	0.57	0.58	0.61	0.61	0.64	0.63	0.67	0.66	0.71	
ρ =0.3	0.60	0.62	0.63	0.64	0.67	0.67	0.70	0.69	0.74	0.71	0.78	
ρ =0.5	0.67	0.69	0.70	0.71	0.73	0.73	0.76	0.75	0.80	0.77	0.84	
ρ =0.7	0.75	0.77	0.77	0.78	0.80	0.80	0.82	0.81	0.86	0.83	0.89	

but does affect the magnitude of the severity (D). The mean has no effect on the severity as it is the difference between the magnitude of the drought variable and the mean itself. So, in the course of mathematical derivations for severity, the mean cancels out, leaving standardized severity, which can be transformed into actual severity D by the relationship mentioned above. The following relationships can therefore be deduced for L_T following the work of Guven (1983).

$$P(L_T \le j) = p(n=0) + \sum_{i=1}^{\infty} [P(L \le j)]^i \cdot p(n=i) \quad (11)$$

Note j takes on discrete values, P(...) stands for the notation of cumulative probability and p(...) for the probability of discrete events. Spells may evolve randomly or in a Markovian fashion and can be regarded to follow the Poisson law of probability. The geometric law of probability adequately simulates the drought length L. The following relationships can be written for probabilities of number of drought runs and length of runs.

$$p(n=i) = \frac{\exp[-Tq(1-r)]\ [Tq(1-r)]^i}{i!} \quad (12)$$

$$P(L_T \le j) = 1 - r^{j-1}; P(L > j) = r^{j-1} \quad (13)$$

where q is the probability quantile defined earlier and r is the conditional probability of any year being a drought year, given that the past year is also a drought year. Substituting equations (12) and (13) into equation (11) and simplifying, one can get the following relationship

$$P(L_T \le j) = \exp\{-Tq(1-r)[1-P(L \le j)]\} \quad (14)$$

The expected value of L_T can be obtained by using the formula

$$E(L_T) = \sum_{j=1}^{\infty} jp(L_T = j) \quad (15)$$

Since $p(L_T = j) = P(L_T \le j+1) - P(L_T \le j)$, one can therefore derive an expression for p(L_T =j) by involving equations (13) and (14), and the resulting equation is as follows.

$$p(L_T = j) = \exp\left[-T(1-r)r^{j-1}\right]\left\{\exp\left[Tq(1-r)^2 r^{j-1}\right]-1\right\} \quad (16)$$

The conditional probability, r, is related to the lag-one serial correlation coefficient ρ, through the following equation.

$$r = q + \frac{1}{2\pi q}\int_0^{\rho} \exp\left[-0.5z_0^2/(1+\tau)\right](1-\tau^2)^{-1/2}\,d\tau \quad (17)$$

where ρ is the lag-one serial correlation coefficient of the Markov process and τ is the dummy variable of integration. Equation (17) can be evaluated by a numerical integration procedure and values of r for given ρ at truncation level z_0 ($z_0 = z_m$ for normal pdf, $Z_0 = Z_{m\gamma}$ for gamma pdf, and $Z_0 = Z_{ml}$ for log-normal pdf) can be computed. It is evident from equation (17) that for independent processes r = q. It should be noted that if the x_i sequence is normal, ρ can be substituted as it is, but for log-normal pdf ρ should be converted to ρ_1, which is the right value in the normalized domain and $Z_0 = Z_{ml}$. The linkage relationship between ρ and ρ_1 is of the following form

$$\rho_1 = \frac{\ln\left\lfloor \rho C_V^2 + 1 \right\rfloor}{\ln(1 + C_V^2)} \quad (18)$$

For a gamme pdf, ρ remains unchanged but $Z_{m\gamma}$ replaces Z_0. Values of q and r for various pdfs, C_V and ρ values are shown in Table 1. It is obvious from Table 1 that q for the normal pdf is constant and is equal to 0.5 regardless of the coefficient of variation, whereas for log-normal pdf it is dependent on the C_V

and in turn on C_s. Values of r are dependent on ρ for normal pdf and on C_v and ρ for gamma and log-normal pdfs. In all cases log-normal distribution tends to have a greater value of q and r for identical values of ρ and C_v in the sequences of the drought variable, indicating that extreme values of the drought duration are going to be larger under the log-normal structure of data representing the drought. With the above procedural details equation (15) can be solved numerically in order to evaluate $E(L_T)$ for the desired return period "T" in years.

2.3 Modeling Extreme Drought Severities

The probabilistic relationship for S_T can be obtained parallel to that for L_T, i.e. equation (11), and can be expressed as follows

$$P(S_T \le Y) = p(n=0) + \sum_{i=1}^{\infty} P(S \le Y)^i \, p(n=i) \quad (19)$$

in which Y can take on values such as 0, 0.1, 0.2, ... , 60 (Y=60 represents an extremely large value) and these values are dimensionless. Plugging the expression for p(n=i), indicated by equation (12), into equation (19), one obtains the following

$$P(S_T \le Y) = \exp\{-Tq(1-r)[1-P(S \le Y)]\} \quad (20)$$

The term S denotes severity (based on the standardized sequences) or the sum of the deficits in each epoch of the drought spell, which can be approximated as normally distributed in view of the central limit theorem. The pdf of S can therefore be written in the following form

$$P(S \le Y) = \frac{1}{\sqrt{2\pi}\sigma_s} \int_0^Y \exp\left[-0.5\left(\frac{S-\mu_s}{\sigma_s}\right)^2\right] ds \quad (21)$$

In a drought spell consisting of k consecutive years (L=k), the expressions for the mean, μ_s, and standard deviation, σ_s, of severity can be written as follows

$$\mu_s = K(\mu_t) \quad (22)$$

$$\sigma_s^2 = k \cdot \sigma_t^2 \left(\frac{1+\rho}{1-\rho} - \frac{2\rho(1-\rho^k)}{k(1-\rho)^2}\right) \quad (23)$$

where μ_t and σ_t are the mean and standard deviation of the individual deficits, and ρ is as defined earlier.

Parallel to the expression for $E(L_T)$ in equation (15), the expression for $E(S_T)$ can be written as

$$E(S_T) = \int_0^{Y=\infty} S_T f(S_T) dS_T \quad (24)$$

Although the pdf of S_T is not known, equation (24) can still be solved numerically. In the numerical procedure, first, equation (21) is integrated numerically in order to evaluate P(S $\leqslant$ Y), and plugging this value into equation (20) yields the estimate of $P(S_T \le Y)$. The value of Y can be allowed to range from 0 to 60 [infinity in equation (24) is approximated by 60] with an increment of 0.1. Let these values of Y be designated as Y_0=0, Yi=0.1, Y_2=0.2, ..., etc., equation (24) can be expressed in the numerical integral form as follows

$$E(S_T) = \sum_{j=0}^{n_1} \left((Y_j + y_{j+1}\right) / 2\left[P(S_T \le Y_{j+1}) - (S_T \le Y_j)\right] \quad (25)$$

In which n_1=60/0.1, and Y_{600}=60.

Since values of $E(S_T)$ are standardized and in non-dimensional form, the actual drought severity designated as D_T can be expressed as

$$D_T = E(S_T)\cdot\sigma_X = E(S_T)\cdot C_V \cdot x_m = x_m - x_m + E(S_T)\sigma_x \quad (26)$$

the last portion of the above equation can be manipulated as

$$D_T = x_m - C_V^{-1}\cdot\sigma_X + E(S_T)\sigma_X = x_m + F_T\cdot\sigma_X \quad (27)$$

where F_T can be called the drought frequency factor and be written in equation form as

$$F_T = \lfloor E(S_T) - C_V^{-1} \rfloor \quad (28)$$

It can be seen that equation (27) is analogous to the flood frequency formula $Q_T = Q_m + K_T\sigma_Q$ commonly cited in hydrological texts.

3. Application

The Dongzhou reservoir is located at the Chaiwen River of the Dawen Basin within the downstream of the Yellow River, which controls the area of 189 km^2. The main water supply is for irrigation as well as for drinking water. The design irrigation area is 8667 hm^2. The average annual runoff within the controlled area amounts to 39×10^6 m^3, C_v=0.40. The flows tend to be log-normally distributed with a negligible level of carryover (ρ). The reservoir should meet the demand 1 in 100 years drought. Therefore there is a need to estimate the volume of water to be stored for designing the reservoir. The solution of the problem starts by estimation q for C_v=0.40 $(\sigma_x = 16\times10^6 m^3)$ in equation (1) and using the values of q and r (r=q for independent flows) in equations (15) and (16). The value of q equals to 0.58, and $E(L_T)$=7.15, then $F_T = \lfloor 7.15 - 0.40^{-1} \rfloor = 4.65$, $D_T = 0.39 + 4.65\times0.16 = 1.134 \times10^8$ m^3.

Had the discharge is normal distribution, then $q = 0.5$, $E(L_T) = 5.78$, $D_T = 92 \times10^6$ m^3. If the

discharge is gamma distribution, the calculated results are $q = 0.55$, $E(L_T) = 6.74$, and $D_T = 1.07 \times 10^8$ m^3. When $\rho \neq 0$, if $\rho = 0.5$, then, for log-normal discharge, $q = 0.58$, $r = 0.73$, $E(L_T) = 10.63$, $D_T = 1.69 \times 10^8$ m^3, for normal distribution, $q = 0.5$, $r = 0.67$, $E(L_T) = 8.57$, $D_T = 1.36 \times 10^8$ m^3, for gamma distribution of discharge, $q = 0.55$, $r = 0.71$, $E(L_T) = 9.92$, $D_T = 1.43 \times 10^8$ m^3. The above calculation mainly demonstrates the role of skewness and the carryover effects in the storage needs during drought periods.

Therefore, when it is difficult to identify the pdf of the drought variable, the assumption of log-normality allows a conservative design, which is a desirable feature. The assumption of normality leads to the requirement for least storage under identical conditions of C_v and of the dependence structure of the rainfall or the runoff sequences.

4. Conclusions

The results of the present analysis can be stated as follows:

1. The non-normal pdf of the drought variable influences the behavior of $E(L_T)$ and $E(S_T)$ significantly. The log-normal pdf tends to lengthen the values of $E(L_T)$ and enlarge the values of $E(S_T)$ for identical conditions of C_v, C_s, ρ and T, followed by the gamma and normal pdfs. The effect of skewness is accordingly reflected in the increased values of the above parameters in relation to the normal pdf.

2. For the purpose of designing storage structures for drought periods, one can safely assume $E(S_T) \approx E(L_T)$, or the drought intensity ≈ 1 (in the standardized terms) for C_v=0.2～1, ρ=0～7, and a return period of 25～1000 years. The above approximation leads to a conservative design for water storage facilities during drought periods.

3. The skewness and the persistence in the sequences of the drought variable enhance the extremal drought durations and the severities. In particular, the effect of skewness on the extreme drought durations cannot be regarded as insignificant, contrary to the existing belief in the hydrological literatures.

4. A drought frequency formula can be derived to estimate the drought severity in relation to the return period, analogous to the flood frequency formula. The drought frequency factor, F_T, is equal to $[E(S_T)-C_v^{-1}]$ and can easily be computed by knowing pdf, C_v and ρ of the drought variable, and the desired return period "T".

This research has been supported by IDSS developing for water resources optimum allocation and management {20025700003} and by Innovatory found in Henan Province, China.

Correspondence to: Zhenmin Zhou
20 Zhenghua Road
Zhengzhou, Henan 450045, China
Telephone: 0086-0371-5790658
Cellular phone: 13015542843
E-mail: zzm1022@yahoo.com.cn

References

Bogardi JJ, et al. Practical generations of synthetic rainfall event time series in a semi-arid climatic zone. J Hydrol 1998;103:357-73.

Guven O. A simplified semiempirical approach to probabilities of extreme hydrologic droughts. WRR 1983;19:441-53.

Song H, Zhang S. Basic Analysis on Regional Drought Statistic Features. Advances in Water Science J. China. 1994;3.

Wavelet Network Model and Its Application to the Prediction of Hydrology

Wensheng Wang, Jing Ding

Department of Hydrology and Water Resources, Hydraulic School of Sichuan University, Chengdu, Sichuan 610065, China, wangws70@sina.com

Abstract: Based on the multi-time scale and the nonlinear characteristics of the observed time series, a new hybrid model between wavelet analysis and artificial neural network (ANN): wavelet network model, has been suggested. The present model absorbs some merits of wavelet transform and artificial neural network. Case studies, the short and long term prediction of hydrological time series, have been researched. The comparison results revealed that the suggested model could increase the forecasted accuracy and prolong the length time of prediction. The wavelet network model is satisfied. [Nature and Science 2003;1(1):67-71].

Keywords: wavelet analysis; artificial neural network; wavelet network model; prediction of hydrology

1. Introduction

The accuracy prediction of hydrology and water resource can give important information for the city planning, land use, the design of civil project and water resource management. Hydrology system is influenced by many factors, such as weather, land with vegetal cover, infiltration, evaporation and transpiration, so it includes the good deal of stochastic dependent component, multi-time scale and highly nonlinear characteristics. In general, the hydrology system is predicted with regressive analysis, stochastic theory models (Ding, 1988) and Grey model method (Deng, 1992). In recent years, artificial neural network (ANN), fuzzy theory and chaos theory have been widely applied in the sphere of hydrology and water resource. The studies have demonstrated these forecasted approaches are not very satisfied in precision because of only considering some aspects of its property. In order to raise the forecasted precision and lengthen the forecasted time, the hybrid model based on some methods should be probed. In this paper, a new hybrid model: wavelet network model, which is combined with wavelet analysis and ANN, has been proposed.

A wavelet network model makes use of the merits of wavelet analysis and ANN, so it has excellent performance in simulation and forecast. Some case studies are presented (in section 5) in which wavelet network model has been developed using the suggested methodology (in section 4) to forecast hydrological time series in China. The results show the technique and the model are feasible. The conclusions of the study are given in section 6.

2. Study Review

Wavelet analysis has become a research hot point. Wavelet analysis has good time and frequency multi-resolution, and can effectively diagnose signal's main frequency component and abstract local information of the time series. It has huge advances in signal processing, image compress and encoding, tongue encoding, mode identification and nonlinear science fields. The researches and applications of wavelet analysis have already begun in hydrology and water resources. The document (Li, 1997) points out the potential applications of wavelet analysis to hydrology and water resources. Li et al (1999) probe long time interval forecast of hydrological time series with combing neural network models based on wavelet transform. Wang et al (2000) have proposed a wavelet transform stochastic simulation model, which generate synthetic streamflow sequences that are statistically similar to observed streamflow sequences. The multi-time scale characteristics of hydrological variable have been studied by Wang et al (2002). Wavelet analysis will make a new research approach for the system of hydrology and water resources and broaden the content of hydrology greatly.

ANN is highly flexible function approximator that has self-learning and self-adaptive feature. Many studies attempted to model runoff by ANN. For example, Half et al (1993) designed a three-layer feed-forward ANN using the observed rainfall hyetographs as inputs and hydrographs as output to predict runoff from a watershed. Tokar (1999) reported that their ANN model had better prediction accuracy and flexibility than statistical regression and simple conceptual models. Applications of ANN are widely reported in the hydrological literature (French, 1992; Raman, 1995; Hu, 2001; Qing, 2002). ANN models have shown their utility in a broad rang of water resources application and are powerful tool for forecasting and prediction.

3. The Theory of Wavelet Analysis

3.1 Wavelet Transform

Wavelet analysis is multi-resolution analysis in time and frequency domain, and is the important milestone of the Fourier Transform. Wavelet function $\psi(t)$ is called mother wavelet, which has shock properties and can reduce zero rapidly. It can be defined as $\int_{-\infty}^{+\infty}\psi(t)dt = 0$ mathematically. $\psi_{a,b}(t)$ can be acquired through compressing and expanding $\psi(t)$:

$$\psi_{a,b}(t) = |a|^{-1/2}\psi(\frac{t-b}{a}) \quad b \in R, a \in R, a \neq 0 \qquad (1)$$

Where $\psi_{a,b}(t)$ is successive wavelet; a is scale or frequency factor, b is time factor; R is the domain of real number.

If $\psi_{a,b}(t)$ satisfies equation (1), for the energy finite signal or time series $f(t) \in L^2(R)$, successive wavelet transform of $f(t)$ is defined as:

$$W_\psi f(a,b) = < f, \psi_{a,b} > = |a|^{-\frac{1}{2}} \int_R f(t)\overline{\psi}(\frac{t-b}{a})dt \qquad (2)$$

Where $\overline{\psi}(t)$ is complex conjugate functions of $\psi(t)$. Equation (2) describes that wavelet transform is the decomposition of $f(t)$ under different resolution level (scale). In other words, the essence of wavelet transform is to filter wave for $f(t)$ with different filter.

In real application successive wavelet is often discrete. Let $a = a_0^j$, $b = kb_0a_0^j$, $a_0>1$, $b_0 \in R$, k, j are integer number. Discrete wavelet transform of f(t) is written as:

$$W_\psi f(j,k) = a_0^{-j/2}\int_R f(t)\overline{\psi}(a_0^{-j}t - kb_0)dt \qquad (3)$$

When $a_0=2$, $b_0=1$, equation (3) becomes binary wavelet transform:

$$W_\psi f(j,k) = 2^{-j/2}\int_R f(t)\overline{\psi}(2^{-j}t - k)dt \qquad (4)$$

$W_\psi f(a,b)$ or $W_\psi f(j,k)$ can reflect the characteristics of original time series in frequency (a or j) and time domain (b or k) at the same time. When a or j is small, the frequency resolution of wavelet transform is low, but the time domain resolution is high. When a or j becomes large, the frequency resolution of wavelet transform is high, but the time domain resolution is low. That is, wavelet analysis is a mathematic microscope.

3.2 The Algorithm of Wavelet Transform

In real world observed time series are discrete, such as rainstorm process, flood process, monthly streamflow process, and daily runoff sequence. So discrete wavelet transform must be selected for decomposition and reconstruction of time series. There are many discrete wavelet transform algorithm, such as Mallat algorithm (Mallat, 1989; Mallat, 1989) and A Trous algorithm (Shensa, 1992; Aussum, 1997). A Trous algorithm has been adopted in the paper.

Let Z(t) (or C0(t)) denote the original discrete time series. A Trous decomposition algorithm as following:

$$C_i(t) = \sum_{\ell=-\infty}^{+\infty} h(\ell)C_{i-1}(t+2^i\ell) \quad (i = 1,2,\cdots) \qquad (5)$$

$$W_i(t) = C_{i-1}(t) - C_i(t) \quad (i = 1,2,\cdots) \qquad (6)$$

Where $h(\ell)$ is the discrete low-pass filter; $C_i(t)$, $W_i(t)$ (i=1,2, $\cdots$) are scale coefficient (background information) and wavelet coefficient (detail information) at the resolution level *i* respectively. $W_1(t), W_2(t), \cdots, W_P(t)$ *and* $C_P(t)$ are called discrete wavelet transform with the resolution level *P*. In equation (5), extending of boundaries may be carried out in different ways. We took an intuitively acceptable approach by taking *C(n+k)=C(n-k)*.

The wavelet coefficients, $W_i(t)$ (i=1,2,$\cdots$), provide the "detail" signal, which can capture small features of interpretational value in the data; the "residual" term $C_P(t)$ represents the data's "background" information. Because of simplicity of $W_1(t), W_2(t), \cdots, W_P(t), C_P(t)$ (we can see from section 4), some interesting characteristics, such as period, hidden period, dependence, jump, can be diagnosed easily through wavelet components $W_1(t), W_2(t), \cdots, W_P(t), C_P(t)$.

It is possible to reconstruct the original hydrological time series from wavelet components $\{W_1(t), W_2(t), \cdots, W_P(t), C_P(t)\}$. The wavelet reconstruction of the original time series, in term of wavelet coefficients, is given by

$$Z(t) = C_p(t) + \sum_{i=1}^{p} W_i(t) \qquad (7)$$

Equation (7) provides a reconstruction formula for original time series. That is A Trous reconstructing algorithm. A Trous decomposition and reconstructing algorithm are simple and rapid. It's key is to determine the discrete low-pass filter.

4. Wavelet Network Model

4.1 Main Idea

First, original time series can be decomposed into a certain number of sub-time series $\{W_1, W_2, \cdots, W_P, C_P\}$ by wavelet transform algorithm. $W_1, W_2, \cdots, W_P$ are detail time series, and C_P is background time series. These play different role in the original time series and the behavior of each sub-time series is distinct. So the contribution to original time series varies from each other. Then, ANN is constructed in which the sub-time series at *t* time are input of ANN and the original time series at *t+T* time are output of ANN, where *T* is the time length of forecast. Last, the wavelet network model (WNM) is formed in which the weighs are learned with some algorithm. The key of wavelet network model is wavelet decomposition of time series and the

construction of ANN.

4.2 Decomposition of Observed Time Series

The low-pass filter h, which is a B_3 spline, defined as $(\frac{1}{16},\frac{1}{4},\frac{3}{8},\frac{1}{4},\frac{1}{16})$, is used. This is of compact support and point-symmetric. First the resolution level P must be determined. In general there is $INT(\ell g\, n)$ resolution scale number, where n is the length of time series and *INT* stands for integer number, the $\ell g\, n$ is common logarithm.

The wavelet coefficients and scale coefficients of the monthly groundwater level time series derived from A Trous decomposition algorithm are shown in Figure 1. In Figure 1 $W_1(t)$ and $W_2(t)$ denote wavelet coefficients at the resolution level 1 and 2 respectively; $C_2(t)$ denotes scale coefficients at resolution level 2.

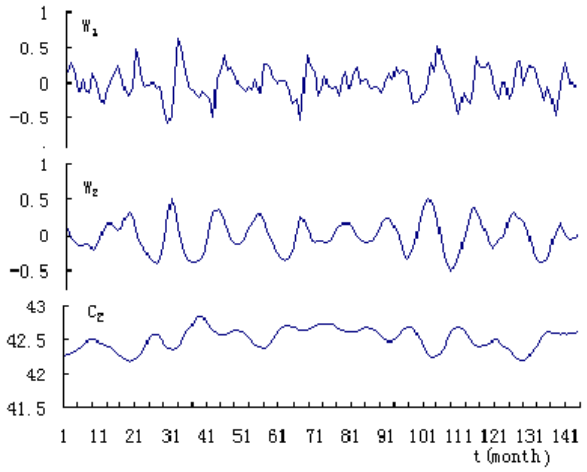

Figure 1. Wavelet Decomposed Process of Monthly Groundwater Level Time Series

4.3 The Structure of ANN

ANN is widely applied in the forecasting of hydrology and water resource. In ANN, BP network models are common to engineer. So called BP network models, that is the feed-forward artificial neural network structure and a back-propagation algorithm (BP). It has proved that BP network model with three-layer is satisfied for the forecasting and simulating in the science of water.

The input of BP network is $X=[W_1(t),W_2(t),\cdots,W_P(t),C_P(t)]^T$, and the nodes of input layer are P+1. The output is $Y=[L(t+T)]$, and the node is 1. The nodes of hidden layer are determined by trial and error. The network weights are learned by standard BP algorithm or self-adapted BP algorithm and so on. The details on BP algorithm are available in the references, hence these are not repeated here.

5. Cases Studies

5.1 Case One: Shallow Groundwater Level Forecast

There is 12-year (1983-1994) record of shallow monthly groundwater level in Beijing of China from the literatures (Lu, 1997), that is $\{Z(t),t=1,2,\ldots,144\}$. The first nine years time series are used for calibration /training of the model, and the remaining three years data are used for verification or testing purposes. In this research $n=9\times12$, then the scale number P=2.

Through A Trous algorithm, the groundwater level time series are decomposed into the sub-time series: $\{W_1(t),W_2(t),C_2(t)\}$, and are listed in Figure 1. Here three-layer network: input layer, hidden layer and output layer, is adopted. The number of nodes in hidden layer is equal to 3. So the structure of WNM is 3-3-1. The weight parameters of network are estimated by self-adapted BP algorithm. The number of training of WNM is 5000.

Given four forecasting periods (T=1 month, 2 month, 3 month, and 4 month), the fitting and forecasting results of groundwater level are shown in Table 1. The forecasted results of groundwater level of 1992~1994 are shown in Figure 2 (T=1 month) and Figure 3 (T=3 month). In order to compare, the results of calibration and verification of ARMA model (Lu, 1997) and threshold autoregressive model (TAR) based on genetic algorithm (Jing, 2000) are listed in Table 1. From Table 1 it can be seen that, for T=1 month, the calibration precision of WNM is almost good as ARMA and TAR, but the verification precision is better than the latter. At the same time, when the forecasting period (Table 1, Figure 3, Figure 4) is become long, the fitting and testing precision of WNM is also very higher than the other models (not listed).

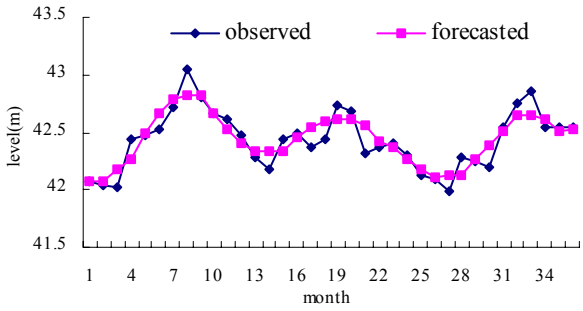

Figure 2. Comparison of the Original Groundwater Level Time Series and Forecasted Time Series of WNM (Where T=1 Month)

5.2 Case Two: Daily Discharge Forecast

Daily discharge data for Yangtze River basin of China at Cuntan Station are used. The years 1992-2001 are selected, the first 8 years data are used for build the wavelet network model, and the remaining two years data are used for verification of WNM. Here $n=8\times365$, then scale number P=3.

Table 1. Error Analysis of Validation and Verification of WNM

Model	Percent of calibration absolute error falling into the demarcation				Percent of verification absolute error falling into the demarcation			
	[0,0.1]	[0,0.2]	[0,0.3]	[0,0.4]	[0,0.1]	[0,0.2]	[0,0.3]	[0,0.4]
ARMA (T=1)	79.0	99.0	100	100	30.0	59.0	81.0	92.0
TAR (T=1)	51.0	82.3	94.8	96.9	47.2	80.6	91.7	100
WNM (T=1)	57.4	87.0	99.1	100	60.0	91.4	100	100
WNM (T=2)	73.2	98.2	100	100	73.5	100	100	100
WNM (T=3)	60.2	91.7	98.2	100	51.5	90.9	100	100
WNM (T=4)	52.8	83.3	94.4	98.2	43.8	71.8	93.8	100

Table 2. The Calibrated and Validated Results of Wavelet Network Model (%)

Model	Percent of validation			Percent of verification		
	<10%	<20%	<30%	<10%	<20%	<30%
TAR(T=1d)	83.9	95.9	98.7	84.9	95.2	98.2
TAR(T=2d)	63.0	86.3	94.7	64.3	86.6	94.0
TAR(T=3d)	52.2	77.5	89.9	52.9	78.0	89.3
TAR(T=4d)	45.4	72.4	86.6	45.8	72.9	84.8
TAR(T=54d)	40.5	67.6	83.5	42.3	68.0	82.3
WNM(T=1d)	76.4	96.1	99.7	89.4	97.9	99.6
WNM(T=2d)	83.3	97.5	99.9	95.2	99.5	99.9
WNM(T=3d)	77.8	97.2	99.9	87.1	99.0	99.9
WNM(T=4d)	66.2	93.1	98.7	78.2	94.1	98.9
WNM(T=5d)	69.1	93.6	98.7	80.6	95.3	98.5

Through A Trous algorithm, the daily discharge time series are decomposed into the sub-time series: $\{W_1(t),W_2(t),W_3(t),C_3(t)\}$. Three layers network is adopted too. The number of nodes in hidden layer is equal to 4. So the structure of WNM is 4-4-1. The weight parameters of network are estimated by modified BP algorithm. The number of training of WNM is 2000.

Given five forecasting periods (T=1 day, 2 day, 3 day, 4 day and 5 day), the fitting and forecasting results of daily discharge are shown in Table 2. The forecasted results of daily discharge of 2001 year are shown in Figure 4 (T=1 day) and Figure 5 (T=3 day). In order to compare, the results of validation and verification of TAR model are listed in Table 2. It was noticed that WNM is better than TAR model.

6. Conclusions

This paper has reported a new hybrid model wavelet network model. It plays an important role in improving the precision and prolonging the forecasting time period

or hydrology and water resource time series.

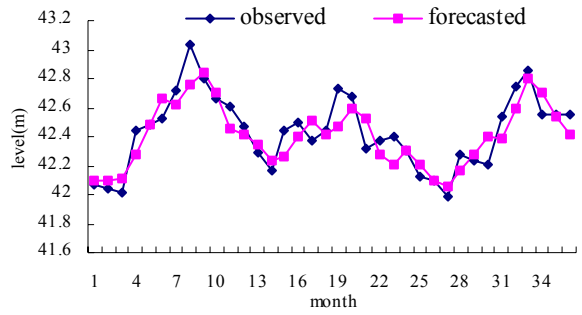

Figure 3. Comparison of the Original Groundwater Level Time Series and Forecasted Time Series of WNM (Where *T*=3 Month)

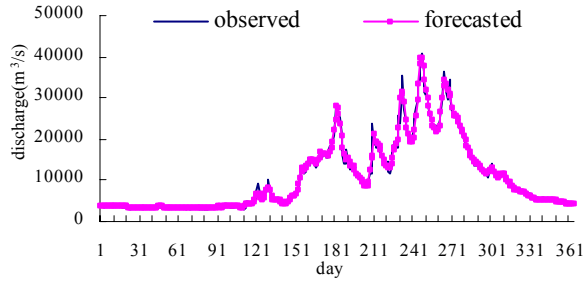

Figure 4. Comparison of the Original Daily Discharge Time Series and Forecasted Time Series of WNM (Where T=1 Day)

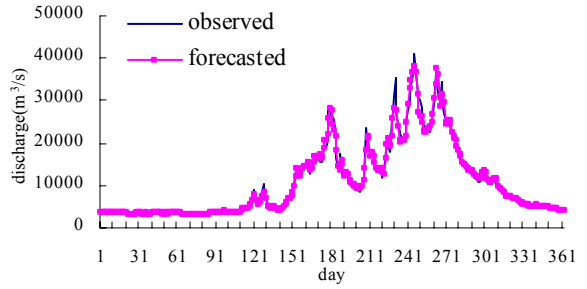

Figure 5. Comparison of the Original Daily Discharge Time Series and Forecasted Time Series of WNM (Where *T*=3 day)

Calibration and verification of wavelet network model for prediction of hydrology and water resource in case studies have shown that the method is functional. The suggested strategy is suit to any other water resource time series.

Elementary attempt at developing the hybrid model is success. Future studies will be opened up from the manner of recombined with wavelet analysis and ANN to applications of wavelet network model.

We would like to thank the National Science Foundation Committee of China to support this research project (No: 50279023).

Correspondence to:
Wensheng Wang
Hydraulic School of Sichuan University
Chengdu, Sichuan 610065, China
Telephone: 001186-28-8540-3347
E-mail: **wangws70@sina.com**

References

Aussum A, Campbell J, Murfagh F. Wavelet-based feature extraction and decomposition strategies for financial forecasting. Journal of Computational Intelligence in France 1997:1-17.

Chui CK, ed. Wavelet—A Tutorial in Theory and Applications. Xian Jiaotong University Press, Xian, China, 1995:66-287 (in Chinese).

Deng J, ed. Grey Prediction and Grey Decision. Huazhong Ligong University Press, Wuhan, China, 1992:74-192 (in Chinese).

Ding J, Deng Y, ed. Stochastic Hydrology. Chengdu University of science and technology Press, Chengdu, China, 1988:190-230 (in Chinese).

French MN, Krajewski WF, Cuykendall RR. Rainfall forecasting in space and time using a neural network. J Hydrol 1992;137:1-31.

Half AH, Halff HM, Azmoodeh M. Predicting runoff from rainfall using artificial neural networks. Proc Engng Hydrol 1993; ASCE:761-5.

Hu T, Lam KC, Ng ST. River flow time series prediction with a range dependent neural network. Hydrol Sci J 2001;46(5):729-45.

Jing J, Ding J, ed. Genetic Algorithm and Its Application to Water Science. Sichuan University Press, Chengdu, China, 2000:25-160 (in Chinese).

Li X, Ding J, Li H. Combing neural network models based on Wavelet transform. Journal of Hydraulic 1999; 2:1-4 (in Chinese).

Li X, Ding J, Li H. Wavelet analysis and its potential application to hydrology and water resources. Journal of Sichuan Union University (Engineering Science) 1997;1(4): 49-52 (in Chinese).

Liu G, Ding J. Groundwater level forecast with Bp network model. Journal of Xian Geology College, 1997;2:45-50 (in Chinese).

Lu H. Forecast of shallow groundwater level in Beijing. Geotechnical Investigation & Surveying, 1997;1:67-71.

Mallat S G. Multifrequency channel decomposition of images and wavelet models. IEEE Trans on ASSp 1989;37(12):2091-110.

Mallat SG. A theory for multiresolution signal decomposition: the wavelet representation. IEEE Trans on PAMI 1989;11(7):674-93.

Qing G, Ding J, Liu G. Self-adapted BP algorithm and its application to flood forecast of river. Advance in Water Science 2002;13(1):37-41(in Chinese).

Raman H, Sunilkumar N. Multivariate modeling of water resource time series using artificial neural network [J]. Hydrol Sci J 1995;40(21):145-63.

Shensa MJ. Discrete wavelet transform: wedding the A Trous and Mallat algorithm [J]. IEEE Transactions on Signal Processing 1992;40:2464-82.

Tokar AS, Johnson PA. Rain-runoff modeling using artificial neural network. J Hydrol Engng ASCE 1999;4(3):232-9.

Wang W, Ding J, Xiang H. The multi-time scale analysis of hydrological time series with wavelet transform. Journal of Sichuan University 2002;35(4):14-7 (in Chinese).

Wang W, Yuan P, Ding J. Wavelet analysis and its application to the stochastic simulation of daily discharge process. Journal of Hydraulics 2000;11:43-8 (in Chinese).

Zhang L, ed. Artificial neural network models and its application. Fudan University Press, Shanghai, China. 1994:10-65 (in Chinese).

Applying on RAGA in Estimating Internal Rate of Return of Hydropower Project

Xiaorong Huang*, Chuan Liang*, Zhiyong Liu**

* School of Hydropower Engineering, Sichuan University, Chengdu, Sichuan 610065, China, Hxiaorong@163.net; ** School of Network, Sichuan University, Chengdu, Sichuan 610065, China

Abstract: Internal rate of return, a kind of important economic analysis index, is often used by evaluating economic feasibility for engineering. Substantively, estimating internal rate of return is to solve higher-order equation with one unknown. Due to its precision disadvantage, complicated calculation, and especially theories lacks, traditional linear interpolation is unsuited to do with these questions. Real Coding Accelerating Genetic Algorithm (RAGA), a new method, has overall optimization ability, less calculation quantity, adaptability to interspace size of the optimistic search variety, swiftly calculation and high accuracy. It can be used and proved to calculate internal rate of return effectually. [Nature and Science 2003;1(1):72-74].

Key words: RAGA; internal rate of return; linear interpolation

Introduction

The investment of hydropower engineering was gradually taken back by its net income of each year. If everything is OK, at the end of economic life, the amount of the investment can be returned at the right moment. Because this process has nothing to do with outside factors, only with its own investment, net income of each year and increment rate of possessive funds, the rate of discount is so called as internal rate of return. Solving higher-order equation with one unknown usually can get internal rate of return, an unknown rate. Unfortunately, at present, a simple and effectual solution method cannot be really obtained because linear interpolation, which is often used before, can't attain satisfactory accuracy for that there is no linear relation between rate of discount and internal rate of return (Liu, 2003). Real Coding Accelerating Genetic Algorithm (RAGA) can resolve this problem nicely, and it can acquire desired result from big scope, meanwhile its accuracy is obviously higher than what traditional linear interpolation can do. Moreover, RAGA does not need attempt to calculate it many times, then the calculation is reduced greatly, and also overcome the result which varied with different persons only because this linear interpolation method is adopted. As we know, Internal rate of return can make sure the capital income and foreshow the biggest interest rate afforded without financial crisis. Hydropower engineering usually possessing big project investment, a long project constructing and project repayment period, needs higher accuracy that can reflect the income ability of investment well. In this way, RAGA provides the new method for us with the way of thinking. Scientific and dependable data can be available.

1. The Brief Introduction of RAGA

Standard Genetic Algorithm (SGA), the traditional genetic algorithm, usually adopts the coding method of binary system. Its individual genotype is also called binary coded string that only uses coding sign 0 and 1. Binary coding is not only simple and easy to proceed its crossover, selection and mutation etc., but also easy to make good use of the mode axioms to theoretically analyze algorithm. In despite of this, Standard Genetic Algorithm's shortage is still obvious: it can't reflect the special structure characteristics of a problem enough, and its part-search ability is also worse due to its random attributes when optimization question of continuous functions is handled. Furthermore, to research optimization question of continuous functions containing many dimensions and needing higher accuracy, the binary coding shows disadvantages. Firstly, the binary coding exits mapping error when continuous functions proceed to discrete process. If the length of coding string is shorter, the requested accuracy cannot be obtained. If the length of coding string is longer, even though its accuracy is improved, the search scope of genetic algorithm swiftly extends. Secondly, the binary coding cannot reflect particular attributes of problems well. It is difficult to generate special genetic operator for special problems. As a result, many precious experiences from research on classic optimal algorithm cannot be made good usage, and special restricted condition isn't easy to be handled. In order to overcome these shortages of binary coding method, we may adopt real number coding, and make the individual coding length fitly equal to decision variable number. This kind of coding has a few advantages: (1) be qualified to denote bigger number; (2) be qualified to obtain higher accuracy; (3) be qualified to search from big scope; (4) reduce the calculation complexity and improve calculation efficiency; (5) be easy to unite genetic algorithm and classic optimal algorithms; (6) be easy to design genetic operators aiming to specialized

problems; (7) be easy to handle complicated restricted conditions.

2. The Estimation of Internal Rate of Return

Internal rate of return is kinds of discount rate, which can make total amount of net present value of each year in project economic life, happen to be equal to zero. We now introduce the expression below:

$$\sum_{t=0}^{n} (CI - CO)_t (1 + IRR)^{-t} = 0 \qquad (1)$$

Equation inside: IRR——internal rate of return;

$(CI-CO)_t$——net present value of T year

n——life period of project

As we know, equation (1) is a higher-order equation with one unknown. Hence, it isn't easy to be solved. At present, the linear interpolation method is usually used. Its expression is as the following:

$$IRR = i_1 + \frac{NPV_1}{NPV_1 + |NPV_2|}(i_2 - i_1) \qquad (2)$$

i_1——lower rate of return that we attempt to calculate;

i_2——higher rate of return that we attempt to calculate;

NPV_1——net present value we calculate by i_1 (positive value);

NPV_2——net present value we calculate by i_2 (negative value).

Because hydropower engineering's lifetime is long (several decades), it is difficult to calculate internal rate of return by traditional mathematics method. According to the equations above, we consider that the accuracy of the linear interpolation method is low and its calculation is complicated. Hence, we attempt to turn equation （1） to minimization problem, another method to calculate internal rate of return. From equation（2－1）, they obtain

$$\min Q = \min \left| \sum_{t=0}^{n} (CI - CO)_t (1 + IRR)^{-t} \right| \qquad (3)$$

Therefore, internal rate of return is really to solve non-linear optimization problem, and RAGA is easy to handle it.

3. The Process That Model Realizes

Figure 1 shows the steps and calculation process of RAGA. In comparison, selection, crossover and mutation of RAGA proceed to parallel computation. In consequence, RAGA's search scope is bigger than SGA's, and there are more chances to get optimal value. RAGA can gradually narrow the scope of optimistic variable by making use of accelerating circulation. The accuracy of solution is improved quickly.

RAGA's control parameters are made up of community scale n, excellent individual number s, mutation probability P_m, crossover probability P_c, and their value will influence final optimistic value. Having done a great deal of numerical experiments and actual application, we obtain experimental relation between n and s:

$$s/n > 6\% \qquad (4)$$

When we apply RAGA, we suggest n: over 300 number, s: over 20, P_m: 0.8, P_c: 0.8 (Jin, 2000). If these are satisfied, we can get better result.

Figure 1. Flow Chart for RAGA

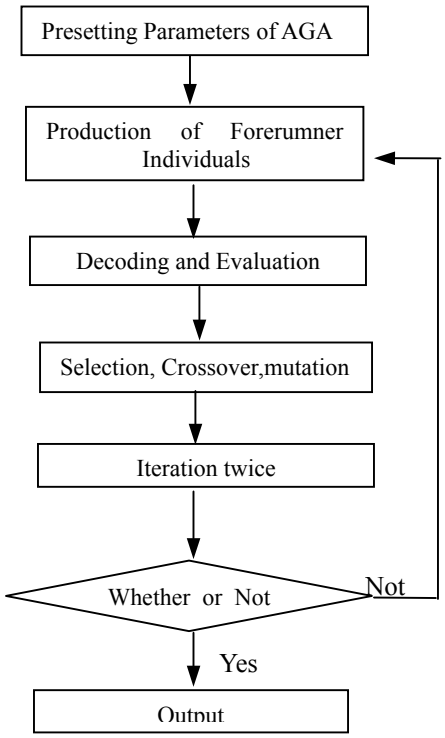

4. Example Analysis

Zipingpu water conservancy project, located at 6 km and on the upstream from Dujiangyan, Chengdu, China, is a key project to exploit the upstream of Minjing River reasonably. It tackles the difficulties of water and power shortage and flood control in Dujianyan irrigation area and Chengdu city. Its main functions are irrigation and municipal water supply, comprehensive benefits of generation, flood control, tourism and aquaculture. Its installed capacity has 0.76 million KW, average annual energy output has 3.417 billion KW.h. The total static investment reaches 5.75039 billion yuan (Chinese dollar)

and the total dynamic investment reaches 6.23600 billion yuan. Its construction period will last 7 years and operation period will last 30 years, so the total economic calculation period will last 37 years. The net cash flow of each year is shown in Table 1, and the calculation of the internal rate of return of Zipingpu engineering by different measures according to equation (3) is shown in Table 2.

Table 1. Zipingpu Project Net Cash Flow (unit: ten thousand Chinese yuan)

Year	1	2	3	4	5	6	7	8
NCF	–26274	–63040	–96349	–116874	–122121	–84969	–28916	53465
Year	9	10	11	12	13	14	15	16
NCF	59031	76491	76047	75575	75010	74415	73786	73122
Year	17	18	19	20	21	22	23	24
NCF	73059	72996	72932	72869	72806	72742	72679	72616
Year	25	26	27	28	29	30	31	32
NCF	72553	72489	72426	56881	56818	56754	56691	56628
Year	33	34	35	36				
NCF	56628	56628	56628	–263074				

Table 2. The Internal Rate of Return of Zipingpu Engineering (unit: ten thousand Chinese yuan)

result \ method	Internal rate of return	Remains value Q
Linear interpolation	8.81%	997.945
Fminbnd function	8.79%	97.021
RAGA（accelerate once）	8.7870%	38.4226
RAGA（accelerate two times ）	8.7880%	6.7341
RAGA（accelerate three times）	8.7878%	2.2189

It must be pointed out that the RAGA method is applied straight when the mark of cash flow change once. If it changes many times, all this shows that the income from the engineering investment is laid out some other external engineering. The external rate of return isn't always as same as the internal rate of return. If so, firstly we should convert the surplus income into external investment according to the external rate of return, then this part fund is further returned to internal engineering. The literatures suggest that we may estimate the internal rate of return by net investment examination method to any cash flow, whose expression would be of the form:

$a_0, a_1, a_2, \cdots, a_n$, r means internal rate of return, e means external rate of return, so the net investment of j year can be written in the form:

$$NI_0 = a_0 \qquad (5)$$

$$NI_j = N_{j-1}(1+i) + a_j, (j = 1,2,\cdots,n) \qquad (6)$$

If $NI_{j-1} < 0(j = 1,2,\cdots,n)$, the parameter i is set by internal rate of return. If not, the parameter i is set by external rate of return. At the same time, the net investment of n year must be equal to zero. We now introduce the expressions below:

$$NI_n = NI_n(r) = 0 \qquad (7)$$

Furthermore, we obtain

$$\min \quad Q = |NI_n(r)| \qquad (8)$$

Finally, we may apply the RAGA method to proceed the calculation.

5. Conclusion

Estimating the internal rate of return is actually to solve a kind of complicated and non-linear problem, by the RAGA method, higher accuracy, less error, more rationality we can obtain. When the cash flow mark of engineering change over twice, we should avoid confusing external rate of return and internal rate of return, otherwise it will bring important error for decision-making.

Correspondence to:
Xiaorong Huang
School of Hydropower Engineering, Sichuan University
Chengdu, Sichuan 610065, China
Telephone: 01186-28-8540-5610
Cellular phone: 01186-13608058560
E-mail: **Hxiaorong@163.net**

References

Jin J, Ding J. Genetic Algorithm and Its Applications to Water Science. Publishing House of Sichuan University. Chengdu, China. 2000;112-33.

Liu X. Engineering Economy Analysis. Publishing House of Xinan Jiaotong University. Xian, China. 2003;71-4.

Science and Technology Product Development Centre of Fei Si. The Assistant Optimizing Calculation and Design of the MATHLAB 6.5. Publishing House of Electronics Industry. Beijing, China. 2003;41-2.

Applying Self-Organizing Competition Artificial Neural Networks to Classify the Soil

Xiangdong Ma*, Qiang Fu**

* School of Water Resources & Environment, Hohai University, Nanjing, Jiangsu 210024, China;
** School of Water Conservancy & Civil Engineering, Northeast Agricultural University, Harbin, Heilongjiang 150030, China, fuqiang100@371.net

Abstract: Through applying the clustering function of Self-Organizing Mapping (SOM) network, the writer uses MATLAB 5.3 software to classify 21 kinds of soil samples in Sanjiang Plain. Through comparing the result with references that uses the method of fuzzy clustering, the paper concludes that the SOM network can reflect the complicated information among each soil samples. The effect of classification is good, and can be applied on soil classification. [Nature and Science 2003;1(1):75-81].

Key words: SOM network; soil classification

1. Introduction

Soil classification is not only the basis of soil science, but also the synthetic symbol of the developed level of soil science (Liu, 1988; Fu, 2003). The soil analyzing system studied out by human in different period can reflect the understanding level and soil science seedtime of this period. At present, the study on soil classification has developed toward the direction of using evaluated index and quantity index (Liu, 1988; Xie, 2000; Liu, 1997; Zhao, 2000). Fuzzy clustering analysis has been applied broadly. But in fuzzy clustering analysis, there are different methods used by different people to demarcating the data, such as correlation coefficient method, distance method and so on. Different methods can obtain different fuzzy similarity matrix. The final result of classification has partial difference. Different demarcating method can use and pick-up different information in the soil samples. Otherwise, when we calculate the best-classified result (the best threshold value λ), we often apply the method of mathematical statistics. That means that the best threshold value will be calculated through building statistical value F. We will analyze and judge further whether the threshold value λ is the best or not. These show that a certain soil classification method can only provide a tool and thought. For a concrete issue, we should combine the practical condition to making a right judgement. Based on this, the author put forward a new method to classify the soil. This is Self-Organizing Feature Map (SOM) network that has the function of clustering.

2. SOC Artificial Neural Networks

2.1 Brief Introduction of SOC Networks

Self-organizing compete (SOC) artificial neural networks is a kind of networks without teaching. It has the function of self-organizing. Through training by itself, it can classify the input samples automatically. The basic thought of SOC networks is that each nerve cell in completed layer completes the responded chance to input mode. At last, only one nerve cell becomes the winner. At the same time, it can adjust the linked weights relative to the winner nerve cell toward the better direction. So, self-organizing compete artificial neural networks can be applied to classification aspect (Wen, 2000; Wang, 1995).

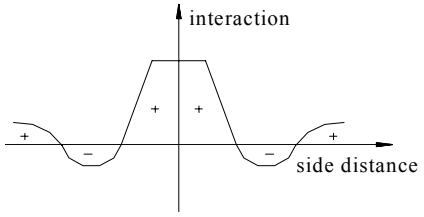

Figure 1. The Relation of Lateral Interaction

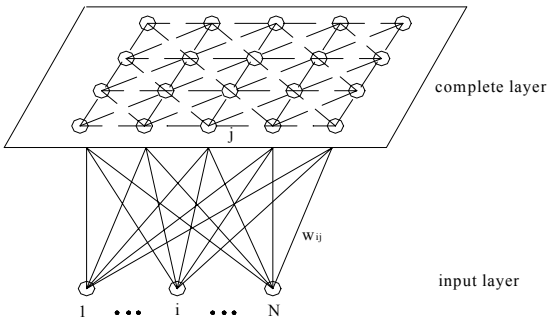

Figure 2. The Structure of Self-organizing Character Mapping Network

2.2 Self-Organizing Feather Map (SOM) Artificial Neural Networks (Wen, 2000; Wang, 1995)

SOM has been put forward in 1981 by professor

Kohonen. The corporate feature of nerve cell is that the neighbouring two nerve cells excite through stimulating each other, and the farside nerve cells restrain each other. The farther nerve cells have a little excitement. This kind of part mutual relation can be described in Figure 1. The network configuration sees to Figure 2. The number of nerve cell in input layer is n. The competed layer composes $M = m^2$ nerve cells. Thus, these nerve cells build up a two-dimension plane array. The nerve cells in input layer are all linked with the nerve cells in competed layer. Sometimes, side controlled links each nerve cell in competed layer. There are two linked weights in the networks. One is to respond to exterior input. The other one is among the nerve cells. The function of the second weight is to control the interaction of every nerve cell.

2.3 The Learning and Working Rule of SOM Networks (Wen, 2000; Wang, 1995)

In Figure 2, let the input mode is

$P_k = (p_1^k, p_2^k, \cdots, p_N^k)$, $k = 1,2,\cdots,q$.

The nerve cell vector in competed layer is

$A_j = (a_{j1}, a_{j2}, \cdots, a_{jm})$, $j = 1,2,\cdots,m$.

Where: P_k —— continue value; A_j —— number quantity.

The linked weight between nerve cells j in competed layer and nerve cells in input layer is as follows.

$W_j = (w_{j1}, w_{j2}, \cdots, w_{ji}, \cdots w_{jN})$, $i = 1,2,\cdots,N$, $j = 1,2,\cdots,M$.

The learning and working rule is as follows.

(1) Initialize. Endow the linked weight ($\{w_{ij}\}$) of networks with random value in the region of [0,1]. $i = 1,2,\cdots,N$, $j = 1,2,\cdots,M$. Define the original value of learning rate $\eta(0)$ ($0 < \eta(0) < 1$) and neighbouring threshold $N_g(t)$. ($N_g(t) = N_g(0)$). The total learning time is T.

(2) Select any one mode (P_k) in the total mode (q) to input layer. At the same time, we should normalize the data as follows.

$$\overline{P_k} = \frac{P_k}{\|P_k\|} = \frac{(p_1^k, p_2^k, \cdots p_n^k)}{\left[(p_1^k)^2 + (p_2^k)^2 + \cdots + (p_n^k)^2\right]^{1/2}}$$

(3) Normalize the linked weight $W_j = (w_{j1}, w_{j2}, \cdots, w_{ji}, \cdots w_{jN})$. Calculate the distance between $\overline{W_j}$ and $\overline{P_k}$.

$$\overline{w}_j = \frac{w_j}{\|w_j\|} = \frac{(w_{j1}, w_{j2}, \cdots, w_{jn})}{\left[(w_{j1})^2 + (w_{j2})^2 + \cdots + (w_{j3})^2\right]^{1/2}}$$

$$d_j = \left[\sum_{i=1}^{N} (\overline{p}_i^k - \overline{w}_{ji})^2\right]^{1/2}, \quad j = 1,2,\cdots,M$$

(4) Find out the least distance d_g. Define the winner nerve cell g. $d_g = min\{d_j\}$, $j = 1,2,\cdots,M$

(5) Adjust the linked weight. Modify all the linked weight between the nerve cells in the neighbouring threshold ($N_g(t)$) in competed layer and in input layer.

$$\overline{w_{ji}(t+1)} = \overline{w_{ji}(t)} + \eta(t) \cdot \left[\overline{p_i^k} - \overline{w_{ji}(t)}\right], \quad j \in N_g(t),$$

$j = 1,2,\cdots,M$, ($0 < \eta(0) < 1$)

(6) Select another learning mode to networks input layer. Return to step (3). The learning process will not end until all the learning modes have been provided to networks.

(7) Renovate the learning rate $\eta(t)$ and $N_g(t)$.

$$\eta(t) = \eta(0)(1 - \frac{t}{T})$$

$\eta(0)$ ——original learning rate; t ——learning time; T ——the total learning time.

Now, let the coordinate value of any nerve cell (g) in competed layer is (x_g, y_g). The scope of neighbouring region is a square. The top right corner of the square is $(x_g + N_g(t), y_g + N_g(t))$. The down left corner of the square is $(x_g - N_g(t), y_g - N_g(t))$. The revised formula is $N_g(t) = INT\left[N_g(0)(1 - \frac{t}{T})\right]$.

$INT[x]$ —— the symbol of getting the integer; $N_g(0)$ is the original of $N_g(t)$.

(8) Let: $t = t + 1$. Return to step (2). The whole process will not end until $t = T$.

3. Soil Classification Based on SOM Networks.

Now, we use the data of Liu (1988). There are 21 samples in Songhua River area. There are 9 indexes of each sample. The original data see to Table 1.

Ensure the input mode of the networks is $P_k = (p_1^k, p_2^k, \cdots, p_N^k)$, $k = 1,2,\cdots,q$. ($q = 21$, $N = 9$).

Calculate these data based on software MATLAB 5.3.

(1) Using function newsom（P，[D1，D2，…Di]）to build up a SOM networks.

P——input vector. i——the dimension number.

We should give the scope of each input vector.

net=newsom([0 1;0 1;0 11;0 10;0 50;0 70;0 70;0 2;0 50]，[6 1]（The number can be adjusted）);

Table 1. Soil Sample and Its Character Index

Sample number	Soil name	Total nitrogen (%)	Total phosphor (%)	Soil character: Organic matter (%)	pH	Substitution quantity (me/100)	Cultivated depth (cm)	Physical clay content (%)	Capability $g \cdot cm^{-3}$	Field moisture capacity (%)
1	Folium mucosity bottom white slurry black soil	0.270	0.142	6.46	5.5	35.8	21	45.3	1.03	29.3
2	Thick-level mucosity bottom black soil	0.171	0.115	3.46	6.3	33.0	60	45.3	0.78	38.9
3	Folium mucosity bottom black soil	0.114	0.101	2.43	6.4	26.5	25	51.0	1.13	31.6
4	Thick-level mucosity bottom black soil	0.173	0.123	3.30	5.8	28.9	65	45.6	1.09	36.1
5	Folium mucosity bottom black soil	0.145	0.131	3.28	6.0	28.5	25	51.0	1.03	30.5
6	Thick-level black meadow	0.173	0.140	3.45	5.8	33.4	60	49.0	0.98	35.2
7	Middle-level black meadow	0.250	0.177	5.51	7.2	42.5	45	46.6	0.93	29.8
8	Folium black meadow soil	0.237	0.189	5.37	6.1	32.9	27	45.0	1.00	33.0
9	Folium gully black meadow soil	0.319	0.227	7.04	5.8	35.9	24	39.3	1.03	28.8
10	Thick-level flat meadow soil	0.163	0.124	3.73	6.2	30.6	61	48.1	1.28	26.0
11	Middle-level flat meadow soil	0.194	0.201	4.50	5.7	30.9	35	47.4	1.25	43.9
12	Thick-level gully meadow soil	0.142	0.185	3.79	6.4	32.5	55	51.0	1.10	22.8
13	Thick-level gully latent raised meadow soil	0.240	0.217	4.92	6.5	37.3	41	63.6	1.17	35.5
14	Folium gully latent raised meadow soil	0.253	0.172	4.63	6.8	35.7	20	44.1	1.15	33.0
15	Thick-level plat carbonate meadow soil	0.357	0.289	7.21	7.5	42.1	40	48.3	0.80	33.0
16	Middle-level gully carbonate meadow soil	0.280	0.204	10.68	6.7	42.5	31	41.5	1.05	41.0
17	Middle-level meadow	0.164	0.141	3.05	4.8	19.7	30	30.9	1.22	29.0
18	Arenaceous meadow soil	0.095	0.099	1.51	6.0	16.0	20	26.4	1.27	26.0
19	Eroded dark and brown soil	0.392	0.240	6.62	5.3	37.3	14	34.7	1.10	26.7
20	Folium white slurry soil	0.267	0.208	6.25	5.8	39.5	19	42.4	1.10	28.0
21	Yellow and white slurry soil	0.137	0.111	3.04	5.1	23.7	18	43.1	1.37	34.0
	Average value	0.2160	0.1684	4.7729	6.0810	32.6286	35.0476	44.7429	1.0886	32.0048

(2) Using function train () and function sim () to train and simulate. Let the training time is 5000. The final classified results see to Table 2. From Table 2 we can see that the character of sample (4) and (6) is very close. They all belong to thick-level mucosity bottom black soil. Sample (9) and (20) belong to the same kind. Sample (3) and (5) are all folium mucosity bottom black soil, and have the similar character. If we classify all the samples to two groups, we can see that most of folium soil belongs to one group. The soil of thick and middle-level belong to another group. SOM networks can classify the soil according to the different networks

dimension. So, the dimension number determines the final results. But the total trend varied a little. From Table 2 we know that the result can reflect the practical complexion.

Table 2. Soil Classify Based on SOM Network (Trained 5000 times)

Networks dimension	Numbers of classification	Serial number of sample x_i
[1 1]	1	(1 2 3 4 5 6 7 8 9 10 11 12 13 14 15 16 17 18 19 20 21)
[2 1]	2	(2 4 6 7 10 11 12 13 15 16)(1 3 5 8 9 14 17 18 19 20 21)
[3 1]	3	(2 4 6 10 12)(7 11 13 15 16)(1 3 5 8 9 14 17 18 19 20 21)
[4 1]	4	(2 4 6 10 12)(7 11 13 15 16)(1 3 5 8 9 14 20)(17 18 19 21)
[5 1]	5	(2 4 6 10 12)(7 13 15)(11 16)(1 3 5 8 9 14 20)(17 18 19 21)
[6 1]	6	(2 4 6 10 12)(7 13 15)(11 16)(17 18)(19 21)(1 3 5 8 9 14 20)
[7 1]	7	(2 4 6 10)(12)(7 13 15)(11 16)(1 3 5 8 9 14 20)(19 21)(17 18)
[8 1]	8	(2 4 6 10)(12)(7 13 15)(11 16)(3 5 8)(1 9 14 20)(19 21)(17 18)
[9 1]	9	(2 4 6 10)(12)(7)(13 15)(11 16)(3 5 8)(1 9 14 20)(19 21)(17 18)
[10 1]	10	(2 4 6 10)(12)(7)(13 15)(11 16)(3 5 8)(1 14)(9 19 20)(21)(17 18)
[11 1]	11	(2 4 6 10)(12)(7)(13 15)(11 16)(3 5)(8)(1 14)(9 19 20)(21)(17 18)
[12 1]	12	(2 4 6 10)(12)(7)(13 15)(11 16)(3 5)(8)(1 14)(9 19 20)(21)(17 18)
[13 1]	13	(2 4 6)(10)(12)(7)(13)(15)(11 16)(3 5)(8)(1 14)(9 19 20)(21)(17 18)
[14 1]	14	(2)(4 6)(10)(12)(7)(13)(15)(11 16)(3 5)(8)(1 14)(9 19 20)(21)(17 18)
[15 1]	15	(2)(4 6)(10)(12)(7)(13)(15)(11)(16)(3 5)(8)(1 14)(9 19 20)(21)(17 18)
[16 1]	16	(2)(4 6)(10)(12)(7)(13)(15)(11)(16)(3 5)(8)(1 14)(9 19 20)(21)(17)(18)
[17 1]	17	(2)(4 6)(10)(12)(7)(13)(15)(11)(16)(3 5)(8)(1)(14)(9 19 20)(21)(17)(18)
[18 1]	18	(2)(4 6)(10)(12)(7)(13)(15)(11)(16)(3 5)(8)(1)(14)(9 20)(19)(21)(17)(18)
[19 1]	19	(2)(4 6)(10)(12)(7)(13)(15)(11)(16)(3)(5)(8)(1)(14)(9 20)(19)(21)(17)(18)
[20 1]	20	(2)(4 6)(10)(12)(7)(13)(15)(11)(16)(3)(5)(8)(1)(14)(9)(20)(19)(21)(17)(18)
[21 1]	21	(2)(4)(6)(10)(12)(7)(13)(15)(11)(16)(3)(5)(8)(1)(14)(9)(20)(19)(21)(17)(18)

4. Fuzzy Clustering Method to Classify the Soil

We can apply fuzzy clustering method to classify the soil samples. The final result of classification is as follows.

If λ =1.0, we can divide it into 21 kinds.

If λ =0.9810, we can divide it into 20 kinds.

$\{x_4, x_6\}, \{x_1\}, \{x_2\}, \{x_3\}, \{x_5\}, \{x_7\}, \{x_8\}, \{x_9\}, \{x_{10}\}, \{x_{11}\}, \{x_{12}\}, \{x_{13}\}, \{x_{14}\}, \{x_{15}\}, \{x_{16}\}, \{x_{17}\}, \{x_{18}\}, \{x_{19}\}, \{x_{20}\}, \{x_{21}\}$;

If λ =0.9801, we can divide it into 19 kinds.

$\{x_4, x_6\}$, $\{x_9, x_{20}\}$, $\{x_1\}$, $\{x_2\}$, $\{x_3\}$, $\{x_5\}$, $\{x_7\}$, $\{x_8\}$, $\{x_{10}\}$, $\{x_{11}\}$, $\{x_{12}\}$, $\{x_{13}\}$, $\{x_{14}\}$, $\{x_{15}\}, \{x_{16}\}, \{x_{17}\}, \{x_{18}\}, \{x_{19}\}, \{x_{21}\}$;

If λ =0.9719, we can divide it into 18 kinds.

$\{x_4, x_6\}, \{x_9, x_{20}\}, \{x_5, x_{13}\}, \{x_1\}, \{x_2\}, \{x_3\}, \{x_7\}, \{x_8\}, \{x_{10}\}, \{x_{11}\}, \{x_{12}\}, \{x_{14}\}, \{x_{15}\}, \{x_{16}\}, \{x_{17}\}, \{x_{18}\}, \{x_{19}\}, \{x_{21}\}$;

If λ =0.9694, we can divide it into 17 kinds.

$\{x_4, x_6\}, \{x_9, x_{20}\}, \{x_5, x_8, x_{13}\}, \{x_1\}, \{x_2\}, \{x_3\}, \{x_7\}, \{x_{10}\}, \{x_{11}\}, \{x_{12}\}, \{x_{14}\}, \{x_{15}\}, \{x_{16}\}, \{x_{17}\}, \{x_{18}\}, \{x_{19}\},$

$\{x_{21}\}$;

If λ =0.9693, we can divide it into 16 kinds.

$\{x_4, x_6\}, \{x_9, x_{19}, x_{20}\}, \{x_5, x_8, x_{13}\}, \{x_1\}, \{x_2\}, \{x_3\}, \{x_7\}, \{x_{10}\}, \{x_{11}\}, \{x_{12}\}, \{x_{14}\}, \{x_{15}\}, \{x_{16}\}, \{x_{17}\}, \{x_{18}\}, \{x_{21}\}$;

If λ =0.9674, we can divide it into 15 kinds.

$\{x_4, x_6\}, \{x_9, x_{19}, x_{20}\}, \{x_5, x_8, x_{13}, x_{14}\}, \{x_1\}, \{x_2\}, \{x_3\}, \{x_7\}, \{x_{10}\}, \{x_{11}\}, \{x_{12}\}, \{x_{15}\}, \{x_{16}\}, \{x_{17}\}, \{x_{18}\}, \{x_{21}\}$;

If λ =0.9665, we can divide it into 14 kinds.

$\{x_4, x_6\}$, $\{x_9, x_{19}, x_{20}\}$, $\{x_3, x_5, x_8, x_{13}, x_{14}\}$, $\{x_1\}$, $\{x_2\}$, $\{x_7\}$, $\{x_{10}\}$, $\{x_{11}\}$, $\{x_{12}\}$, $\{x_{15}\}, \{x_{16}\}, \{x_{17}\}, \{x_{18}\}, \{x_{21}\}$;

If λ =0.9659, we can divide it into 13 kinds.

$\{x_4, x_6\}, \{x_1, x_9, x_{19}, x_{20}\}, \{x_3, x_5, x_8, x_{13}, x_{14}\}, \{x_2\}, \{x_7\}, \{x_{10}\}, \{x_{11}\}, \{x_{12}\}, \{x_{15}\}, \{x_{16}\}, \{x_{17}\}, \{x_{18}\}, \{x_{21}\}$;

If λ =0.9635, we can divide it into 12 kinds.

$\{x_4, x_6\}, \{x_1, x_9, x_{19}, x_{20}\}, \{x_3, x_5, x_8, x_{13}, x_{14}, x_{16}\}, \{x_2\}, \{x_7\}, \{x_{10}\}, \{x_{11}\}, \{x_{12}\}, \{x_{15}\}, \{x_{17}\}, \{x_{18}\}, \{x_{21}\}$;

If λ =0.9576, we can divide it into 11 kinds.

$\{x_2, x_4, x_6\}, \{x_1, x_9, x_{19}, x_{20}\}, \{x_3, x_5, x_8, x_{13}, x_{14}, x_{16}\}, \{x_7\}, \{x_{10}\}, \{x_{11}\}, \{x_{12}\}, \{x_{15}\}, \{x_{17}\}, \{x_{18}\}, \{x_{21}\}$;

If λ =0.9550, we can divide it into 10 kinds.

$\{x_2, x_4, x_6\}, \{x_1, x_3, x_5, x_8, x_9, x_{13}, x_{14}, x_{16}, x_{19}, x_{20}\}, \{x_7\}, \{x_{10}\}, \{x_{11}\}, \{x_{12}\}, \{x_{15}\}, \{x_{17}\}, \{x_{18}\}, \{x_{21}\}$;

If λ =0.9504, we can divide it into 9 kinds.

$\{x_2, x_4, x_6\}, \{x_1, x_3, x_5, x_8, x_9, x_{13}, x_{14}, x_{16}, x_{19}, x_{20}\}, \{x_{10}, x_{12}\}, \{x_7\}, \{x_{11}\}, \{x_{15}\}, \{x_{17}\}, \{x_{18}\}, \{x_{21}\}$;

If λ =0.9470, we can divide it into 8 kinds.

$\{x_2, x_4, x_6\}, \{x_1, x_3, x_5, x_8, x_9, x_{13}, x_{14}, x_{16}, x_{19}, x_{20}\}, \{x_7, x_{15}\}, \{x_{10}, x_{12}\}, \{x_{11}\}, \{x_{17}\}, \{x_{18}\}, \{x_{21}\}$;

If λ =0.9414, we can divide it into 7 kinds.

$\{x_2, x_4, x_6\}, \{x_1, x_3, x_5, x_7, x_8, x_9, x_{13}, x_{14}, x_{15}, x_{16}, x_{19}, x_{20}\}, \{x_{10}, x_{12}\}, \{x_{11}\}, \{x_{17}\}, \{x_{18}\}, \{x_{21}\}$;

If λ =0.9271, we can divide it into 6 kinds.

$\{x_2, x_4, x_6, x_{10}, x_{12}\}, \{x_1, x_3, x_5, x_7, x_8, x_9, x_{13}, x_{14}, x_{15}, x_{16}, x_{19}, x_{20}\}, \{x_{11}\}, \{x_{17}\}\{x_{18}\}, \{x_{21}\}$;

If λ =0.9260, we can divide it into 5 kinds.

$\{x_2, x_4, x_6, x_{10}, x_{12}\}, \{x_1, x_3, x_5, x_7, x_8, x_9, x_{11}, x_{13}, x_{14}, x_{15}, x_{16}, x_{19}, x_{20}\}, \{x_{17}\}, \{x_{18}\}, \{x_{21}\}$;

If λ =0.9109, we can divide it into 4 kinds.

$\{x_1, x_2, x_3, x_4, x_5, x_6, x_7, x_8, x_9, x_{10}, x_{11}, x_{12}, x_{13}, x_{14}, x_{15}, x_{16}, x_{19}, x_{20}\}, \{x_{17}\}\{x_{18}\}, \{x_{21}\}$;

If λ =0.8997, we can divide it into 3 kinds.

$\{x_1, x_2, x_3, x_4, x_5, x_6, x_7, x_8, x_9, x_{10}, x_{11}, x_{12}, x_{13}, x_{14}, x_{15}, x_{16}, x_{19}, x_{20}\}, \{x_{17}, x_{21}\}\{x_{18}\}$;

If λ =0.8712, we can divide it into 2 kinds.

$\{x_1, x_2, x_3, x_4, x_5, x_6, x_7, x_8, x_9, x_{10}, x_{11}, x_{12}, x_{13}, x_{14}, x_{15}, x_{16}, x_{17}, x_{19}, x_{20}, x_{21}\}, \{x_{18}\}$;

If λ =0.7881, we can divide it into 1 kinds.

$\{x_1, x_2, x_3, x_4, x_5, x_6, x_7, x_8, x_9, x_{10}, x_{11}, x_{12}, x_{13}, x_{14}, x_{15}, x_{16}, x_{17}, x_{18}, x_{19}, x_{20}, x_{21}\}$。

The results of dynamic clustering see to Figure 3. The best threshold value λ can be calculated by statistical quantity F (Table 3). In Table 3, r is the number of the classifications.

From Table 3 we can see that there are 11 F to satisfy the inequation $F > F_{0.05}(r-1, n-r)$. Now, let's check （F - F_α）. We can select the （F - F_α）that has rather big value as the main result of classification. λ =0.9470（8 kinds），λ =0.9260（5 kinds）. So, the best soil classification is 5 kinds or 8 kinds.

4.3 Analyze the Result

When λ =0.8712, these soil samples can be divided into two kinds as follows.

$$\left\{\begin{matrix} x_1, x_2, x_3, x_4, x_5, x_6, x_7, x_8, x_9, x_{10}, x_{11}, x_{12}, x_{13}, \\ x_{14}, x_{15}, x_{16}, x_{17}, x_{19}, x_{20}, x_{21} \end{matrix}\right\}, \{x_{18}\}$$

Table 3. Calculating F to Obtain the Best Threshold Value λ in Soil Classify

λ	1.0000	0.9810	0.9801	0.9719	0.9694	0.9693	0.9674	0.9665	0.9659	0.9635	0.9576
r	21	20	19	18	17	16	15	14	13	12	11
F	0	15.1063	17.2141	4.4997	4.4751	5.1556	4.9366	5.6952	6.6561	5.8316	6.9994
$F_{0.05}(r-1,n-r$		247.5	19.4	8.68	5.84	4.62	3.96	3.55	3.28	3.10	2.98
$(F-F_{\alpha})$	---	---	---	---	---	0.5356	0.9766	2.1452	3.3761	2.7316	4.0194
λ	0.9550	0.9504	0.9470	0.9414	0.9271	0.9260	0.9109	0.8997	0.8712	0.7881	
r	10	9	8	7	6	5	4	3	2	1	
F	5.4332	6.6171	8.1403	6.5647	7.3600	8.6611	1.6738	2.4192	2.398	0	
$F_{0.05}(r-1,n-r$	2.90	2.85	2.83	2.85	2.90	3.01	3.20	3.55	4.38		
$(F-F_{\alpha})$	2.5332	3.7671	5.3103	3.7147	4.46	5.6511	---	---	---	---	

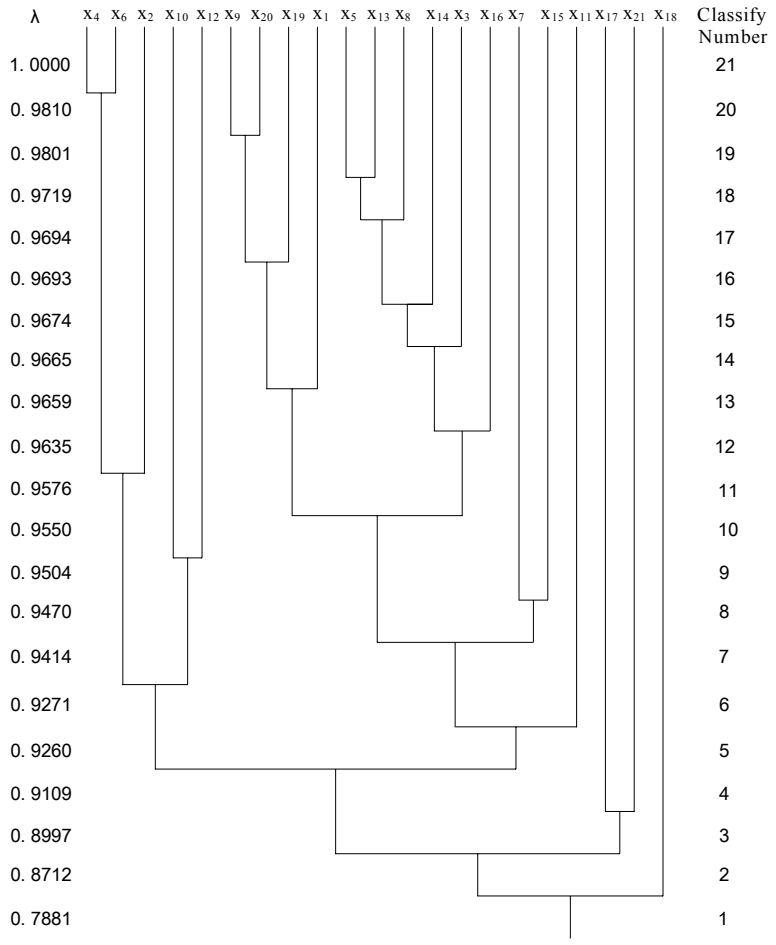

Figure 3. Fuzzy Dynamic Clustering of Soil

The sample 18 belongs to one kind itself. It shows that the indexes of total nitrogen, total phosphor, substitution quantity, organic matter and so on are all lower than other soil samples. So that, it is reasonable for that it has been divided into a single kind.

If λ=0.9260, we can divide it into 5 kinds. One is $\{x_2, x_4, x_6, x_{10}, x_{12}\}$.

It shows that the character of most of thick soil is close.

Another is

$\{x_1, x_3, x_5, x_7, x_8, x_9, x_{11}, x_{13}, x_{14}, x_{15}, x_{16}, x_{19}, x_{20}\}$.

It shows that the character of most of folium soil is close.

The others are $\{x_{17}\}, \{x_{18}\}$ and $\{x_{21}\}$.

If λ=0.9470, we can divide it into 8 kinds.

$\{x_2, x_4, x_6\}$, $\{x_1, x_3, x_5, x_8, x_9, x_{13}, x_{14}, x_{16}, x_{19}, x_{20}\}$, $\{x_7, x_{15}\}, \{x_{10}, x_{12}\}, \{x_{11}\}, \{x_{17}\}, \{x_{18}\}, \{x_{21}\}$.

It can reflect the same information as other classification. This information is accord with the practical complexion.

5. Discussions

According to Liu (1988), the fuzzy similarity matrix is built by distance method. The method used the distance information among every sample. The final result of the best classification is 12 kinds or 17 kinds. In this paper, the authors apply the method of correlation coefficient. The best classification is 5 kinds or 8 kinds. In SOM network, the training function Linkdist（pos）adopts the distance method also, and the final result is closer to Liu (1988). The different result shows that different methods to build up demarcated matrix can pickup different information in the original data. Thus, the result will have part difference. But the above three methods can reflect the practical complexion. They have the similar classified configuration.

On the other hand, it is very easy to use SOM networks to classify the soil samples. SOM network can train, learn and compete by itself. It can give us the best-classified result according to the people's wish. Especially when we use the SOM-ANN toolbox in MATLAB 5.3 software, we can make the problem of soil classification much simply. At last, we should give the right result according to combine with practical complexion.

Fund Item: Chinese National "863" High-Technique Programme (No. 2002AA2Z4251-210041).

Correspondence to:
Qiang Fu
School of Water Conservancy & Civil Engineering
Northeast Agricultural University
Harbin, Heilongjiang 150030, China
Telephone: 01186-451-5519-0298
Cellular phone: 01186-13936246215
E-mail: fuqiang100@371.net

References

Fu Q, Xie YG, Wei Z.M. 2003. Application of Projection Pursuit Evaluation Model Based on Real-Coded Accelerating Genetic Algorithm in Evaluating Wetland Soil Quality Variation in the Sanjiang Plain, China [J]. Pedosphere 2003;13(3):249-56.

Liu X. Applying fuzzy clustering to soil classification. Journal of Northeast Agricultural College 1988(2):112-26.

Liu ZG, Ma XH. Effect of reclamation on soil environment in Sanjiang Plain. Pedosphere 1997;7(1):73-8.

Wang W. The principle of ANN——Introduction and Application. Publishing Company of Beijing Aviation Spaceflight University, Beijing, China. 1995:157-65.

Wen X, Zhou L, Wang D. Design the ANN with MATLAB. Science Publishing Company, Beijing, China. 2000:271-85.

Xie J, Liu C. Fuzzy Mathematics Method and Its Application. Middle China Technique Publishing Company, Wuhan, Hubei, China. 2000:81-106.

Zhao QG. Resource and environmental quality changes and adjustment principles for sustainable development in rapidly developing coastal region of Southeastern China. Pedosphere. 2001;11(4):289-99.

Flood Disaster Loss Evaluation Model Based on Projection Pursuit

Juliang Jin, Yu Zhang, Libing Zhang

College of Civil Engineering, Hefei University of Technology, Hefei, Anhui 230009, China,
jinjl66@xinhuanet.com

Abstract: In order to resolve the non-uniformity problem of evaluation results of disaster loss indexes, and to raise the evaluation result precision of flood disaster loss, a projection pursuit（PP）based flood disaster loss model is suggested, where the results of flood disaster loss evaluation are real numbers. A scheme of PP modeling is also presented to reduce the computational amount, and a new function of projection indexes is given. It is suggested that both the function of projection indexes and the parameters of PP model can be optimized by using a real coding based genetic algorithm. The calculation example shows that the model is effective and general, which can be applied to evaluating other natural disaster loss. [Nature and Science 2003;1(1):82-85].

Key words： flood disaster loss; evaluation; projection pursuit (PP); genetic algorithm

1. Introduction

Flood disaster loss evaluation is to evaluate the damage degree caused by flood disaster according to flood disaster loss evaluation criterions, existing flood disaster loss evaluation index values and disaster loss evaluation model (Jin, 2002). The result of disaster loss evaluation, named as disaster loss grade, disaster grade or disaster degree (Yu, 1993; Zhao, 1993) is of important instructional significance to the flood disaster management. Flood disaster loss is involved with many factors including the natural environment and social economy etc. There are still no uniform evaluation index systems and grade criterions of flood disaster loss internationally. So evaluation problem of flood disaster loss is still one of difficulties and hotspots of researches on flood disaster.

Due to the non-uniformity of the flood disaster loss evaluation results of all indexes, it is difficult to evaluate disaster loss by directly using the disaster loss index criterions determined by historical experience of flood disaster (Jiang, 1996). So some models for evaluating disaster loss, including disaster loss degree measurement method, fuzzy comprehensive evaluation, matter element analysis, neural network and so on, have been presented one after the other (Jin, 2002;Yu, 1993; Zhao, 1997; Li, 1994). Their evaluation results are always discrete disaster grades, and the disaster grade precision is coarse. While the disaster loss indexes of actual flood disaster are usually continuous real numbers, in other words, even though the flood disasters are of the same disaster grade according to the actual models for evaluating disaster loss grade, their corresponding disaster loss index values are often different remarkably. So it is inconvenient to guide the flood disaster management.

How to synthesize a multi-index problem into a single-index problem scientifically and objectively is still the focus of researches on flood disaster loss evaluation, because only being in one dimension space makes it possible to flood disaster loss evaluate (Ren, 1998). Therefore, as an exploratory data analysis method, projection pursuit (PP) model for evaluating flood disaster loss, where the parameters are optimized by real coding based accelerating genetic algorithm (RAGA) (Jin, 2000), is suggested and applied to a case in this paper.

2. Flood Disaster Loss Evaluation Model Based on Projection Pursuit

PP is a kind of exploratory statistical method to analyze and process non-normal and high dimension data (Friedman, 1974; Li, 1997). Its basic idea is to project high dimension space data to projective values in low dimension space, to describe some structure by using a projective index function, to search the optimal projective index function, and to analyze the structure characters of the high dimension space data by the projective values, or to construct mathematical model according to the scattering dot figure formed by the projective values and the researched system output values. The problem to construct and optimize projective index function is the key to successfully applying PP method. The problem is very complex, and the computation of traditional PP methods is large (Friedman, 1974; Li, 1997), which restricts the wide application of PP technique and the deep study on it.

Here a simple scheme is presented, where a PP model for evaluating flood disaster loss is founded by using RAGA, which includes three steps as follows：

Step 1: to construct projective index function. Let $y(i)$

be the experiential grade of a certain flood disaster, which is produced according to the grade criterion table of flood disaster loss evaluation, and let $\{x^*(j,i)|j=1\sim p, i=1\sim n\}$ be the sample set of the disaster loss indexes, where n is the number of the flood disaster and p is the number of disaster loss indexes, respectively. The more the disaster loss is, the greater the disaster loss indexes are, and the higher the grades of the flood disaster loss are. Let the lowest grade of disaster loss be 1, and let the highest grade of disaster loss be N. Founding the model for evaluating flood disaster loss means constructing mathematical relation between $\{x^*(j,i)|j=1\sim p\}$ and $y(i)$. Here the aim of PP method is to synthesize the p dimension data $\{x^*(j,i)|j=1\sim p\}$ to one dimension $z(i)$ named projective value with the projective direction $\alpha=(\alpha(1), \alpha(2), \cdots, \alpha(p))$ by the following formula

$$z(i)=\sum_{j=1}^{p}\alpha(j)x(j,i) \tag{1}$$

where α is an unit length vector, then we can construct mathematical relation according to the scattering dot figure of $z(i)$ and $y(i)$. Equation (2) can be used to standardize the indexes both to eliminate the dimensional effect and to make the PP model be of generality:

$$x(j,i)=[x^*(j,i)-E_x(j)]/S_x(j) \tag{2}$$

where $\{x(j,i)|j=1\sim p\}$ are the standardized values of $\{x^*(j,i)|j=1\sim p\}$, $E_x(j)$ and $S_x(j)$ are mean value and standard deviation of the disaster loss index series $\{x^*(j,i)|i=1\sim n\}$.

When synthesizing projective value, the projective values should contain as much variation information of $\{x(j,i)\}$ as possible, in other words, the standard deviation S_z of $z(i)$ is as great as possible. Meanwhile, absolute value $|R_{zy}|$ of the related coefficient of $z(i)$ and $y(i)$ should be as great as possible. So the synthesized projective values can contain as much variation information of independent variable system $\{x(j,i)|j=1\sim p\}$ as possible, and can guarantee that the projective value is of good interpretability to attributive variable $y(i)$ (Ren, 1998). Based on the above demands, a projective index function can be designed as follows:

$$Q(\alpha)=S_z+|R_{zy}| \tag{3}$$

where $|\ |$ is to calculate absolute value, S_z is standard deviation of projective value $z(i)$, namely

$$S_z=\left[\sum_{i=1}^{n}(z(i)-E_z)^2/(n-1)\right]^{0.5} \tag{4}$$

and R_{zy} is the related coefficient of $z(i)$ and $y(i)$, namely

$$R_{zy}=\frac{\sum_{i=1}^{n}(z(i)-E_z)(y(i)-E_y(i))}{\left[\sum_{i=1}^{n}(z(i)-E_z)^2\sum_{i=1}^{n}(y(i)-E_y(i))^2\right]^{0.5}} \tag{5}$$

In equations (4) and (5), E_z and E_y are the mean values of the series $\{z(i)\}$ and $\{y(i)\}$, respectively.

Step 2: to optimize the projective index function. The value of the projective index function $Q(\alpha)$ is changed only according to the variation of the projective direction α when the grade sample set of flood disaster loss $\{y(i), i=1\sim n\}$ and the disaster index set $\{x^*(j,i)|j=1\sim p, i=1\sim n\}$ have been determined. Different projective directions reflect different data structure character, and the optimal projective direction is the direction that best discovers some structure character of the high dimension sample data. The optimal projective direction can be estimated by resolving the following optimal problem:

$$\max\ Q(\alpha)=S_z+|R_{xy}| \tag{6}$$

$$\text{s.t.}\quad \sum_{j=1}^{p}\alpha^2(j)=1 \tag{7}$$

It is a complex and nonlinear optimization problem, where the optimized variables are $\{\alpha(j)|j=1\sim p\}$, and it is difficult to resolve the problem by using the traditional methods (Friedman, 1974; Li, 1997). As a kind of general optimization methods based on the mechanics of natural selection and natural genetics, RAGA can be applied to deal with the optimization problem easily and effectively (Jin, 2000).

Step 3: to found the PP model of evaluating flood disaster loss. The projective value $z^*(i)$ of the ith flood disaster can be gained by substituting the equation (1) with the optimal projective direction α^* according to Step 2. Then we can found the corresponding mathematical model according to the scattering dot figure of $z^*(i)\sim y(i)$. Present writers find what the scattering dot figure of $z^*(i)\sim y(i)$ reflecting here is monotonically increasing relation between $z^*(i)$ and $y(i)$: when $z^*(i)$ is greater than a certain threshold, it is determined to be the highest grade of flood disaster (Grade N); when $z^*(i)$ is less than another certain threshold, it is determined to be the lowest grade of flood disaster (Grade 1); when $z^*(i)$ is between the two thresholds, it is determined to be the medium grade of flood disaster. This is a relation that both the upper segment and the lower segment have limits, and the middle segment varies and increases rapidly and progressively. So it is appropriate to take Logistic Curve as the model of evaluating flood disaster loss, namely (Jin, 1997).

$$y^*(i)=\frac{N}{1+e^{c(1)-c(2)z^*(i)}} \tag{8}$$

where $y^*(i)$ is the calculated value of the grade of the ith flood disaster; the highest grade N is the upper limit of the Logistic Curve; $c(1)$ and c(2), being undetermined parameters, are integral constant and increase rate, and they can be determined by resolving the following minimization problem with using RAGA (Jin, 2000; Jin,

1997):

$$\min F(c(1),c(2)) = \sum_{i=1}^{n} [y^*(i) - y(i)]^2 \quad (9)$$

3. Case Study

Flood disaster area $x^*(1,i)$ and direct economic loss $x^*(2,i)$ are taken as the grade evaluation indexes of flood disaster loss. The frequency analysis was done of the actual series data of Henan Province of China between 1950 and 1990, and then the grade criterions of flood disaster loss of Henan Province are gained (Table 1) (Jiang, 1996).

Table 1. Evaluation Criterions of Flood Disaster Loss of Henan Province of China (Jiang, 1996)

evaluation indexes	ordinary disaster	fairly great disaster	great disaster	super disaster
flood disaster area (km^2)	<46.7	46.7~136.7	136.7~283.3	>283.3
direct economic loss (10^8 yuan)	<9.5	9.5~31.0	31.0~85.0	>85.0

Random evaluation indexes values and corresponding sample series of experiential grades of flood disaster loss can be gained by using the steps as follows: 1) The values of experiential disaster loss grades 1,2,3 and 4 are for the four values of ordinary disaster, fairly great disaster, great disaster, and super disaster, respectively. 2) The index value of the left extreme point of ordinary disaster can be determined as 0.5 times the index value of the right extreme point of ordinary disaster, and the index value of the right extreme point of the super disaster can be determined as 3 times the index value of the left extreme point of the super disaster. So every disaster loss grade has its index value range. 3) Five values can be gained by using uniform random number in the index value range of each disaster loss grade. The direct economic loss and the flood disaster area should have the same uniform random number in the same sample dot, considering that direct economic loss and flood disaster area are generally of positive relativity. 4) Every boundary value is chosen once from Table 1, and the corresponding disaster loss grade value is chosen as the arithmetic mean value of two disaster loss grade values related to the boundary value. So 23 sample dots are gained from No.1 to No.23 in Table 2.

Table 2. Comparison between Experiential Grade Values and Calculated Grade Values of PP Model

No.	evaluation indexes		$z^*(i)$	grades of flood disaster loss		No.	evaluation indexes		$z^*(i)$	grades of flood disaster loss	
	$x^*(1,i)$	$x^*(2,i)$		experiential	PP model		$x^*(1,i)$	$x^*(2,i)$		experiential	PP model
1	38.70	7.900	-1.179	1.0	1.375	17	157.30	38.600	-0.472	3.0	2.486
2	38.50	7.800	-1.180	1.0	1.374	18	283.30	85.000	0.424	3.5	3.499
3	32.10	6.500	-1.215	1.0	1.323	19	556.90	67.100	2.174	4.0	3.966
4	24.20	4.900	-1.257	1.0	1.264	20	649.50	194.900	2.766	4.0	3.987
5	36.40	7.400	-1.191	1.0	1.358	21	602.30	180.700	2.464	4.0	3.979
6	46.70	9.500	-1.136	1.5	1.438	22	446.50	134.000	1.468	4.0	3.897
7	97.60	21.700	-0.843	2.0	1.896	23	694.90	208.500	3.056	4.0	3.992
8	60.40	12.800	-1.057	2.0	1.558	1950	72.92	9.900	-1.047	2.0	1.573
9	112.60	25.200	-0.757	2.0	2.035	1954	148.13	20.656	-0.690	2.0	2.143
10	56.20	11.800	-1.081	2.0	1.521	1956	203.92	27.521	-0.437	3.0	2.538
11	80.60	17.600	-0.941	2.0	1.739	1957	179.10	24.858	-0.545	3.0	2.373
12	136.70	31.000	-0.618	2.5	2.258	1963	375.46	94.927	0.827	4.0	3.722
13	259.10	76.100	0.252	3.0	3.364	1964	301.24	47.836	0.092	3.0	3.213
14	200.10	54.400	-0.167	3.0	2.915	1975	141.97	116.439	0.295	3.0	3.400
15	280.10	83.800	0.401	3.0	3.482	1982	279.84	121.127	0.792	4.0	3.707
16	236.10	67.600	0.088	3.0	3.209	1984	172.06	51.619	-0.287	3.0	2.755

The disaster grade index values $\{x^*(j,i)|j=1\sim2, i=1\sim23\}$ in Table 2 are transformed into standardized series $\{x(j,i)|j=1\sim2, i=1\sim23\}$. The standardized series and disaster loss grade value series $\{y(i)| i=1\sim23\}$ substitute the equations (1), (4), (5) and (6) in turn, and then the projective index function of the example is gained. After the function is optimized by using RAGA, its maximum value is 2.34, and the optimal projective direction is α^*= (0.7066, 0.7076). Making α^* substitute the equation (1), and then the projective values $z^*(i)$ is gained (Table 2). The scattering dot figure of $z^*(i)$~$y(i)$ shows that equation (8) can be used to describe the relation of $z^*(i)$ and $y(i)$, where N is 4, $c(1)$ and $c(2)$ in equation (8) can be estimated by using RAGA to optimize equation (9). Then PP model for evaluating flood disaster loss grade in Henan Province is

$$y^*(i) = \frac{4}{1+e^{-1.2578-1.6152z^*(i)}} \qquad (10)$$

where $y^*(i)$ is the calculated disaster loss grade value of the ith flood disaster. The calculated grade value of each flood disaster of PP model is in Table 2, and the result of error analysis between $y^*(i)$ and $y(i)$ is listed in Table 3.

Table 3. Error Analysis between Experiential Grade Values and Calculated Grade Values of PP Model

percent of absolute error falling the following range (%)						mean absolute error (disaster grade)	mean relative error (%)
[0,0.1]	[0,0.2]	[0,0.3]	[0,0.4]	[0,0.5]	[0, 0.6]		
34.78	43.48	60.87	82.61	95.65	100.00	0.22	13.42

Comparing the experiential grade values and the calculated grade values of PP model in Table 2 with the grade criterions in Table 1, the calculated values are reasonable, which more exactly describe the influence of the quantity difference of disaster loss index values on determining the disaster loss grade.

Table 3 shows that PP model can be used to describe the relationship between the projective values of flood disaster loss and the disaster loss grades. The 9 great disaster loss samples of 41 years data, which took place from 1950 to 1990 in Henan Province (Jiang, 1996), have been evaluated by using PP model, and their evaluation results can be seen from No.1950 to No.1984 in Table 2. Their experiential grade values are chosen as the evaluation results of the neural network model (Jin, 2002). The evaluation results of the two models are consistent basically, and the grade precision of disaster loss of PP model is higher. Now most of the calculated disaster loss grade values of other evaluation models are discrete, and they lack necessary transition range between the adjacent disaster loss grades. Take the flood disaster of 1950 for example, the disaster loss indexes of flood disaster area and direct economic loss are all near the bounders of the ordinary disaster and fairly great disaster, so it is reasonable that this year's disaster loss grade is evaluated as 1.573 by using PP model.

4. Conclusion

At the present time, the calculation results of the presented models for evaluating flood disaster loss are mostly discrete grades, and the grade precision of the calculation results are also coarse. For the sake of raising evaluation precision, a new model – PP model, where disaster loss grades are continuous real numbers, is suggested for evaluating flood disaster loss. A scheme of PP modeling is presented to reduce the computational amount and a new projection index function is given. It is suggested that both the function and the parameters of PP model can be optimized by using a real coding based genetic algorithm developed by the authors. The calculation example shows that PP model is effective and general, which can be applied to evaluating other natural disasters loss.

Foundation Item: The Excellent Young Teachers Program in Higher Education Institute of MOE, P.R.C. [Department of Education and Person (2002)350], Anhui Provincial Science and Technology Fund of Excellence Youth, Anhui Provincial Natural Science Foundation (No. 01045102), Chinese National Natural Science Fund Project (No. 40271024).

Correspondence to:
Juliang Jin
College of Civil Engineering
Hefei University of Technology
Hefei, Anhui 230009, Chnia
E-mail: jinjl66@xinhuanet.com

References

Friedman J H, Turkey J W. A projection pursuit algorithm for exploratory data analysis. IEEE Trans. on Computer 1974;23(9):881-890.

Jiang J, Ji X, Liu L, et al. Preliminary analysis of flood and drought disasters between 1950 and 1990 in Henan province. Journal of Catastrophology 1996;11(4):69-73 (in Chinese).

Jin J, Yang X, Ding J. Real coding based accelerating genetic algorithm. Journal of Sichuan University (Engineering Science Edition) 2000;32(4):20-24 (in Chinese).

Jin J, Yang X, Liu Y, et al. Application of genetic algorithm for estimating logistic curve parameters. System Sciences and Comprehensive Studies in Agriculture 1997;13(3):186-190 (in Chinese).

Jin J, Zhang X, Ding J. Projection pursuit model for evaluation grade of flood disaster loss. Systems Engineering—Theory & Practice 2002;22(2):140-144 (in Chinese).

Li Z, Deng X. Preliminary exploration of natural disaster loss assessment model based on matter element analysis. Journal of Natural Disasters 1994;3(2):28-33 (in Chinese).

Li Z. Projection pursuit technology and its progress of application. Journal of Nature in China 1997;19(4):224-227 (in Chinese).

Ren R, Wang H. Theory, methods and examples of data analysis for multi-variable statistics. Chinese National Defence Industry Press. 1998:109-113, 149-163 (in Chinese).

Yu Q. Localization and its improvement of disaster degree measurement method. Journal of Natural Disasters 1993;2(2):8-10 (in Chinese).

Zhao A, Ma Z. Research on assessment index system of natural disaster loss. Journal of Natural Disasters 1993;2(3):1-7 (in Chinese).

Zhao L, Wang K, Qiu P. Synthetic evaluation of disaster. Systems Engineering—Theory & Practice 1997;17(3):63-69 (in Chinese).

Experimental Study on Intelligent Gear-Shifting Control System of Construction Vehicle Based on Chaotic Neural Network

Zhenyu Zhu, Chunxin Xu

College of Mechanical Science and Engineering，Jilin University, Changchun, Jilin 130025, China,
zhu_zhy@hotmail.com

Abstract: In this paper, taking power-shifting transmission of ZL50 wheel loader as control object, an autocontrol system based on Intel-51 single-chip microcomputer has been developed. Chaotic neural networks (CNN) control technology in which chaotic optimizing algorithms is applied to improve neural networks' learning efficiency makes gear-shifting control system possess intelligentized characteristics. The results of experiment show that the intelligent control system could reliably and exactly realize an automatic transmission according to changed working conditions after gear-shifting strategy has been successfully regulated. The intelligent electronic control unit (ECU) works steadily and can accurately and duly complete gear-shifting. Finally, the study is helpful for designing intelligentized construction machinery. [Nature and Science 2003;1(1):86-90].

Keywords: construction vehicle; chaotic neural network; intelligent gear-shifting control; micro-controller

1. Introduction

The automatic transmission (AT) is a key technology to improve performance of vehicles. With the synthesized applications of mechatronics technology, computer technology, autocontrol technology on vehicles, development of modern vehicle technology is stepping into a completely new age with the characteristics of intelligence, in which one of the most primary symbols is automatization of vehicle transmission system, i.e., to realize automatic gear-shifting of the transmission. As a kind of special vehicle, construction vehicles possess very important status in vehicle family. As view of the complexity of operation, the badness of working condition and the variety of working tasks, which result in the frequent gear-shifting of the drivers for meeting the demands of vehicle power force, to realize automatic transmission on construction vehicle have special significance on improving vehicle performance, promoting working efficiency, lightening labor intension and utilizing in reason energy sources (Yi, 1998).

At present, in China, the driver makes decision on current gear of construction vehicle based on working tasks, conditions of road surface and vehicle running status, which brings on that the work efficiency of vehicle mainly depends on the experience of the driver. Moreover, automatic gear-shifting control system with the characteristics of intelligence can simulate the driver's operation and learn the optimal gear-shifting strategy and realize complex control by making use of learning and memory capability of chaotic neural network (CNN) technology that does not have to analyze control process and inner structure of the system. So intelligent gear-shifting control system is adopted on automatic transmission of the powertrain system of modern construction vehicle.

In this paper, theory analysis and experiment research have been combined. A set of intelligent gear-shifting controller with CNN technology for construction vehicle, which has auto-adaptability and on-line learning capability, is developed and a testing experiment is carried out on test-bench of the powertrain system.

2. Control Principle

2.1 Gear-shifting Strategy

Gear-shifting strategy is the core of intelligent control system of automatic transmission, because it is related to whole performance of the powertrain system and it directly affects vehicle's driving power, fuel economy and auto-adaptability to environment. Gear-shifting strategy is the rules of changing the time of automatic shifting between gears, and that the time varies with control parameters. It is a one-to-one correspondence, that there is only one output variable to every group of input variable. In order to assure the optimal driving output of construction vehicle and exert power potential of engine, gear-shifting point should be the intersection point of two gears' driving power curves in the traction trait picture when the angle of throttle is kept no change (Wang, 2001), as Figure 1 shows. According to the principle, gear-shifting rules under each angle of throttle can be obtained. When speed of vehicle is as x-axis and angle of throttle as y-axis, the optimal driving power gear-shifting curves may be drawn. In Figure 2, the real lines are rising-gear curves and the broken lines are falling-gear curves. It is seen from Figure 2 that the gear-shifting curves are composed of two or more changed rules segments, which is called the combination gear-shifting strategy. It is the integration of equal-delay type, radiating type and converging type gear-shifting strategy. The assembled rules make it

possible to attain different vehicle performances under each angle of throttle (Ge, 1993).

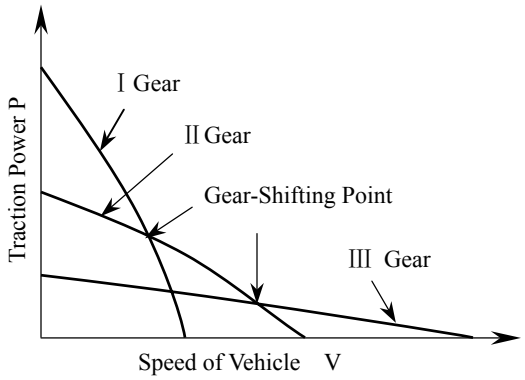

Figure 1. Principle of Optimal Driving Power Gear-Shifting

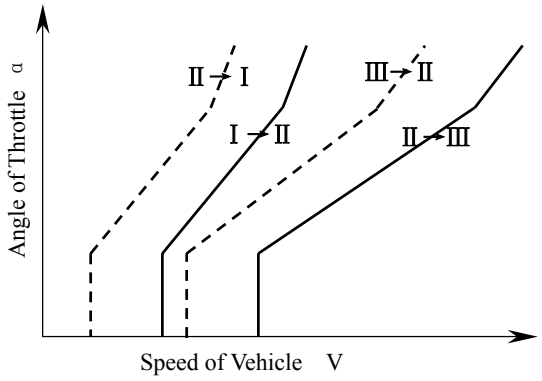

Figure 2. Sketch Map of Gear-Shifting Strategy

2.2 Design of Neural Network Control System

The optimal gear-shifting strategy is a nonlinear and multipartite function that describes the relation between vehicle state parameters (speed, angle of throttle, etc.) and the optimal gear. Owing to the complex mathematic model, it is hard to obtain the proper gear only with generic seeking methods. At the same time, the gear-shifting curves above-mentioned are altered all the time along with constantly changed working conditions of construction vehicle. In this instance, the proleptic control goal can not be achieved if old gear-shifting rules continue to be used. Neural network control methods possess great predominance on resolving nonlinear problems and distilling control rules from experimental data. So in this paper auto-adaptability and auto-learning mechanism of neural networks is introduced to construct the intelligent control system, which makes construction vehicle obtain automatically gear-shifting rules and adapt automatically to working conditions and realize the function of learning on-line, so as to assure that construction vehicle can exert optimal working efficiency and control performance （Baumann, 1998）.

For automatic transmission control of construction vehicle, the gear of transmission is controlled output parameter. The angle of engine throttle and speed of vehicle can describe running states of vehicle and ascertain traction power by selecting appropriate gear （Hiroshi, 1993）.

Model of three layers forth-feedback neural network is designed based on the theory above-mentioned, as Figure 3 shows. Neural networks adopt two inputs x_1 （angle of engine throttle）, x_2（speed of vehicle）, one output y （gear of transmission） and one middle layer （seven nerve cells）, that is to say, the structure of neural networks employed in the study is 2-7-1 format. $x_i^{(k)}$ is the output of No.*i* nerve cell in No.*k* layer nerve networks, $w_{ij}^{(k)}$ is the connection right from No.*j* nerve cell in No.*k-1* layer to No. *i* nerve cell in No.*k* layer; *n* is the number of nerve cells in No.*k* layer; $\theta_i^{(k)}$ is the threshold value of No.*i* nerve cell in No.*k* layer, hereby, the output of nerve cells in No.*k* layer can be educed in the light of the states of nerve cells in No.*k-1* layer according to formula（1）and（2） (Yuan, 1999)：

$$x_i^{(k)} = f(o_i^{(k)}) = [1 + \exp(-o_i^{(k)})]^{-1} \quad (1)$$

$$o_i^{(k)} = \sum_{j=0}^{n-1} w_{ij}^{(k)} x_j^{(k-1)} - \theta_i^{(k)} \quad (2)$$

2.3 Chaotic Optimizing Algorithm

The former multilayer nerve networks often adopt error-back propagation algorithms to modify right values and threshold values, which has the flaws of slow convergence speed and easily getting into part extremum. Even though the algorithms could be improved on by adding momentum item to the adjusting formula for right values, this method is so hard to meet the demands of making neural networks' total error converge to admissible error limit that it has influenced actual effect of control system. Therefore in this study chaotic nerve networks optimizing algorithms are put forward to carrying through networks' learning. The method, in which a nonlinear feedback item is joined in dynamics equation of nerve networks' connection right, is a iterative algorithms on the basis of grads descending method that can accelerate networks' convergence speed. The nerve networks employing chaotic optimizing algorithms, which make networks hold chaotic kinetic action in right space, can synthetize the virtues of randomicity and definitude so as to take on more flexible dynamics characteristics and higher search efficiency (Li, 2001).

Define that error function is square type. The equation is:

$$E_p = \frac{1}{2} \sum_j (y_{jp} - d_{jp})^2 \quad (3)$$

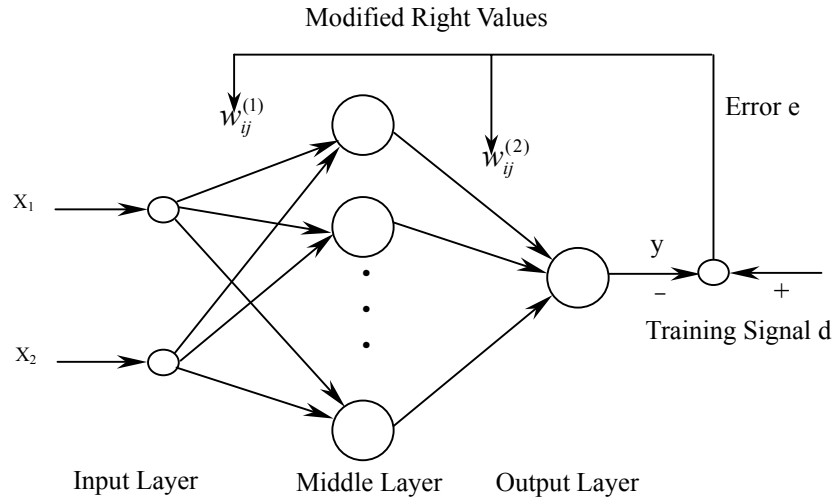

Figure 3. The Model of Three Layers Neural Networks

In above formula, y_{jp} and d_{jp} respectively is anticipant output and factual output; p is the swatch number of trained aggregate. The total error is：

$$E = \sum E_p \qquad (4)$$

Defining two variables:

$$\delta_i^{(k)} = -\frac{\partial E_p}{\partial o_i^{(k)}} = -\frac{\partial E_p}{\partial x_i^{(k)}} \frac{\partial x_i^{(k)}}{\partial o_i^{(k)}} \qquad (5)$$

$$\Delta w = \frac{dw_{ij}^{(k)}}{dt} = -\eta \frac{\partial E_p}{\partial w_{ij}^{(k)}} \qquad (6)$$

$$= -\eta \frac{\partial E_p}{\partial o_i^{(k)}} \frac{\partial o_i^{(k)}}{\partial w_{ij}^{(k)}} = -\eta \delta_i^{(k)} x_j^{(k-1)}$$

① If nerve cell i is output nerve cell of the networks, thus

$$\delta_i^{(k)} = (y_{jp} - d_{jp}) f'(o_i^{(k)}) \qquad (7)$$

② If nerve cell i isn't output nerve cell of the networks, defining that m is No. m nerve cell in middle layer, thus

$$\delta_i^{(k)} = f'(o_i^{(k)}) \sum_m w_{mj}^{(k+1)} \delta_{mj}^{(k+1)} \qquad (8)$$

Dynamics equation of right values modified：

$$w_{ij}^{(k)}(t+1) = w_{ij}^{(k)}(t) - \eta \delta_i^{(k)}(t) x_j^{(k-1)}(t) + f[w_{ij}^{(k)}(t) - w_{ij}^{(k)}(t-1)] \qquad (9)$$

$$z = W(t) - W(t-1) \qquad (10)$$

$$f(z) = \tanh(az) \exp(-bz^2) \qquad (11)$$

In above formula, η is learning rate；a and b is adjustable parameters，and different parameters can result in different feedback equation, in this paper, a=0.6，b=0.1.

3. Design Control System

3.1 Function Design of Control System

The function of intelligent control system is to realize gear-shifting manipulation based on gear-shifting strategy. The types of control system include hydraulic-pressure control model and electron-hydraulic control model according to the production of gear-shifting signal and the mode of controlling gear-shifting values (Toyama, 1992; Jiao, 1997）. In the paper, the autocontrol system with electronic control unit （ECU）adopts electron-hydraulic control mode by which electromagnetic values and gear-shifting values are controlled to complete automatic gear-shifting. Intelligent gear-shifting ECU is in charge of gathering the running state parameters of vehicle and making use of chaotic optimizing algorithms equations to learn all kinds of working conditions and gain correct gear-decision based on the well-trained CNN. In succession, ECU sends out gear-shifting signal to drive gear-shifting performing machine to accomplish gear-shifting of transmission. In order to avoid circulatory gear-shifting, it is required not to make rising-gear curves and falling-gear curves overlapped, i.e., to enactment a speed difference of gear-shifting. So two gear-decision neural networks in intelligent control system are introduced to respectively carry through learning and managing rising-gear and falling-gear instances.

3.2 Hardware Design of Intelligent Control System

Because the matrix operation in computer inner of neural networks learning algorithms is relatively complex, the hardware frame of control system consists of 2 parts: main unit and child unit in order to increase operation speed of the process and assure real time sampling and controlling. The main unit equipped with industry-using control computer with PC bus is in

charge of training the parameters of CNN while the child unit assembled with 8032 micro-controller of Intel MCS-51 series is responsible for controlling gear signal output and sampling vehicle state parameters. The two parts carry out data-exchange by extending common Random Access Memory (RAM). The main computer puts the well-calculated data into common RAM and meanwhile analyses the running data imported from micro-controller while single-chip controller reads the control data in common RAM and drives the electromagnetic values to perform gear-shifting operation (Wang, 2002). The hardware structure of control system is shown in Figure 4.

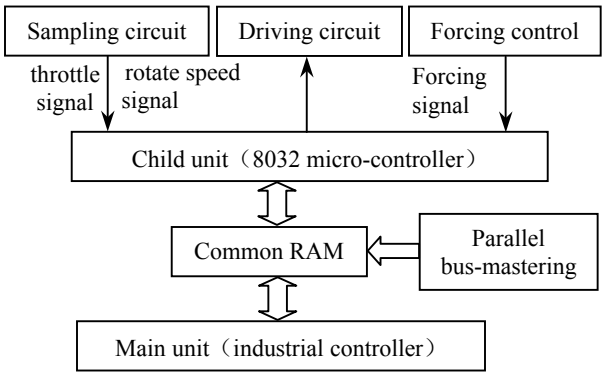

Figure 4. Hardware Design of Control System

4. Experiment and Results Analysis

4.1 Structure of Test-Bench for Powertrain System

In this experiment, the powertrain system equipped on ZL50 wheel loader is taken as controlled object. The main devices include X6130 diesel engine, YJ355 hydrodynamic torque converter （three components, single grade, single posture）, 4D180 hydrodynamic transmission box equipped with 4 forward-gear and 4 back-gear, torque sensor, rotate speed sensor and PD-WC575 power-measure machine with electric vortex. To test the whole performance of the gear-shifting controller, the designed intelligent gear-shifting control system is connected with the performing machine, and torque and rotate speed sensors are laid on the output port of the engine and transmission, and the measuring and controlling apparatus for engine and power-measure machine is employed to respectively control the angle of engine throttle and the output of power-measure machine. During the running process of the system, data-watch system ever and again transmits the vehicle state parameters to the intelligent electronic control unit. The structure of experimental system is shown in Figure 5.

4.2 Self-Learning Experiment of Neural Networks

The experiment begins after having completed electromotive demarcation of the control system. The trained-data acquired from many groups which working conditions is provided for networks with the control aim of keeping the powertrain system exert optimal driving power. The system is loaded by controlling power-measure machine. Under this condition of keeping maximal power output of the powertrain system, the gears of transmission and the throttle of engine are artificially chosen and registered as trained-data when the system has steadily run. The process above is repeatedly carried out till 40 groups running data as a batch is collected for the learning of neural networks. During the learning course, the parameters of nerve networks are continually adjusted in order to make it possible to improve the intelligent gear-shifting control system's identification capability on running rules of the powertrain system. Define that learning rate of nerve networks is 0.01 and training precision of networks is 0.002.

4.3 Gear-Shifting Control Experiment and Results Analysis

The experimental aims are to prove the correct of CNN gear-shifting theory mentioned above and to test the reliability of CNN controller on the test-bench for hydrodynamic mechanical transmission. At the same time, it is important for the control system utilizing the acquired running rules to test its gear-decision-making capability on any working conditions. The powertrain system is loaded by adjusting power-measure machine while the running data is registered by data-watch system. Here, intelligent electronic control unit makes gear-decision and export gear-shifting signals. The results of experiment on 100 points drawn in Figure 6 show that the powertrain system can normally work, and the design of CNN gear-shifting controller is successful. Under continuously changed load conditions the gear-shifting control system can realize automatic transmission by means of gear-shifting strategy acquired from working. So, it may be proven that the decision-making precision and velocity of CNN can meet control demands and ECU can duly and exactly respond to any testing working condition.

5. Conclusions

In this paper, design problems of the intelligent gear-shifting control system from experiment have been solved. Conclusions have been gained as follows：

1．The algorithms and structure of nerve networks in intelligent gear-shifting control system have been improved. The feasibility of chaotic nerve networks （CNN） technology applied to gear-shifting control of construction vehicle has been proved by the experiment on test-bench of the powertrain system.

2. Gear-shifting electronic control unit (ECU) with the core of 8032 micro-controller has been developed.

3. The intelligent gear-shifting control system designed in this study has conquered nerve networks technology's own defect on delayed and imprecise control aspects. The system that possesses the haracteristic of adapting automatically to working conditions by means of learning from operation can realize automatic transmission of construction vehicle.

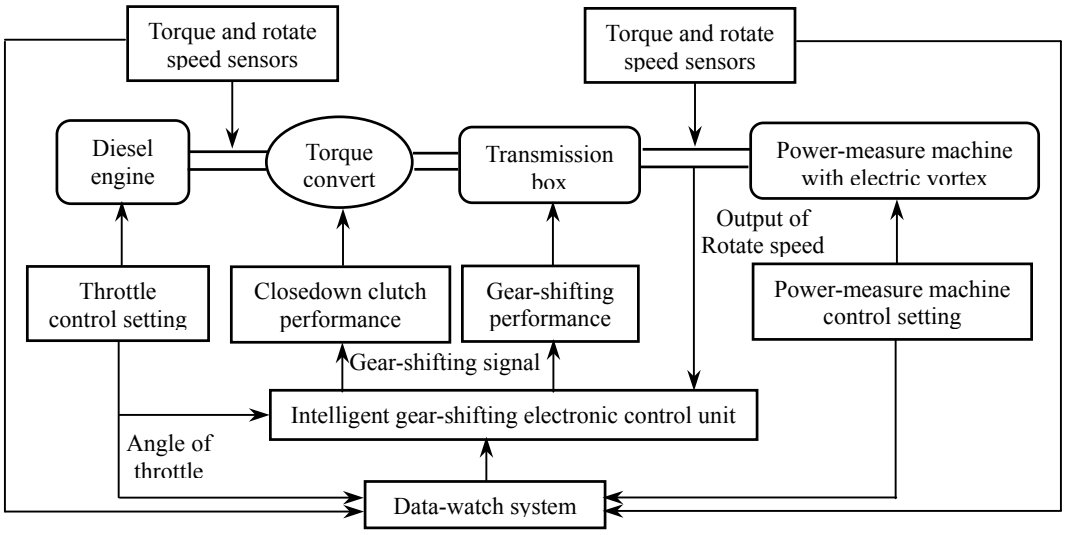

Figure 5. The Structure of Experimental System

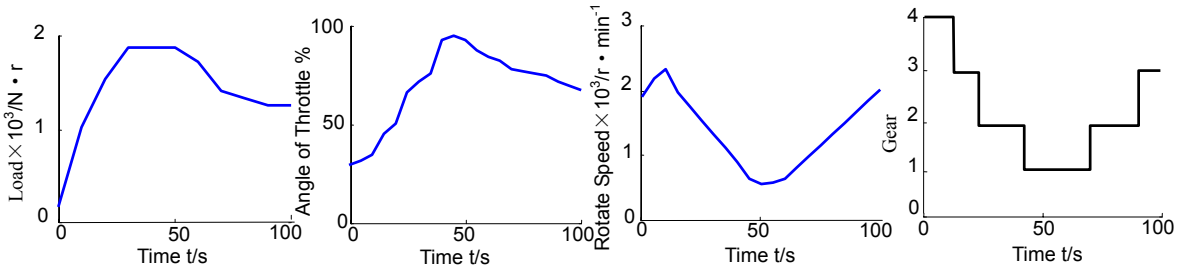

Figure 6. The Results of Experiment

This project is financially supported by the National Natural Sciences Fund of China. The project name: Research on Automatic Transmission Technology for Construction Machinery (Serial number: 50075033).

Correspondence to: Zhenyu Zhu
142 Renmin Avenue
College of Mechanical Science and Engineering
Jilin University
Changchun, Jilin 130025, China
Telephone: 01186-431-5701742
Mobile: 01186-13504463984
E-mail: zhu_zhy@hotmail.com

References

Baumann B, Rizzoni G, Washington G. Intelligent control of hybrid vehicle using neural networks and fuzzy logic. SAE 1998;981061:125-33.

Ge A. Theory and design of automatic transmission for vehicle. Machine Industry Publishing Company, Beijing, China. 1993:136-45.

Hiroshi Y. Automatic transmission shift schedule control using fuzzy logic. SAE 1993; 930674:1077-88.

Jiao S, Xu A, Meng L. Automatic transmission control system of modern construction machinery. Road Machinery & Construction Mechanization 1997;14(3):17-20.

Li K, Chen T. Prediction of noisy time series using Chaotic neural network. Nankai University Transaction （Natural Sciences） 2001;34(3):28-31.

Toyama M, Asai Y. New transmission control system for bulldozers, SAE 1992;921689:481-9.

Wang X, Xu C, Zhao K, Zhao D, Nie F. Simulation of automatic shift-control on construction vehicle. China Journal of Highway and Transport 2001;14(3):113-6.

Wang X. Study on intelligent control for mechanical transmission of construction machinery. Doctoral degree dissertation, Changchun, 2002:85-90.

Yi J. Modern vehicle automatic transmission. Sichuan Technology Publishing Company, Chengdu, China. 1998:35-50.

Yuan Z. Artificial nerve networks and its applying, Tsinghua University Publishing Company, Beijing, China. 1999:66-8.

The Technology of the Municipal Solid Wastes Composting

Zimin Wei*, Shiping Wang**, Jinggang Xu*, Yuyuan Zhou*

* Life Science College, Northeast Agricultural University, Harbin, Heilongjiang 150030, China; ** China Agricultural University, Beijing, China, Weizm691120@163.com

Abstract: Compost is one of the most important ways in China. This paper took Daqing Meishang compost plant as example, and introduced the modern municipal solid wastes composting technology, which including composting engineering flow, process indexes and disposal technology. [Nature and Science 2003;1(1):91-94].

Key words: composting; engineering flow; process indexes; pollutant

Introduction

With the increasing of population quantity as well as industry and economy developing, the output of the municipal solid wastes (MSW) has been increasing in China. At present, the output of MSW has been exceeded a hundred million tons in most cities of China. In fact, the MSW output has been increasing at 10% each year and now it has been accumulated gradually to ninety hundreds million tons in the past years. Most cities in China have been surrounded by the MSW. Because the calorific value of the MSW in China is lower than that in other countries, incineration treatment will be much expensive (Nie, 2000; Sun, 1999). On the other hand sanitation landfill would occupy a lot of lands, and lead to two-step solution by less developed technology (Zhong, 1999). In recent years, the technology of the MSW microbial composting has been accepted gradually by Chinese citizen, because the organic matter content of China MSW exceed 60%, and water content is about 50%, after the MSW was classified by machines, the residual organic matter is suitable for composting, and the composting production could be served as soil fertilizer. At present, Daqing Meishang Company in China owns unique technology in such field. This article would use this MSW composting technology to test its effect.

1. The Engineering Flow of the MSW Composting

The microbial composting technology was used to treat different and comprehensive utilization in Daqing MSW treatment plant. The MSW treatment technology include the MSW classify, composting fermentation, and late treatment system. The engineering flow chart could be seen in Figure 1.

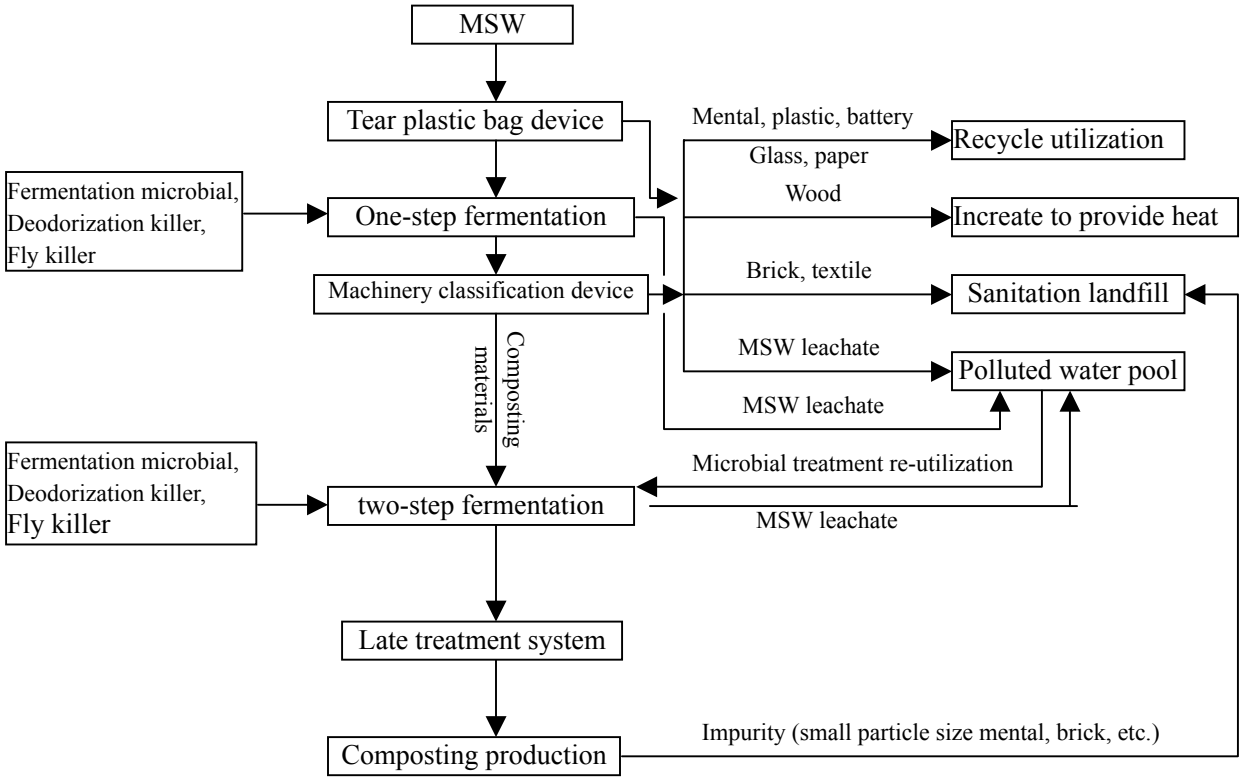

Figure 1. The MSW Composting Engineering Flow Chart

The two-step fermentation was adopted in the composting process and the fermentation period would last about 40 days. Because the water content in the MSW is high (about 55%) and the classification rate is low, the project will divide machinery classification into two steps: one-step fermentation and two-step fermentation, so the classification rate and the quality of the MSW composting could be increased.

1.1 One-step Fermentation

The purpose of one-step fermentation is to decompose carbohydrate, starch and protein, as well as reduce the water content of the MSW. This could lower the losing of organic matter when screening.

The MSW one-step fermentation was completed in 10 fermentation storerooms that were isolated from each other.

Each storeroom area: 54 m (length) × 27 m (width) = 458 m^2.

The height of the fermentation MSW pile: 3 m.

First, MSW was transported into composting plant and the plastic and paper would be removed from the MSW by wind classification and tearing plastic bag device. Then the residual matters would be transported into one-step fermentation storeroom. During the piling of the MSW, the microbial fermentation solution and deodorization killer were sprayed into it, and the oxygen in the fermentation storerooms would be forced to apply to the composting pile at regular interval. The whole period of one-step fermentation would last about 20 days. When water content of the MSW decreased to 30%, transport machinery could transport the one-step fermentation matter to classification liner.

1.2 Classification Technology

The project adopted automatic classification, gravity-wind classification and spring classification. After one-step fermentation finished, MSW was transported to classification liner： metals, plastics, papers, glasses were picked out for recycle utilization； wood and textile were incinerated to apply heat； bricks were landfilled in sanitation landfill plant; the residual organic matters were transported to two-step fermentation area.

1.3 Two-step Fermentation

The MSW was piled in bar shape in two-step fermentation area, and microbial fermentation solution was sprayed into it. Each bar compost pile was 150 m long. Its cross section was triangle, 4.5 m in width and 150 m high. At the primary period of two-step fermentation, the water content was controlled at 50%, compost temperature and pH were determined every day and machinery turned over the fermentation piles once a week. When the compost temperature decreased to 30℃, it indicated that the compost had been maturity. Two-step fermentation period would last about 20 days.

1.4 Late Treatment Technology

Late treatment technology included organic matter classification and package. After two-step fermentation finished, the samples of organic fertilizer were took from fermentation pile, and maturity indexes were tested. After organic fertilizer quality checked, it was transported to screening machinery system, and picked out the small particle size impurity (glass and stone etc), then the organic fertilizer was grinded to package. The organic fertilizer productions were transported to storeroom.

2. Process Indices (Haug, 1979; Crombie, 1982; Smith, 1992; Miller, 1985; Jimenez, 1991)

2.1 Classification Technology Indices

Water content of MSW: 30%.

Classification rate: ≥95%.

MSW volume weight: 0.6 t/m^3.

2.2 One-step Fermentation Technology Indices

Organic matter content: 40%~60%.

Fermentation period: 20 days.

Water content of input organic matter: 55%.

Water content of output organic matter: 30%.

Oxygen density: ≤10%.

C/N (the ratio carbon to nitrogen): 28:1.

Compost temperature: 55℃≤T≤75℃, lasted more than 5 days.

Ventilation quantity: 0.11 m^3/min·m^3 MSW (adjust according to production).

Fermentation pile high: 3.0 m.

Volume weight of input organic matter: 0.5 t/m^3.

Volume weight of output organic matter: 0.6 t/m^3.

2.3 Two-step Fermentation Technology Indices

Fermentation period: 20 days.

Water content of input organic matter: 30%.

Control water content at two-step compost primary period: 50%.

Water content of output organic matter: 25%~30%.

pH of output organic matter: 7.5.

Oxygen density: ≤10%.

C/N: 20:1.

Ventilation quantity: 0.05 m^3/min·m^3 MSW (adjust according to production).

Fermentation pile high: 2.2 m.

Volume weight of input organic matter: 0.5 t/m^3.

Volume weight of output organic matter: 0.6 t/m^3.

Turn over the fermentation piles: once a week.

2.4 Compost Maturity Indices

Water content: 25%~30%.

C/N: ≤20:1.
Compost temperature: <30℃.
Aerobic rate: gradually stable.

2.5 Organic Fertilizer Production Quantity Indices
Smell: without malodorous.
pH: 6.5~7.
Organic matter content: 25%~35%.
Water content: 25%.
Color: brown.
C/N: 15:1~20:1.

3. Pollutant Disposal Technology
The pollutant source came from malodorous gases, MSW leachate and noise.

3.1 Malodorous Gases (Xie, 1997; Brauet, 1981)
MSW was collected from citizen, then transported to the MSW treatment plant the following day. In this period, the simple organic matter would be anaerobic fermentation, rot and decompose. As a result, the malodorous gases (NH_3, H_2S, CH_3SH, etc) were produced and discharged during one-step fermentation and classification process.

The project adopted physics and microbial method to deal with the malodorous gases. The gases collection device was installed in the main compost workroom. Collected the malodorous gases, then passed them through two step water membrane to get rid of dust, wood scraps, activate carbon, furthermore, passed them through microbial membrane to get rid of malodorous (Figure 2). The depurated malodorous gases were discharged to atmosphere through chimney (30 m high). At last, the discharged malodorous gases density were: H_2S, 2.54 mg/m^3; NH_3, 18.8 mg/m^3; CH_3SH, 0.268 mg/m^3. The ejected rates were: H_2S, 0.87 kg/h; NH_3, 9.40 kg/h; CH_3SH, 0.134 kg/h. All of the parameters conform to China malodorous ejection standard (H_2S, 1.3 kg/h; NH_3, 20 kg/h,; CH_3SH, 0.17 kg/h).

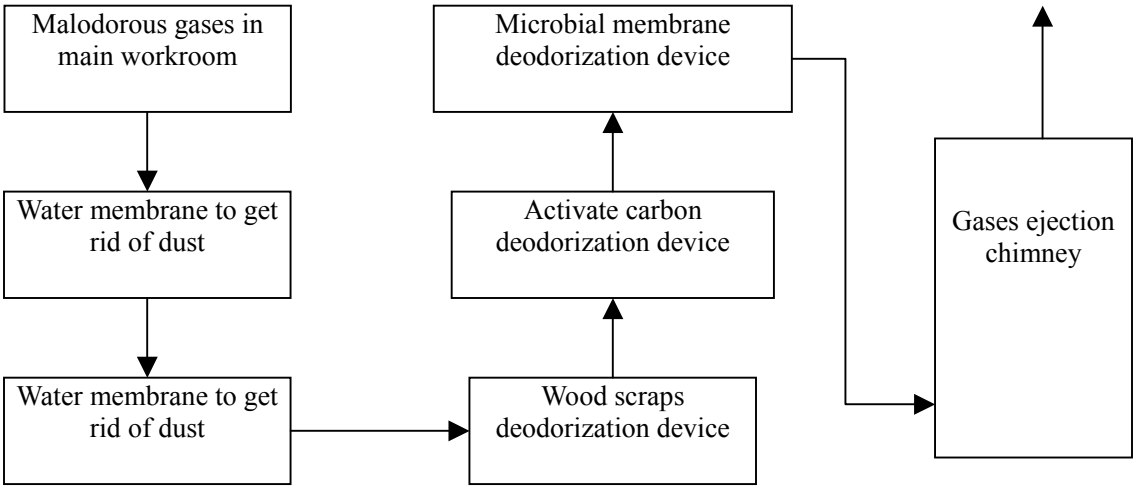

Figure 2. Malodorous Gases Deodorization Technology

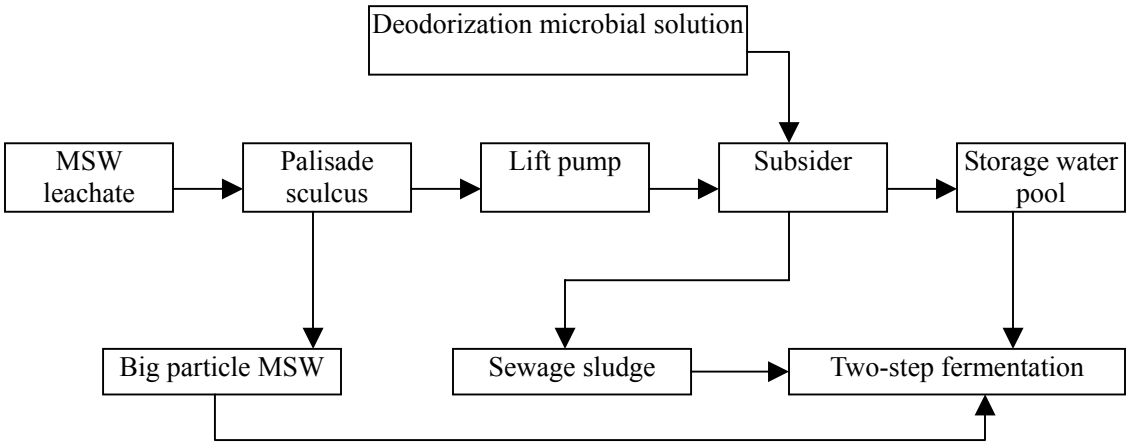

Figure 3. MSW Leachate Disposal System

3.2 MSW Leachate

The MSW leachate main come from one-step fermentation and machinery classification process. As pollution substance solution was very high in MSW leachate, to get rid of pollution substance and drift them to river will cost much. The project adopted physics and microbial method to deal with it (Figure 3). The MSW leachate was collected through drainage ditch, then passed through palisade sculcus to pick out big particle MSW, and deposit to get rid of sedimentation particle substance at the same time, deodorization microbial solution was sprayed into it, finally the treated MSW leachate was sprayed into two-step fermentation.

3.3 Solid Wastes

Solid wastes were picked out by classification process, which including plastic, metal, wood, textile, paper, brick, glass, battery etc. Its disposal ways were shown in Table 1.

Table 1. The Solid Wastes Disposal Ways

Solid waste types	Yield （t/d）	Disposal methods
Plastic	55	Recycle
Metal	8.3	Recycle
Wood	13.5	Incineration
Textile	28.5	Incineration
Paper	7	Recycle
Brick	12	Sanitation landfill
Glass	40	Recycle
Battery	0.1	Storage

4. Discussions and Conclusions

Daqing Meishang plant has composted the MSW for three years. It has produced organic fertilizer 115 tons per day and recycled plastic 64 tons and paper 22 tons per day, and gained enormous economic and environment results. At the same time, many questions have risen in MSW organic fertilizer sale and utilization. As the nutrient of the MSW organic fertilizer is lower (N, 1.23%, P_2O_5, 0.98%, K_2O, 1.34%) and the fertilizer application quantity is higher in soil than that of chemical fertilizer, that would waste a large number of labors. At present, not all farmers in China accept the MSW organic fertilizer. Therefore, how to increase the MSW nutrient and decrease the fertilizer application in soil is the main work for environment protection and fertilizer worker in the future.

The financial support provided by the Harbin City Technology Item 2002AA3CN109.

Correspondence to:
Shiping Wang
Wood Street 59
Gongbin Road, Xiangfang District
Harbin, Heilongjiang 150030, China
Telephone: 01186-451-5519-1377
Cellular phone: 01186-13845081243
E-mail: weizm691120@163.com

References

Crombie G. Evolution of a compost plant. Biocycle 1982;23(6):17-25.

Brauet H, Varma G. Air pollution control equipment. Berlin, Heidiberg. New York. 1981.

Haug RT. Engineering principles of sludge composting. J Water Pollut Control Fed 1979;51:2189-206.

Jimenez EI, Garcia VP. Composting of domestic refuse and sewage sludge. I. Evalution of temperature, pH, C/N ration and cation exchange capacity. Resources, Conservation and Recycling 1991;6:45-60.

Miller RC, Finstein MS. Materials balance in the composting of waste water sludge as affected by process control strategy. Journal Water Pollution Control Federation 1985;57(2):127.

Nie YF, Liu FQ, Wang JJ. Assessment on the way to develop MSW incineration in China. Research of Environmental Sciences 2000;3:19-23.

Smith WH, Margolis ZP, Janonis BA. High attitude sludge composting. Biocycle 1992;8:68-91.

Sun H, Li Y, Zhang W. The economic analysis of the MSW incineration to electric and apply heat. Beijing Energy Conserve Action, China. 1999;2:1-4.

Xie B, Shi JL, Xu YT. A review of odorous gases treatment using microbes. Journal of Environment Introduction, China. 1997;1:6-8.

Zhong ZY, Zhou QX. Sanitation landfill technology for refuse. Urban Environment & Urban Ecology. China. 1999;2:1-7.

Nature and Science, Volume 1, Number 1, November 2003, ISSN 1545-0740

NATURE AND SCIENCE

(Volume 1, Number 1)

Author Index

Nobel Prize Winners in 2003

Nobel Prize has been awarded annually since 1901 according to Alfred Nobel's testament. The following is the information of the Nobel Prize Winners in 2003:

1. Physics:

(1) **ALEXEI A. ABRIKOSOV** (1928 Moscow of Russia, Russian and American; Materials Science Division, Argonne National Laboratory of USA) - Theory of superconductors and superfluids.

(2) **VITALY L. GINZBURG** (1916 Moscow of Russia, Russian, P.N. Lebedev Physical Institute of Russia, ginzburg@lpi.ru), and ANTHONY J. LEGGETT (1938 Washington, DC of USA, Briton and American, Dept of Physics, University of Illinois of USA, aleggett@uiuc.edu) - Theory of superconductors and superfluids.

(3) **ANTHONY J. LEGGETT** (1938 Washington, DC of USA; Briton and American; Dept of Physics, University of Illinois; aleggett@uiuc.edu) - Theory of superconductors and superfluids.

2. Chemistry:

(1) **PETER AGRE** (1949 Northfield, Minnesota of USA, Johns Hopkins University School of Medicine, pagre@jhmi.edu) - Discovery of water channels.

(2) **RODERICK MACKINNON** (1956 Burlington, MA of USA, Rockefeller University of USA, mackinn@rockefeller.edu) - Structural and mechanistic studies of ion channels.

3. Physiology-medicine:

(1) **PAUL C. LAUTERBUR** (1929 Sidney, Ohio of USA; American; Biomedical Magnetic Resonance Laboratory, University of Illinois; pc@uiuc.edu) - Discoveries concerning magnetic resonance imaging.

(2) **SIR PETER MANSFIELD** (1933 London of UK; Briton; Magnetic Resonance Centre of University of Nottingham; Melanie.Stretton@nottingham.ac.uk) - Discoveries concerning magnetic resonance imaging.

4. Economics:

(1) **ROBERT F. ENGLE** (1942 Syracuse, NY of USA; American; New York University; rengle@stern.nyu.edu) - Methods of analyzing economic time series with time-varying volatility (ARCH).

(2) **CLIVE W. J. GRANGER** (1934 Swansea, Wales of UK; Briton; University of California, San Diego; cgranger@ecsd.edu) - For methods of analyzing economic time series with common trends (cointegration).

5. Literature:

JOHN MAXWELL COETZEE (1940 Cape Town of South Africa; Australian; University of Adelaide of Australia) - Innumerable guises portrays the surprising involvement of the outsider.

6. Peace:

SHIRIN EBADI (1947 Iran; Iranian) - Efforts for democracy and human rights.

Price: US$5.00

Nature and Science

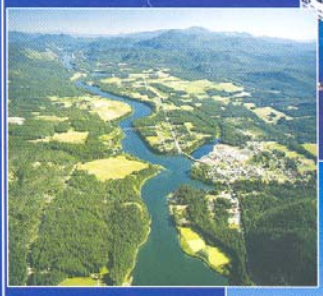

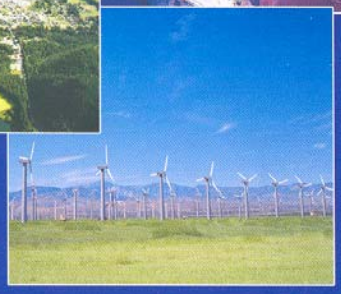

Marsland Company
P.O. Box 753
East Lansing,
Michigan 48826
The United States
Tel: (517) 862-6881

E-mail: editor@sciencepub.net
Homepage: http://www.sciencepub.net